Electrophysiological characterization of Na^+ and T-type Ca^{2+} channel alterations and their impact on action potential generation in rodent models of neuropathic pain

Dissertation

zur

Erlangung des Doktorgrades (Dr. rer. nat.)

der

Mathematisch-Naturwissenschaftlichen Fakultät

der

Rheinischen Friedrich-Wilhelms-Universität Bonn

vorgelegt von

Omneya Taha Hanafi

aus

Aachen

Bonn 2014

Angefertigt mit Genehmigung der Mathematisch-Naturwissenschaftlichen Fakultät
der Rheinischen Friedrich-Wilhelms-Universität Bonn

1. Gutachter: Prof. Dr. Heinz Beck
2. Gutachter: Prof. Dr. Christa E. Müller
Tag der Promotion: 26.08.2014
Erscheinungsjahr: 2014

Acknowledgements

First, I would like to express my gratitude to my supervisor Prof. Dr. Heinz Beck, for giving me the opportunity to conduct my PhD studies and perform experimental work in his laboratories. I would also like to thank him for his expert advice and constructive help during the research time.

I am very grateful to Dr. med. Monika Jeub for giving me the chance to conduct my PhD studies in her group. To me she was a constructive supervisor who was always guiding and understanding.

My deep thank to Dr. Thoralf Opitz, for his professional help and assistance, as well as his continuous encouragement and patience during my work.

My deep thank to PD Dr. Ildikó Rácz for her kind cooperation with our research group as well as her professional support and advice for my experiments.

I am also grateful to Dr. med. Markus Mueller for his kind cooperation with our research group and his help in performing part of the experiments.

Many sincere thanks to the laboratory members who not only provided help and encouragement but mostly also ensured the friendly working environment in the lab.

Special thanks to my friends Elisabet Reyes and Victoria Peeva for their moral support and constant encouragement during my work.

I am forever indebted to my husband and my family for their continuous and kind encouragement and true help and support during the course of this study.

Table of contents

List of Figures

List of Tables

Abbreviations

ADP	Spike afterdepolarization
AHP	Spike afterhyperpolarization
AIDP	Acute inflammatory demyelinating polyradiculoneuropathy
AP	Action potential
ATP	Adenosine triphosphate
BSA	Bovine serum albumin
Cap^-	Capsaicin negative
Cap^+	Capsaicin positive
CCD	Chronic compression of DRG
CCI	Chronic constriction injury
cDNA	Complementary deoxyribonucleic acid
CFA	Complete Freund's Adjuvant
CNS	Central nervous system
dNTP	Deoxyribonucleosidetriphosphate
DRG	Dorsal root ganglion
EAE	Experimental autoimmune encephalomyelitis
EAN	Experimental autoimmune neuritis
GBS	Guillain–Barré syndrome
HVA	High voltage activated (calcium channels)
HW	Half width
IASP	International Association for the Study of Pain
IB_4	Isolectin B_4
ICFA	Incomplete Freund's Adjuvant
I_h	hyperpolarization-activated current
I_{NaP}	Persistent Na^+ current
I_{NaT}	Transient Na^+ current
KO	Knock-out
LVA	Low voltage activated calcium channel
mRNA	Messenger ribonucleic acid
n.s.	Not significant
PBS	Phosphate buffered saline
PCR	Polymerase chain reaction
PDN	Painful diabetic neuropathy
PNL	Partial sciatic nerve ligation
PNS	Peripheral nervous system
PWT	Paw withdrawal threshold
RMP	Resting membrane potential
SNI	Spared nerve injury
SNL	Sciatic nerve ligation
TNF-α	Tumor necrosis factor alpha
TTX	Tetrodotoxin
TTX_R	TTX-resistant
TTX_s	TTX-sensitive
$V_{1/2}$	Voltage of half maximal activation
VGCC	Voltage gated calcium channels
VGSC	Voltage gated sodium channels
wt	Wild type
τ_{Decay}	Decay time constant

Summary

The pathomechanism underlying neuropathic pain is still unclear and for some diseases such as Guillain-Barré-Syndrome almost unexplored. For this, experimental autoimmune neuritis (EAN), a rat model of Guillain Barré-Syndrom (GBS), was established in our laboratory to detect nociceptive neurons for changes in their membrane properties that might be correlated to severe pain. EAN rats developed motor deficits, weight loss as well as mechanical allodynia, all symptoms resembling the clinical and pathological features of GBS. Current clamp recordings of small DRG neurons of EAN rats revealed a significant reduction in AP duration as well as signs of enhanced excitability such as lower rheobase and higher frequency of evoked AP discharge. These alterations have been detected in a subtype of DRG neurons that display sensitivity to capsaicin. Changes in these membrane properties were also accompanied by alterations of Na^+ currents in the same subgroup of neurons. The transient TTX_S Na^+ current was clearly up-regulated in EAN animals, while the transient TTX_R Na^+ current tends to be down-regulated, leaving the total transient Na^+ current unchanged. This switch in Na^+ currents was again demonstrated in the significantly faster inactivation kinetics of the total transient Na^+ current, reflecting the predominant role of the fast TTX_S Na^+ current in EAN DRG neurons. In addition, EAN induced a reduction in the magnitude of the total persistent Na^+ current of cap^+ DRG neurons that could be attributed to the TTX_S I_{NaP}. These changes in Na^+ currents can be considered as potential basis for the altered electrical properties observed in cap^+ DRG neurons of EAN rats.

Previous studies reported contradicting results concerning the role of T-type Ca^{2+} currents in supporting neuropathic pain. For this, in the second part of this study changes in T-type Ca^{2+} currents in nociceptive DRG neurons were analysed in a mouse model of partial nerve ligation-induced neuropathic pain. Our results show that the PNL animals suffered an increase in nociceptive sensitivity that was paralleled by a significant up-regulation of T-type Ca^{2+} currents in cap^+ DRG neurons. Pharmacological experiments revealed that this increase was attributed to a Ni^{2+} resistant current component, a result that stands in contrast with a pronociceptive role of $Ca_V3.2$ in neuropathic pain suggested previously. However, mice lacking $Ca_V3.2$ still suffered pain hypersensitivity following nerve injury. Also, T-type Ca^{2+} currents were significantly enhanced in DRG of PNL $Ca_V3.2$ KO mice. Moreover, RT-PCR revealed a lack of up-regulation of these channel subunits on the mRNA level. Collectively, our data suggest an up-regulation of one or both of the Ni^{2+} insensitive T-type subunits ($Ca_V3.1$ or $Ca_V3.3$) in small cap^+ DRG neurons after partial nerve ligation. These changes can explain the increased excitability, as evidenced by a considerable reduction of threshold of AP firing in the same subset of neurons.

In conclusion, our present data demonstrate a role of Na^+ currents as well as LVA-currents in the increased cellular excitability and nociceptive sensitivity in different animal models of neuropathic pain. Further studies are required to identify the specific subunits involved and hence allow effective treatment with minimal side effects.

1 Introduction

1.1 The peripheral nervous system/pain pathway

Pain is an unpleasant sensation that alerts the body to potentially damaging stimuli and consequently triggers an appropriate protective response. Acute pain transmission is initiated by a subgroup of primary sensory neurons called nociceptors, which are defined by the International Association for the Study of Pain (IASP) as “a receptor preferentially sensitive to a noxious stimulus or to a stimulus which would become noxious if prolonged”. Accordingly, nociceptors have characteristic thresholds or sensitivities that distinguish them from other sensory nerve fibers (Burgess and Perl 1967).

Pain is induced by an external stimulus (mechanical, thermal, chemical or electrical) of sufficient energy that activates nerve endings of nociceptive neurons in skin, bone, joint, muscle or viscera, thus, initiating action potentials that are conducted towards their central terminals in the dorsal horn of the spinal cord. Consequently, in the dorsal horn, Ca^{2+} influx through VGCC (voltage gated calcium channels) triggers the release of nociceptive neurotransmitters (glutamate) or neuromodulators (e.g substance P), which in turn excite or sensitize secondary sensory neurons in the superficial laminae (I and II) of the dorsal horn. The dorsal horn neurons, in turn, transmit the pain messages to higher brain centers, including the reticular formation, thalamus and the cerebral cortex (Basbaum 2000).

Primary sensory neurons can be classified into three main groups. Aα- and Aβ-fibers have large diameters and thick myelin sheaths. Thus, they are rapidly conducting and involved in detection of innocuous stimuli (Lewin and Moshourab 2004; Smith and Lewin 2009). The thinly myelinated Aδ-fibers have smaller axon diameters and are classified as either low-threshold, D-hair mechanoreceptors or mechanoreceptors activated by noxious stimuli (Aδ-mechanoreceptors) (Lewin and Moshourab 2004; Koltzenburg et al. 1997). The third group of neurons is the unmyelinated C-fibers, which are more abundant than A-fibers (Lewin and Moshourab 2004). Both Aδ- and C-fibres constitute most of nociceptors, where the Aδ-fibers mediate the 'first' rapid, acute sharp pain evoked by noxious stimuli and the C-fibers the 'second', more diffuse, dull pain. The C-fiber nociceptors are mostly polymodal. Hence, they are able to respond to noxious stimuli of all types: mechanical, heat and chemical (Bessou and Perl 1969). Some C-fiber nociceptors, however, respond only to noxious heat or mechanical stimuli, some to mechanical and heat and some to mechanical and cold. Another group of C-fibers, known as "sleeping" or "silent" are not activated by noxious stimuli (Handwerker et al. 1991; Schmidt et al. 1995; Weidner et al. 1999). Nevertheless, these fibers are able to sensitize after incubation with inflammatory mediators, where they become responsive to mechanical and/or heat stimuli (Meyer et al. 1991; Kress et al. 1992). The small diameter nociceptors terminate in the superficial laminae I and II of the dorsal horn, and the large diameter neurons terminate in laminas III and IV.

Primary sensory neurons are pseudounipolar cells, where a single process arising from the cell body in the dorsal root ganglion (DRG) splits into a peripheral axon that

innervates the periphery and a central axon that synapses on second-order neurons in the dorsal horn of the spinal cord (Basbaum et al. 2009). Primary sensory neurons/DRG neurons can be grouped according to their size into small, medium and large neurons. Small DRGs represent the somas of thin Aδ- and C-type sensory fibers and are less than 31 µm in average diameter. Large DRG neurons arise from Aα- and -Aβ-fibers and are larger than 45 µm in average diameter. The medium sized neurons (between 32-45 µm) could belong to either group (Lee et al. 1986; Scroggs and Fox 1992).

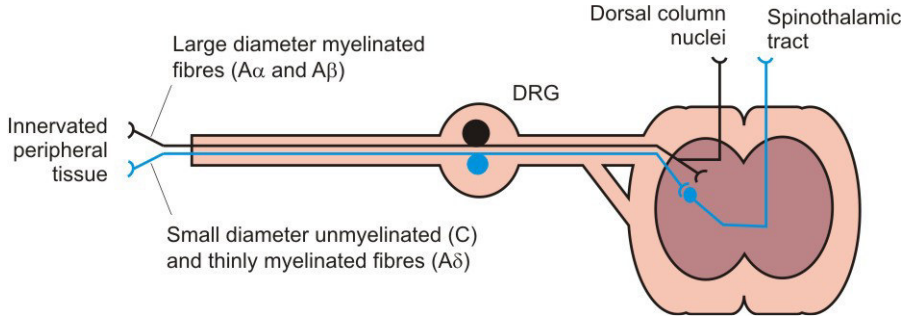

Fig. 1: Anatomy of primary sensory neurons. Sensory information is transmitted by the primary sensory neurons from the peripheral tissue to the spinal cord. The cell bodies of these neurons are located in the dorsal root ganglia. Cell bodies of 15–45 µm in diameter give rise to unmyelinated C and thinly-myelinated Aδ-fibers. Cell bodies >45 µm in diameter give rise to myelinated Aα-and Aβ-sensory fibers (modified after Mantyh 2006).

1.2 Neuropathic pain

Neuropathic pain is a type of pain that does not protect or support healing. It is due to a disruption of the somatosensory system, and can be considered as a disease on its own. Neuropathic pain is defined by the IASP as pain "caused by a lesion or disease of the somatosensory nervous system". Up to one-sixth of the world population is affected and a variety of causes can lead to this maladaptive pain. Examples include mechanical nerve injury, autoimmune diseases (e.g. multiple sclerosis, Guillain–Barré syndrome), metabolic diseases (e.g. diabetic polyneuropathy), infections (e.g. herpes zoster, HIV) and neurotoxicity (e.g. chemotherapy of cancer or pharmacotherapy of tuberculosis). As a general rule, lesions leading to neuropathic pain must directly involve the nociceptive pathways (Campbell and Meyer 2006). Common features of neuropathic pain include burning or coldness, "pins and needles sensation", numbness and itching, attacks of pain without a cause as well as widespread pain not otherwise explainable. Moreover, patients might suffer abnormal sensations such as allodynia (pain response to a normal non-painful stimulus) and hyperalgesia (exaggerated response to a painful stimulus) (Bridges et al. 2001). It should be mentioned that neural damage leads to chronic neuropathic pain only in a minority of patients. The liability of pain varies according to gender, age, and anatomical site of injury.

1.3 Mechanism/pathophysiology of neuropathic pain

Chronic neuropathic pain is a result of maladaptive plasticity within the nociceptive system. Following nerve injury, multiple alterations both central and peripheral take

place and lead to this complex pain phenotype. The plasticity of nociceptors is shown by a process called sensitization, where either non-responsive neurons become responsive, or neurons respond at a reduced threshold and/or produce responses of greater magnitude. Such sensitization is a result of repeated stimulation.

Under normal conditions, the firing threshold of primary afferent neurons is usually not reached without a stimulus. However, following nerve injury there is a large increase in the level of spontaneous firing in the afferent neurons linked to the injury site (Wall and Gutnick 1974). It is suggested, that this ectopic discharge contribute to the development of hyperalgesia, allodynia and ongoing pain associated with nerve injury. Also, it has been observed that the central terminals of large myelinated fibers can form synapses in a part of the dorsal horn that normally receives nociceptive inputs as a consequence of nerve injury (Woolf et al. 1995). This anatomical rearrangement may allow low- threshold sensory information to be interpreted as nociceptive, thus, providing another explanation for the emergence of allodynia after peripheral nerve injury (Bridges, Thompson et al. 2001).

Over time following peripheral nerve injury, the repetitive or prolonged noxious afferent input causes postsynaptic dorsal horn and higher order neurons up to the cortex to contribute to chronic pain. This central sensitization is characterized by lowering of activation thresholds of spinal neurons as well as the appearance of wind-up phenomena (Mendell 1966; Wall and Gutnick 1974). Wind up-phenomenon is defined as the frequency-dependent increase in excitability of spinal cord neurons as a result of repetitive stimulation of C-fiber afferents. It leads to an increase in pain perception.

Furthermore, decreased expression of inhibitory receptors on primary afferent terminals and postsynaptic neurons following nerve injury also contribute to the central sensitization. To this end, primary afferents reduce their expression of μ opioid receptors (Kohno et al. 2005) and a loss of pre- and postsynaptic GABAergic inhibition in the spinal cord has been recognized.

Moreover, neurodegeneration takes place following nerve injury, where both primary sensory and dorsal horn neurons die after peripheral nerve injury (Tandrup et al. 2000; Okamoto et al. 2001).

Immune mechanisms also play a critical role in initiation and maintenance of neuropathic pain. Following peripheral nerve injury, a set of inflammatory mediators are released from injured and inflammatory cells that sensitize nociceptive neurons. This "inflammatory soup" includes kinins, amines, prostanoids, growth factors, chemokines, and cytokines, protons and ATP. The release of cytokines IL-1 and TNF-α for example can directly modulate primary sensory neuron activity and elicit spontaneous action potential discharges (Jin and Gereau 2006; Wolf et al. 2006). In this regards, the deletion of IL-1 receptor type 1 or blocking of TNF-α attenuates pain behavior in neuropathic pain models (Jin and Gereau 2006; Wolf, Gabay et al. 2006). Furthermore, it has been observed that hyperalgesia is temporally linked with Wallerian degeneration and macrophage recruitment (Sommer et al. 1995; Myers et al. 1996) suggesting a direct role of macrophages to nerve injury induced hyperalgesia.

In conclusion, the mechanisms of neuropathic pain develop during the disease to involve both peripheral and central pathophysiology. Therefore, it could be considered as a progressive nervous system disease. Treatment of neuropathic pain is still a challenging issue. Of the current pharmacological drugs used for treatment are the tricyclic anti-depressants that act by blocking noradrenaline and serotonin reuptake (Stahl 1998; Gilron et al. 2006). Certain anticonvulsants as carbamazepine and gabapentin can also relief neuropathic pain by blocking Na^+ or Ca^{2+} channels (McQuay et al. 1996; Sindrup and Jensen 1999). Also opioids as methadone are used in controlling this chronic pain due to their NMDA antagonism as well as μ-opioid agonist properties (Gilron, Watson et al. 2006). However, these drugs relief pain in less than 50% of patients and are associated with considerable side effect (Bridges, Thompson et al. 2001).

1.4 Action potentials and their role in pathological pain processing within the DRG

The cell body of a nociceptor (DRG neurons) is a useful model for various studies as of the mechanism of transduction of noxious stimuli, transmission of electrical signals to the CNS, and release of neurotransmitters and neuropeptides at central and peripheral terminals (Malin et al. 2007; Cummins et al. 2009). The soma expresses a mixture of channels with a wide range of characteristics. These channels are also expressed in free nerve endings, central terminals and the axon (Basbaum, Bautista et al. 2009). Also, the excitability of DRG neuron somatas is affected by a variety of pathologies and injuries (Rush et al. 2007). The relatively easy isolation and spherical shape of these cell somatas as well as their involvement in a variety of diseases have made them a very good model for the study of the roles of different ion channels in electrogenesis. In addition, many functional characteristics of nociceptors are retained when sensory ganglia are dissociated and placed into culture (Kress and Reeh 1996). Hence, it is possible to examine chemical, thermal and mechanical sensitivity (Baccaglini and Hogan 1983; Cesare and McNaughton 1996; McCarter et al. 1999), thus allowing the identification of different DRG neurons as nociceptors and classification into different groups.

Nociceptors are generally electrically silent (Woolf and Ma 2007), transmitting all or none action potentials only when stimulated. The majority of large DRG neurons (Aα- and Aβ-neurons) display fast somatic action potentials and short afterhyperpolarizations (Gallego and Eyzaguirre 1978; Rose et al. 1986; Gurtu and Smith 1988; Koerber et al. 1988; Kim et al. 1998). In contrast, the action potentials of small fiber nociceptors have a characteristic morphology, as they have an unusually wide action potential with a hump or shoulder in the falling phase, and a long lasting afterhyperpolarization (AHP) (Gallego 1983; Ritter and Mendell 1992; Djouhri et al. 1998; Lopez de Armentia et al. 2000). These cells also display a greater overshoot and much greater input resistance as well as slower rate of firing than fast-conducting large diameter neurons (Bessou et al. 1971; Gorke and Pierau 1980; Harper and Lawson 1985 a). A recent study explored the inward cation currents giving the DRG neurons the characteristic shape of the action potential. They showed that Na^+ currents that are TTX-resistant (Tetrodotoxin-resistant) are the major contributors to the AP upstroke,

where TTX_S Na^+ channels also play a significant role especially around the threshold. The shoulder of the AP was mainly carried by TTX_R Na^+ currents and HVA Ca^{2+} currents (Blair and Bean 2002).

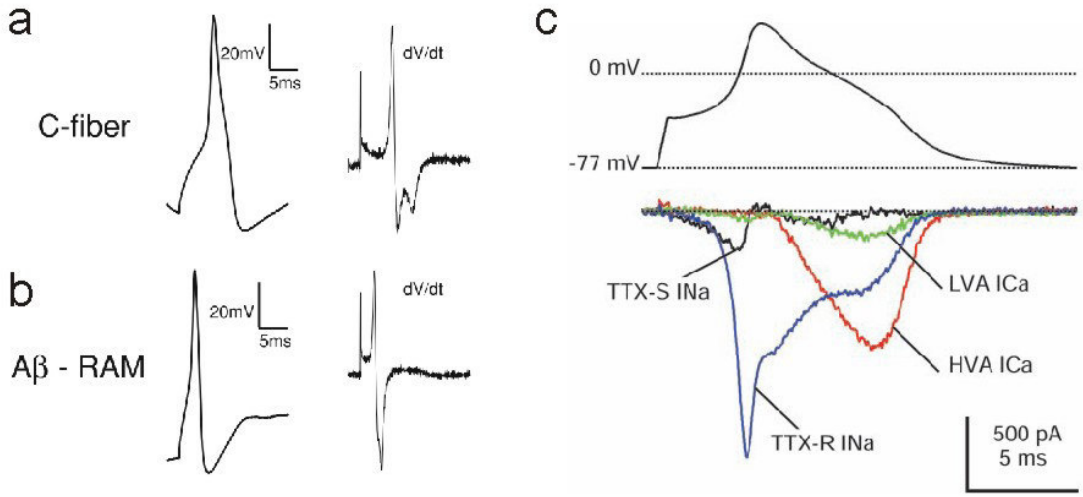

Fig. 2: Action potentials of DRG neurons. (a) Small diameter C-fibers have wide action potential with a hump or shoulder in the repolarizing phase, which can be shown by the appearance of two peaks in the first derivative of the spike (dV/dt). (b) A-fibers, which are wide in diameter, have narrow action potentials. The first derivative of the spike show one peak only. (With permission from Springer: J Comp Physiol A, Volume 195, Smith, E. S. and G. R. Lewin, Nociceptors: a phylogenetic view, 1089-106, Copyright (2009)). (c) Different inward currents during an action potential clamp in a DRG neuron. TTX_S Na^+ marked in black, TTX_R Na^+ in blue, HVA Ca^{2+} in red, LVA Ca^{2+} in green (With permission from SfN: J Neurosci, Volume 22, Blair, N. T. and B. P. Bean, Roles of tetrodotoxin (TTX)-sensitive Na^+ current, TTX-resistant Na^+ current, and Ca^{2+} current in the action potentials of nociceptive sensory neurons, 10277-90, Copyright (2002)).

Nerve injury leads to changes in the electrophysiological properties of nociceptive DRG neurons. An increased excitability (Abdulla and Smith 2001 a; Ma and LaMotte 2005), amplification of responses (burst discharges in response to single stimulus) (Moldovan et al.) and spontaneous discharges (Nystrom and Hagbarth 1981; Nordin et al. 1984) have been found to occur from DRG neuron somatas or within the neuroma (Wall and Devor 1983; Kajander and Bennett 1992; Babbedge et al. 1996; Study and Kral 1996; Millan 1999). Increase in excitability within DRG neurons is associated with changes in the action potential morphology, including lower action potential threshold and higher spike height. The amount of current required to discharge an action potential is also reduced (Gurtu and Smith 1988; Zhang et al. 1997; Kim, Na et al. 1998; Stebbing et al. 1999; Abdulla and Smith 2001 a). However, there is a discrepancy in some spike changes. Where some authors report an increase in spike width (Gallego et al. 1987; Kim, Na et al. 1998; Stebbing, Eschenfelder et al. 1999; Abdulla and Smith 2001 a), others report either small changes (Gurtu and Smith 1988), no effect (Zhang, Donnelly et al. 1997), or even a reduction in the proportion of neurons with an inflection on their repolarizing phase of their APs (Oyelese and Kocsis 1996). Furthermore, some studies show a reduction in AHP of nociceptive Aδ-fibers during peripheral inflammation (Djouhri and Lawson 1999), other studies,

however, find no changes in AHP after nerve injury (Abdulla and Smith 2001 a; Ma and LaMotte 2005). These discrepancies might be explained by the use of different cell types, animal species and/or animal models of neuropathic pain in the different studies.

The alterations of action potential parameters following nerve injury depend on the activity of voltage-dependent ion channels. As mentioned, nociceptive DRG neurons express a wide variety of voltage-gated channels (e.g. Na_V, Ca_V, K_V) that convert the peripheral terminal stimulation into a set of action potentials, thereby encoding the intensity of the noxious stimulation applied. Alterations of cell excitability and firing behavior in neuropathic pain is correlated with changes of these channels as well as those contributing to frequency modulation (e.g. hyperpolarization-activated cyclic nucleotide-gated cation channel [HCN] and A-type $K_V4.3$ and $K_V3.4$ channels) (Hille 2001).

1.5 Voltage gated Na^+ channels

Voltage-gated Na^+ channels (VGSC) are responsible for action potential initiation and propagation in excitable cells. These channels consist of a central α-subunit, that is sufficient for functional expression, and is associated with auxiliary β-subunits (Catterall 2000). The pore-forming α-subunit is composed of four homologous domains labeled I-IV, which fold together creating a central pore. Each domain contains six transmembrane helices labeled S1-S6 and an additional pore loop located between the S5 and S6 segments. These pore loops line the extracellular portion of the pore. This is the entry and the narrowest part of the pore and is responsible for its ion selectivity. The inner exit from the pore is wider and lined by the S5 and S6 segments of the four domains. The voltage sensitivity of VGSC is due to the S4 segments in each domain, which contain positively charged amino acid residues at every third position. These residues are stabilized by forming ion pairs with negatively charged residues of the adjacent transmembrane segments. Membrane depolarization that changes the transmembrane electric field causes the S4 segments to spiral outward. This movement leads to channel activation due to a conformational change that opens the pore. The outward movement is catalyzed by exchange of the ion pair partners (Catterall 2012). Na^+ channels inactivate within 1–2 ms upon activation. This fast inactivation is essential for repetitive firing of action potentials and control of excitability in nerve cells. The short intracellular loop connecting domains III and IV serves as inactivation gate (Vassilev et al. 1988) by folding into the channel structure and blocking the pore from the inside during sustained depolarization of the membrane (Kellenberger et al. 1996).

The α-subunit is associated with one or two β-subunits, which consist of an N-terminal extracellular domain, a single transmembrane segment, and a short intracellular segment (Isom et al. 1992). Four β-subunits have been described (Morgan et al. 2000; Yu et al. 2003), where β1 and β3 interact non-covalently with α-subunits and β2 and β4 form disulfide bonds. β-subunits can modify the kinetics and voltage dependence of channel gating. Furthermore, these subunits play a role in localization and immobilization of Na^+ channels in specific locations in excitable cells (Brackenbury and Isom 2011).

Na^+ channels are closed at resting membrane potential, but open upon membrane depolarization due to a conformational change as previously described. The influx of Na^+ ions through the channel pore leads to further membrane depolarization, which in turn activates more Na^+ channels. However, Na^+ channels remain open only for a short time (few milliseconds), even if depolarization is maintained, due to a process called fast inactivation. Here, the cytoplasmic domains of the channel drop into the inner pore and plug it. Na^+ channels also undergo slow inactivation, a process that involves closing a gate at the extracellular end of the pore. Inactivated channels cannot be activated until the inactivation is removed, leading to a refractory period during which depolarization fails to open the channels. Membrane repolarization or hyperpolarization removes inactivation (Hille 2001).

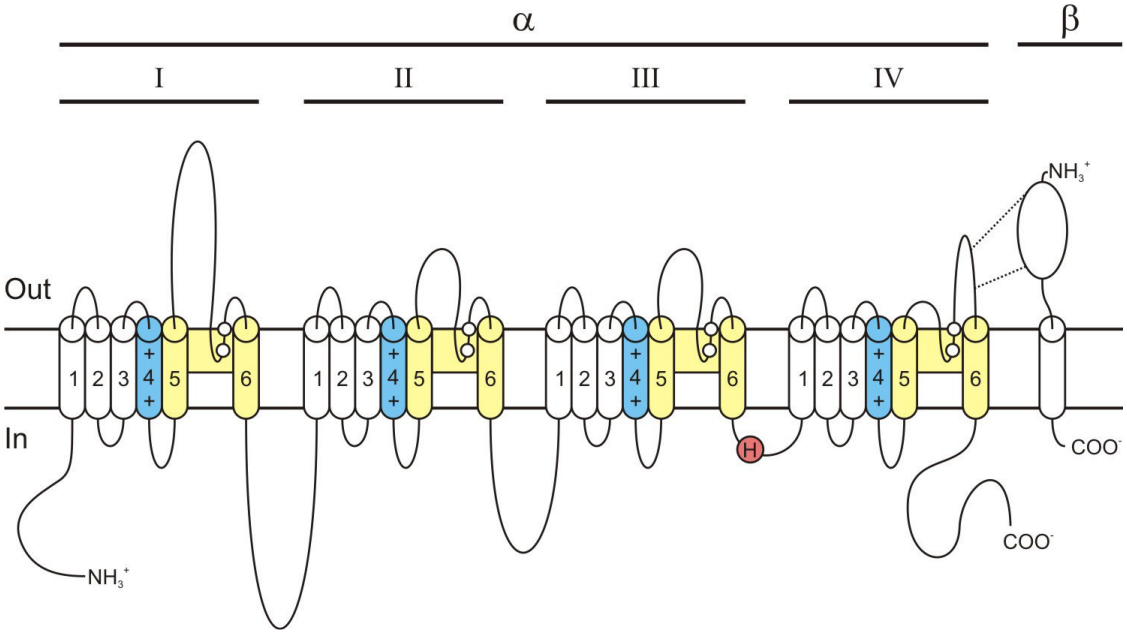

Fig. 3: Voltage gated Na^+ channel primary structure. The α-subunit is composed of four homologous domains (I-IV). Each domain consists of six transmembrane segments (S1-S6) that are represented as cylinders. The polypeptide chains of each subunit are shown as bold lines. Pore-lining segments are marked in yellow. Amino residues that form the ion selectivity filter and the tetrodotoxin binding site are marked in white circles. The S4 voltage sensors are marked in blue and the site involved in forming the inactivation gate is marked in a red circle (modified after Catterall 2012).

There are nine α-subunits ($Na_V1.1$-$Na_V1.9$), which are expressed in different excitable tissues. In addition, closely related Na^+ channel-like proteins have been identified (Na_X), which are not voltage gated and are involved in salt sensing (Watanabe et al. 2000). The Na^+ channels are distinguished by differences in their amino acid sequence, kinetics, Tetrodotoxin (TTX)-sensitivity and expression profiles.

The Na^+ channels give rise to different types of Na^+ currents. The transient Na^+ current (I_{NaT}), which is characterized by fast activation and inactivation, underlies the rising phase of the action potential, and therefore is important for action potential initiation. The noninactivating or persistent Na^+ current (I_{NaP}), on the other hand, has been proposed to have functional roles in setting the membrane potential in a subthreshold

range. For this reason, I_{NaP} can regulate membrane depolarization, repetitive firing and enhance synaptic transmission (Kiss 2008).

Most voltage-gated Na^+ channels can be blocked by nanomolar concentrations of TTX and thereby are termed TTX-sensitive channels. The binding site of TTX, as well as other neurotoxins (saxitoxin, μ-conotoxin), is formed by amino acid residues in the pore loops of domain I. In contrast, $Na_V1.5$, $Na_V1.8$, and $Na_V1.9$ are relatively resistant to this toxin, eliciting a TTX_R current. A single amino acid substitution in the binding site of TTX confers the resistance (Fozzard and Hanck 1996; Catterall 2000).

1.6 The role of Na^+ channels in pain processing within DRG neurons

Table 1: An overview of the different Na^+ channels of DRG neurons (modified after Rush, Cummins et al. 2007).

Na^+ channel isoform	Localization	Kinetics & Pharmacology	Biophysical properties
$Na_V1.1$	widespread	fast TTX_S	unidentified
$Na_V1.2$	embryonic	fast TTX_S	activates & inactivates at depolarized potentials compared to other TTX_S channels, can produce resurgent current
$Na_V1.3$	embryonic	fast TTX_S	rapid repriming characteristics, can produce persistent current in response to slow depolarizing ramps
$Na_V1.5$	embryonic	fast TTX_R	not fully characterized
$Na_V1.6$	widespread	fast TTX_S	rapid repriming characteristics, can produce persistent current as well as resurgent current
$Na_V1.7$	widespread	fast TTX_S	slow repriming characteristics, can produce persistent current in response to slow depolarizing ramps
$Na_V1.8$	widespread	slow TTX_R	rapid repriming characteristics, activates & inactivates at depolarized potentials
$Na_V1.9$	small nocicepctive cells	persistent TTX_R	activates at hyperpolarized potentials and inactivates very slowly

It has been proposed that changes in voltage-gated Na^+ channels in the DRG neurons can participate in the induction of neuropathic pain. The abnormal excitability of injured and uninjured DRG neurons following nerve injury is related to changes in the density, distribution, and functional activity of these channels. In fact, abnormal Na^+ channel accumulation has been observed in the tips of injured axons. Furthermore, the

use of Na^+ channel blockers (such as lidocaine) in patients can effectively relief neuropathic pain of different etiologies (Priest and Kaczorowski 2007).

A variety of Na^+ channels are expressed in the DRG neurons (Kostyuk et al. 1981; Caffrey et al. 1992; Roy and Narahashi 1992; Elliott and Elliott 1993). These include $Na_V1.1$ and $Na_V1.6$ channels, which are expressed at high levels and are known to support TTX-sensitive (TTX_S) Na^+ currents. In addition, small diameter DRG neurons are unique in expression of three other types of Na^+ channels: $Na_V1.7$, which produces a transient TTX_S Na^+ current with slow repriming kinetics (Cummins et al. 1998); $Na_V1.8$ encodes a TTX_R Na^+ current with slow activation, inactivation and rapid repriming kinetics (Jeftinija 1994; Akopian et al. 1996; Sangameswaran et al. 1996) and $Na_V1.9$ expressing a noninactivating (persistent) TTX_R Na^+ current (Dib-Hajj et al. 1998). $Na_V1.8$ has a high activation threshold, whereas $Na_V1.9$ has hyperpolarized voltage dependence of activation near the resting membrane potential, where it may set threshold for activation (Baker and Bostock 1997). The expression of these various types of Na^+ channels is not limited to the cell body and extends along the fibers (Brock et al. 1998; Strassman and Raymond 1999; Black et al. 2002; Black and Waxman 2002; Rush et al. 2005; Rush et al. 2006), which hints to the importance of these channels in conduction and fiber characteristics.

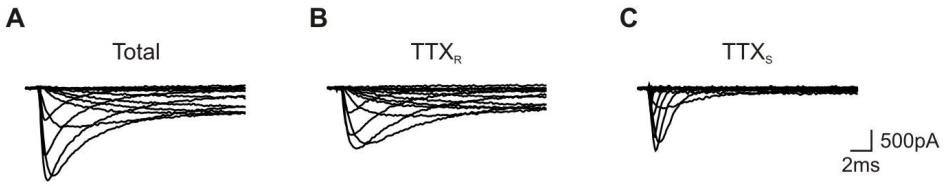

Fig. 4: Na^+ currents in DRG neurons. (A) Total Na^+ current of a DRG neuron. The current can be pharmacologically separated by TTX, allowing the isolation of a TTX_R component (B) and a TTX_S component (C) by subtracting (B) from (A).

Peripheral nerve injury causes a dramatic change in Na^+ channel expression. This was first observed by Waxman et al., who showed that axotomy of the sciatic nerve causes a down-regulation of $Na_V1.8$ and $Na_V1.9$ and an up-regulation of $Na_V1.3$ expression in nociceptive DRG neurons (Waxman et al. 1994; Dib-Hajj et al. 1996; Cummins and Waxman 1997; Dib-Hajj, Tyrrell et al. 1998; Cummins et al. 2000). $Na_V1.3$ is normally only expressed during early stages of development and is undetectable in the adult rat nervous system (Beckh et al. 1989; Waxman, Kocsis et al. 1994; Felts et al. 1997). The up-regulation of $Na_V1.3$ expression is accompanied by the emergence of a rapidly repriming TTX_S current in these cells (Cummins and Waxman 1997). These changes may be the cause of high frequency or spontaneous firing observed after nerve injury. Additionally, loss of persistent currents in DRG neurons after axotomy that participate in setting the resting potential (Stys et al. 1993) could produce a hyperpolarizing shift in resting potential. Again this might increase the amount of TTX-sensitive Na^+ current available for electrogenesis.

Another example demonstrating the plasticity of Na^+ channels is the recording of TTX_S and TTX_R currents in DRG neurons from rats with diabetic neuropathy. The experiment showed increased amplitudes and hyperpolarized conductance voltage and steady state inactivation properties of both currents compared with control DRG

neurons. It has been proposed that changes in the voltage gating properties of the Na^+ currents are related to the phosphorylation of $Na_V1.6$, $Na_V1.7$ and $Na_V1.8$ channel proteins. Changes in current amplitudes are due to an increased expression of $Na_V1.3$ and $Na_V1.7$ and reduced expression of $Na_V1.6$ and $Na_V1.8$ (Hong et al. 2004).

Different injuries can lead to contrasting changes of certain Na^+ channels in the DRG neurons. As mentioned above, $Na_V1.7$ protein and current are both increased in the DRG in a rat model of painful diabetic neuropathy (Hong, Morrow et al. 2004; Chattopadhyay et al. 2008). Interestingly, the amount of $Na_V1.7$ protein is reduced in the DRG neurons after SNI (spared nerve injury) and sciatic nerve axotomy in animals (Kim, Oh et al. 2002; Berta et al. 2008). Another example showing the plasticity of these channels is demonstrated by $Na_V1.8$. The mRNA and protein levels of this subtype are increased following carrageenan injection into the hind paw of rodents, which is paralleled by an increase in TTX_R current (Black et al. 2004; Coggeshall et al. 2004). In contrast to inflammatory pain, peripheral nerve injury is associated with a decrease of $Na_V1.8$ mRNA and protein level as well as loss of TTX_R current in the small diameter neurons of the injured DRG (Cummins and Waxman 1997; Decosterd et al. 2002; Gold et al. 2003; Berta, Poirot et al. 2008).

1.7 Voltage gated Ca^{2+} channels

Voltage gated Ca^{2+} channels are composed of a central transmembrane α1-subunit, which is associated with an $\alpha2\delta$ dimer, an intracellular β-subunit, and a transmembrane γ-subunit (Takahashi et al. 1987). The β-subunit is intracellular and has no transmembrane segments (Ruth et al. 1989). It is attached to the α1-subunit (Pragnell et al. 1994) through the intracellular loop connecting domains I and II. The α2-subunit is a glycoprotein located extracellularly and is attached to the membrane through disulfide linkage to the δ-subunit, that has a single transmembrane region (Gurnett et al. 1996).

Expression of the α1-subunit is sufficient to produce functional Ca^{2+} channels, however with low expression level, abnormal kinetics and voltage dependence (Perez-Reyes et al. 1989). The $\alpha2\delta$ subunit and β-subunit are important for normal gating properties and expression of these channels (Lacerda et al. 1991; Singer et al. 1991).

The transmembrane structure and amino acid sequence of the α1-subunit of Ca^{2+} channels is like that of the voltage-gated Na^+ channels (Tanabe et al. 1987), however with minor differences. The narrow extracellular portion of the pore that is lined by the pore loop contains a pair of glutamate residues in each domain that is required for Ca^{2+} selectivity (Heinemann et al. 1992). The addition of only three glutamate residues in the pore loops of domains II, III, and IV of Na^+ channels are sufficient to confer Ca^{2+} selectivity (Heinemann, Terlau et al. 1992; Sather and McCleskey 2003). The inner exit from the pore, which is lined by the S6 segments, forms the receptor sites for the pore-blocking Ca^{2+} antagonist drugs specific for L-type Ca^{2+} channels (Hockerman et al. 1997).

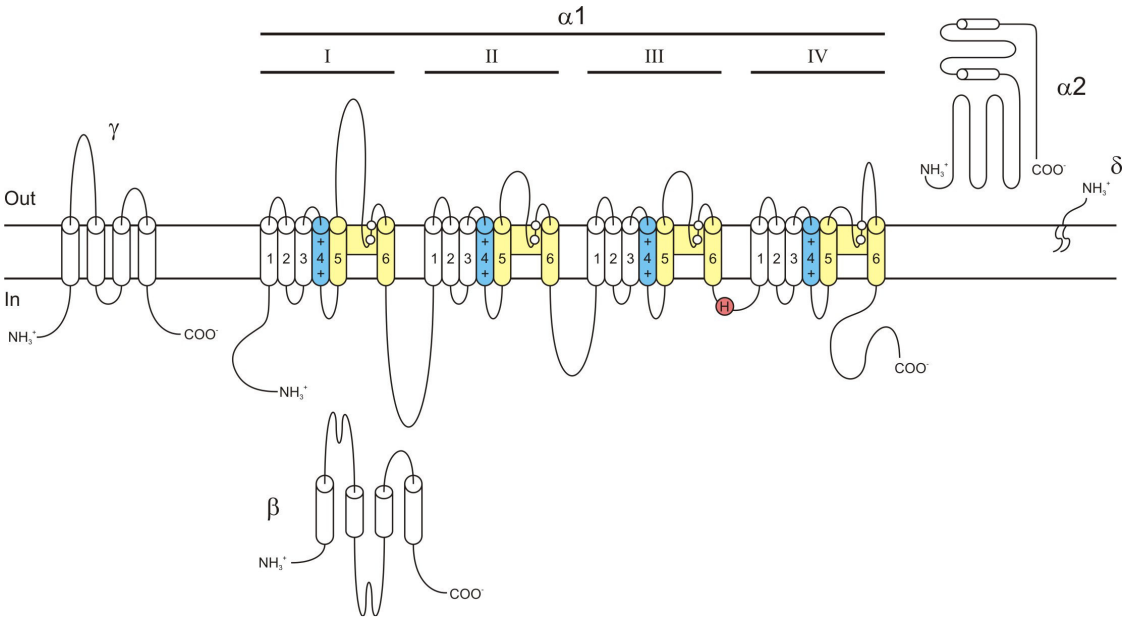

Fig. 5: Voltage-gated Ca^{2+} channel primary structure. The α-subunit is composed of four homologous domains (I-IV). Each domain consists of six transmembrane segments (S1-S6) that are represented as cylinders. The polypeptide chains of each subunit are shown as bold lines. Pore-lining segments are marked in yellow. Amino residues that form the ion selectivity filter are marked in white circles. The S4 voltage sensors are marked in blue and the site involved in forming the inactivation gate is marked in a red circle. The associated α2δ dimer, intracellular β-subunit, and transmembrane γ-subunit are shown. The zigzag line of the δ-subunit represents its glycophosphatidylinositol anchor (modified after Catterall 2011).

There are 10 α1-subunits of voltage gated Ca^{2+} channels, which can be divided into three families: Ca_V1, Ca_V2, and Ca_V3 (Snutch and Reiner 1992; Ertel et al. 2000). Ca_V1 type Ca^{2+} channels mediate L-type Ca^{2+} currents. These currents are called L-type due to their slow voltage dependent inactivation, which makes them long lasting (Tsien et al. 1988). They are inhibited by dihydropyridines, phenylalkylamines and benzothiazepines (Reuter 1979; Tsien, Lipscombe et al. 1988). The Ca_V2 type Ca^{2+} channels form a distinct subfamily. $Ca_V2.1$ subunits (Mori et al. 1991; Starr et al. 1991) give rise to P or Q-type Ca^{2+} currents, which are inhibited by ω-agatoxin IVA. $Ca_V2.2$ subunits mediate the N-type Ca^{2+} currents, which are blocked by ω-conotoxin GVIA (Dubel et al. 1992; Williams et al. 1992). $Ca_V2.3$ subunits form R-type Ca^{2+} channels, which are resistant to the inhibitors of L-type, N-type or P/Q-type Ca^{2+} currents (Soong et al. 1993). Also, this subfamily has intermediate voltage dependence of inactivation, which is more negative and faster than L-type but more positive and slower than T-type (Nowycky et al. 1985). The Ca_V3 Ca^{2+} channels mediate the T-type Ca^{2+} currents (Perez-Reyes et al. 1998). These α1-subunits are not closely related to the other two subfamilies, with 25% amino acid sequence identity. The Ca_V1 and Ca_V2 families form the high voltage activated (HVA) Ca^{2+} channels, while Ca_V3 form the low voltage activated (LVA) or T-type Ca^{2+} channels.

1.8 T-type Ca^{2+} channels and their contribution to neuropathic pain within DRG

Ca_V3 T-type channels are similar in structure to Ca_V1 and Ca_V2, however there is no clear evidence that they interact with the same auxiliary subunits and it is more probable that the $\alpha 1$-subunits function independently.

T-type currents can be differentiated from the HVA currents by their voltage dependence, kinetics, single-channel currents and pharmacology (Bean 1985; Nilius et al. 1985). HVA Ca^{2+} channels have a high voltage of activation, large single channel conductance and slow voltage dependent inactivation (Catterall 2011). In contrast, T-type channels activate at much more negative membrane potentials, and have a fast voltage dependence of inactivation. Hence, they open and inactivate rapidly at potentials near resting membrane potential and also recover rapidly from inactivation. They were named low-voltage activated Ca^{2+} currents for their negative voltage dependence (Carbone and Lux 1984) or T-type Ca^{2+} currents as they are transient (Nowycky, Fox et al. 1985). Near threshold potentials, these currents activate and inactivate relatively slowly, whereas at higher potentials activation and inactivation are faster. This produces a characteristic pattern where successive records cross each other. HVA channels do not produce this criss-crossing pattern because inactivation rates are much slower than activation rates (Randall and Tsien 1997). Furthermore, T-type currents close slowly upon repolarization (deactivate slowly) generating a tail current. They have small, equivalent, single channel conductance of Ba^{2+} and Ca^{2+} and are insensitive to dihydropyridines. These channels also exhibit a window current, as their steady state inactivation occurs over a similar range as activation. Since T-type currents peak at around 30 mV, they can be measured in isolation to test pulses at this potential (Perez-Reyes 2003).

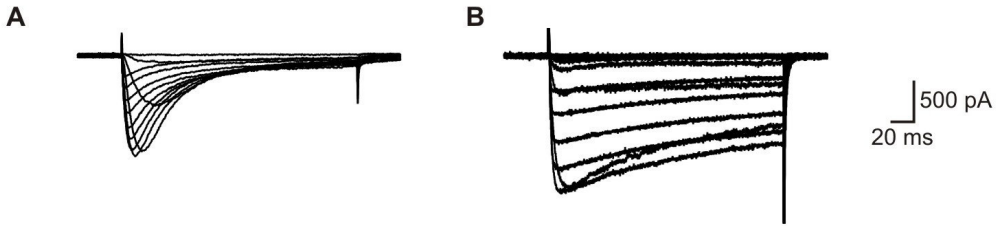

Fig. 6: Ca^{2+} currents in DRG neurons. (A) A family of inward T-type currents measured using a series of step depolarizations of -70 to +40 mV in 10 mV increments. At depolarized potentials T-type currents show faster activation and inactivation kinetics, which forms the typical criss-crossing pattern. (B) HVA-currents were measured using a series of step depolarizations of -70 to +40 mV in 10 mV increments. The currents show a weak inactivation over a 200 ms voltage pulse.

Due to the unique biophysical properties of T-type currents and their ability to function near resting membrane potentials, they have an important role in neuronal excitability that has been shown in different neuronal cell types (Llinas 1988; Huguenard 1996; Perez-Reyes 2003). The entry of Ca^{2+} leads to membrane depolarization, which in turn activates other voltage gated ion channels as Na^+ channels and thus can initiate action potential bursts. A previous study on medium sized DRG neurons showed that these

cells, when held at hyperpolarized potentials (-75 or -66 mV), elicit action potentials with an ADP (afterdepolarizing potentials) that were in conjunction with burst firing. In the same study, T-type currents were found to underlie the generation of ADPs (White et al. 1989).

T-type currents are present in small and medium-sized DRG neurons. In small DRG neurons, the expression of T-type currents is usually of moderate density. A subtype of small DRG neurons called the "T-rich" cells have a high density of T-type current and almost totally lack any HVA-type Ca^{2+} currents (Todorovic and Jevtovic-Todorovic 2007). On the other hand, some of the medium sized neurons express robust (referred to as "gigantic" by Scroggs and Fox) T-type currents. The neurons in this size range belong to Aδ high-and low-threshold mechanoreceptors (Shin et al. 2003; Dubreuil et al. 2004; Fang et al. 2005).

There are at least three subtypes of the pore-forming α1-subunit of T-channels, α1G ($Ca_V3.1$) (Perez-Reyes, Cribbs et al. 1998), α1H ($Ca_V3.2$) (Cribbs et al. 1998) and α1I ($Ca_V3.3$) (Lee et al. 1999). The inactivation and deactivation properties are different in these related channels (Perez-Reyes 2003). $Ca_V3.1$ and 3.2 display fast inactivation, while $Ca_V3.3$ displays slow inactivation. The time course of recovery from inactivation is also different between the three isoforms, where $Ca_V3.1$ channels recover the fastest (Perez-Reyes 2003). The T-type Ca^{2+} channel family can also be pharmacologically distinguished. $Ca_V3.2$ Ca^{2+} channels are sensitive to divalent cations such as nickel (Ni^{2+}, IC_{50} 10 μM) and low micromolar concentrations of zinc (Zn^{2+}) and copper (Cu^{2+}). $Ca_V3.1$ and $Ca_V3.3$, on the other hand, are 20-fold less sensitive (Lee et al. 1999). HVA channels are even less sensitive to Ni^{2+}, except for $Ca_V2.3$ that resembles T-type channels in their sensitivity to Ni^{2+} (IC_{50} 27 μm). However, these channels, unlike T-type channels, require stronger depolarization for channel opening (Zamponi et al. 1996).

In small and medium-sized peripheral sensory neurons, $Ca_V3.2$ is the most abundant isoform of T-type channels, while $Ca_V3.1$ and $Ca_V3.3$ isoforms are much less frequently expressed in these neurons (Talley et al. 1999).

Recent studies have suggested a role of T-type channels in neuropathic pain as several pharmacological blockers and modulators of T-type channels have been shown to alleviate neuropathic pain in vivo. For example (+)-ECN, a T-type channel blocker, has been reported to reverse thermal hyperalgesia in rats with CCI (chronic constriction injury) when injected in peripheral receptive fields of sensory neurons (Pathirathna et al. 2005). Mibefradil and ethosuximide effectively reversed hyperalgesia and allodynia in rats with CCI (Dogrul et al. 2003). However, these compounds do not selectively block T-Type channels, as they affect other voltage gated channels that influence the excitability of nociceptors, as HVA Ca^{2+} channels and voltage gated Na^+ and K^+ channels (Coulter et al. 1989; Jimenez et al. 2000; McNulty and Hanck 2004; Coste et al. 2007). Nevertheless, T-type currents were significantly diminished after application of the oxidizing agent DTNB, which in vivo diminished thermal and mechanical nociception (Todorovic et al. 2004). In a model of streptozotocin-induced diabetic neuropathy, Jagodic et al. found that in parallel with development of diabetic induced pain, T-type current was significantly increased in

medium size DRG cells. This was associated with more frequent ADPs as well as lower threshold of burst firing in these cells (Jagodic et al. 2007). The T-type currents in this study were blocked by Ni^{2+} and enhanced by L-cysteine, suggesting $Ca_V3.2$ isoform as responsible for the up-regulation. Other studies have also demonstrated the role of $Ca_V3.2$ in contributing to neuropathic pain. Bourinet and colleagues showed that intrathecal administration of $Ca_V3.2$ antisense knock-down in DRG cells induced a large reduction of T-type currents, and reversed both thermal and mechanical hyperalgesia in rats with CCI (Bourinet et al. 2005). Moreover, the selective knock-down of DRG $Ca_V3.2$ currents in vivo has effectively reversed mechanical and thermal hyperalgesia in STZ-induced diabetic neuropathy in rats (Messinger et al. 2009). It is however the case, that antisense oligonucleotide knock-down studies might be non specific due to possible off-target effects.

In contrast to these results, Hogan and colleagues (Hogan et al. 2000; McCallum et al. 2003) reported the loss of T-type currents in sensory neurons of rats with neuropathic pain. Additionally, an in-vivo study using $Ca_V3.2$ knock-out mice did not find a difference in thermal and mechanical hyperalgesia in CCI- and control mice (Choi et al. 2007). Other studies support a role of $Ca_V3.1$, where activation of thalamic $Ca_V3.1$ channels may suppress visceral pain transmission. On the other hand, comparing the pain susceptibility of mice lacking $Ca_V3.1$ with that of their wild type littermates, revealed attenuation of neuropathic pain in the knock-out mice (Na et al. 2008).

1.9 Animal models of neuropathic pain

Different animal models of human diseases with neuropathic pain have been developed. These include rodent models of mechanical nerve trauma as chronic constriction injury (CCI: sciatic nerve is subjected to loose ligations), spinal nerve ligation (SNL: L_5 or L_6 spinal nerves are ligated), partial sciatic nerve ligation (PNL: 1/3 to 1/2 of the sciatic nerve is tightly ligated) as well as spared nerve injury (SNI: peroneal and tibial branches of the sciatic nerve are tightly ligated). Furthermore, there are animal models of painful diabetic polyneuropathy (streptozotocin induced diabetic polyneuropathy), polyneuropathy due to chemotherapy (vincristine or paclitaxel induced painful peripheral polyneuropathy) and the acute autoimmune disease Guillain–Barré syndrome (the animal model is called experimental automimmune neuritis).

1.9.1 Experimental autoimmune neuritis

Guillain–Barré syndrome (GBS) is a human acute inflammatory demyelinating neuropathy, which is caused by an autoimmune attack of the peripheral nervous system, and is characterized by motor symptoms such as weakness or paralysis, as well as sensory disturbances (Hughes et al. 1999). There are several subtypes of GBS depending on the primary target of the autoimmune reaction. This includes the acute inflammatory demyelinating polyradiculoneuropathy (AIDP), which is the most common subtype, and the less frequent acute motor and sensory axonal neuropathy (AMSAN) and acute motor axonal neuropathy (AMAN) (Hughes, Hadden et al. 1999; Winer 2001; Hughes and Cornblath 2005). The incidence of GBS is not frequent, between 1–2 cases per 100,000 people annually, but it is the most common cause of

acute non-trauma-related paralysis (Hughes and Cornblath, 2005). GBS involves both cellular and humoral immunity (Ho et al. 1998). It can be triggered by minor infectious disease, where T-lymphocytes become activated, which in turn stimulates B cells to produce autoantibodies. The latter block nerve conduction (Takigawa et al. 2000; Weber et al. 2000), activate complement (Stoll et al. 1991; Sawant-Mane et al. 1996) and facilitate a macrophage attack in the peripheral nerve (Meyer zu Horste et al. 2008). These macrophages, which act as antigen-presenting cells, lead to direct damage of myelinating Schwann cells and axons (Kiefer et al. 2001). The trigger of the cascade of autoimmune response targeting the PNS can be explained by the "molecular mimicry". Surface lipooligosaccaharide structures found on Campylobacter and other microbial species mimic peripheral nervous system (PNS) gangliosides, which have been identified as antigens in GBS (Yuki et al. 2004; Rinaldi and Willison 2008). Hence, a minor infection can cause the T-lymphocytes to become activated due to encountering of the microbial epitopes, and starts a cascade of autoimmune responses leading to the demyelination of the nerve roots and peripheral nerves.

Pain is a common symptom of GBS occurring in 55-85 % of the cases (Ruts et al. 2010). The symptoms include paraesthesia/dysesthesia, backache, neck, muscle, joint or visceral pain and other discomforts (Pentland and Donald 1994; Moulin et al. 1997). The patients with GBS describe the pain as distressing, horrible and require aggressive treatment (Moulin, Hagen et al. 1997). Several studies showed that in GBS patients with acute neuropathic pain, not only large myelinated fibers are affected but also small myelinated and unmyelinated fibers are impaired, which may account for the acute pain symptoms and its maintenance over time (Martinez et al. 2010). However, the exact mechanism of this ongoing pain is still unclear and the current pharmacotherapy are insufficient and are associated with considerable side effect.

Experimental autoimmune neuritis (EAN) is a T-cell mediated acute demyelinating inflammatory disease of the peripheral nervous system, which serves as an animal model of AIDP (Hahn 1996). EAN was first described by Waksmann and Adams in 1955, and can be induced in rats, mice, rabbits and guinea pigs by immunization with peripheral nerve myelin, purified peripheral myelin proteins P0, P2 or PMP-22, or synthetic immunogenic peptides of these proteins (Waksman and Adams 1955; Brostoff et al. 1972; Kadlubowski and Hughes 1979; Milner et al. 1987; Shin et al. 1989; Gabriel et al. 1998). This immunization results in a reproducible disease with clinical and pathological features similar to AIDP (Meyer zu Horste et al. 2007). The pathogenesis of EAN comprises activation of T-cells, which cross the blood-nerve barrier, encounter their similar antigen in the endoneurium, and release mediators that open the blood-nerve barrier. This allows entry of antibodies and macrophages, which get activated by T-cells, invade the myelin sheaths and induce demyelination (Hughes and Cornblath 2005). Two weeks after immunization, animals usually develop weakness and ataxia. The close similarities between EAN and AIDP make EAN a potential model for studies of the mechanisms underlying pain in GBS.

1.9.2 Partial sciatic nerve ligation

Partial sciatic nerve ligation (PNL) is one of the most commonly used models of neuropathic pain, and it simulates the clinical condition of a nerve bruise. In this

model, a tight ligation is created around 33-50 % of the sciatic nerve, leaving the rest of the nerve "uninjured" (Seltzer et al. 1990). An immune response to the ligation leads to nerve swelling and constriction. This is associated with the development of spontaneous pain-like behavior, allodynia and hyperalgesia.

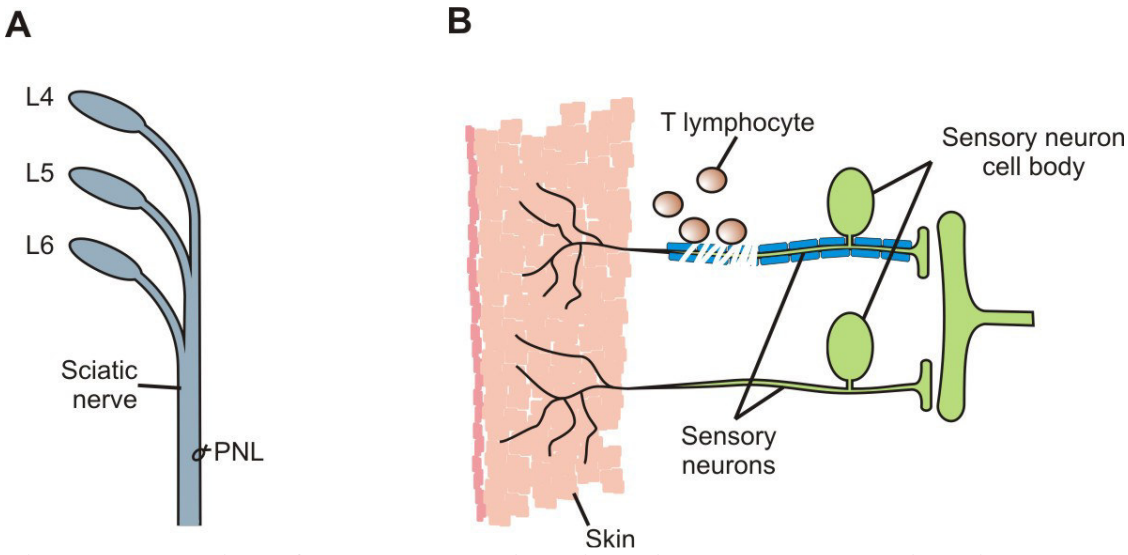

Fig. 7: Illustration of the neuropathic pain animal models used in this doctoral thesis. (A) PNL (partial sciatic nerve ligation): 1/3 to 1/2 of the sciatic nerve is ligated using a medical thread. (B) EAN (Experimental autoimmune neuritis): induced by injection of P2 peptide that leads to an autoimmune response and demyelination of peripheral nerves (modified after Calvo et al. 2012).

1.10 Aims of the thesis

Neuropathic pain is a pathological condition characterized by abnormal pain and is a consequence of the disruption of the somatosensory system by lesions of different etiologies. The pathogenesis of the severe pain is still not fully understood and for some diseases as Guillain–Barré syndrome quite unexplored. Current pharmacotherapies are only partially effective and are associated with considerable side effects. For the development of new specific and effective drugs, a detailed study of the pathomechanism underlying neuropathic pain in each particular disease is required. For this, the first goal of this study was to establish a rat model of Guillain–Barré syndrome (EAN) in our laboratory, and to verify the development of pain (mechanical allodynia) in these animals, as in case of the human GBS. The second purpose of the study was to analyze the nociceptive DRG neurons for changes in their electrophysiological properties that might be correlated to chronic neuropathic pain.

The occurrence of changes in T-type Ca^{2+} currents upon nerve injury has been controversial. Where some studies showed an up-regulation of T-type Ca^{2+} currents in nociceptive DRG neurons (Jagodic, Pathirathna et al. 2007; Jagodic et al. 2008), others reported their loss following nerve injury (Hogan, McCallum et al. 2000; McCallum et al. 2006). Also, the role of $Ca_V3.2$, the most abundant isoform of T-channels, in supporting the pain phenotype is not yet clear. Hence, the purpose of the second part of the study was to clarify the contribution of T-type currents of DRG neurons, especially $Ca_V3.2$, to the pathophysiology of neuropathic pain. Here, a mouse model of partial nerve ligation-induced neuropathic pain was used. Also, $Ca_V3.2$ knock-out mice and wild type littermates were utilized to assess the functional role of this subunit.

2 Materials and methods

2.1 Experimental animal models

All experimental procedures followed the guidelines of the German Animal Protection Law and were approved by local authorities (Landesamt für Natur, Umwelt und Verbraucherschutz NRW; AZ: 8.87-51.04.20.09.353).

Animal husbandry and all behavioral experiments took place in the S1 (Sicherheitsstufe 1, §§ 4-7 GenTSV) animal facility of the university clinics in Bonn („Haus für experimentelle Therapy", HET).

2.1.1 Experimental autoimmune neuritis (EAN)

2.1.1.1 Animals

Experiments were carried out using male Lewis rats 6-7 weeks old. Lewis rats were chosen since they can develop EAN constantly (Hoffman et al. 1980). The animals were purchased from Charles River Laboratories (Sulzfeld, Germany). Maximum four rats were housed in plastic cages under controlled illumination (light-dark cycle: 12:12 h) and environmental conditions (temperature: 22 ± 2 °C; humidity: 55 ± 5 %). Water and food pellets were freely available for all rats. Animals were housed in the cages for at least one week before the start of the experiments.

2.1.1.2 Induction of EAN

Three experimental groups were used: EAN, CFA and ICFA. Each group received a subcutaneous injection of both hind paws with a 100 µl of inoculum containing the following:

- EAN: immunogenic bovine P2 peptide of peripheral myelin and complete Freund's adjuvant (CFA).
- CFA: bovine serum albumin (BSA) and CFA
- ICFA: phosphate buffered saline (1XPBS) and incomplete Freund's adjuvant (ICFA).

For the EAN group, P2 antigen (neuritogeneic P2 peptide amino acids 53-78 synthesized by Charité, Institute for Medicinal Immunology, Germany) was dissolved in 1XPBS to a concentration of 2 mg/ml and emulsified with an equal volume of CFA (Sigma, Germany). CFA contains 1 mg/ml inactivated *Mycobacterium tuberculosis* in mineral oil and was used to enhance the immune response at the site of injection. As it can cause inflammatory pain at higher concentrations two control groups (CFA and ICFA) were used to ensure that the pain phenotype in rats is a consequence of EAN and not due to CFA or the injection. For the CFA and ICFA control groups, an emulsion containing equal volumes of BSA dissolved in 1XPBS (2 mg/ml) and CFA or 1XPBS and ICFA (mineral oil lacking the *Mycobacterium tuberculosis*) (Sigma, Germany) was used. All injections were carried out under isoflurane anesthesia (3% in 95% O_2).

2.1.1.3 Animal monitoring (EAN evaluation)

All animals were scored for clinical sings of EAN. Both clinical scores and body weight were assessed one day before immunization and on day 1, 3, 6, 8, 10, 13, 15, 17, 21, 24, 28 and 31 after immunization (on the same days as the behavioral experiments). Severity of the disease was graded as follows: 0 = no illness; 1 = hanging tail tip; 2 = tail paralysis; 3 = inability to sit up; 4 = movement ataxia; 5 = slight hind leg paresis; 6 = modest hind leg paresis; 7 = strong hind leg paresis; 8 = complete paralysis; 9 = moribund and 10 = death.

2.1.2 Partial sciatic nerve ligation

2.1.2.1 Animals

$Ca_V3.2$ knock-out (KO) mice and wild type (wt) littermates on a C57BL/6N background were used (Chen et al. 2003). Mice were taken from breeding colonies of our own animal facility and the genotype of the animals was determined by PCR (polymerase chain reaction). Due to problems with mouse supply wt mice were purchased in addition from Charles River Laboratories for experiments with only wt mice (action potential measurements and RT-PCR). 12 to 20 weeks old female mice were used for all experiments. The animals were housed in groups of six mice per cage under controlled illumination (light-dark cycle: 12:12 h) and environmental conditions (temperature: 22 ± 2 °C; humidity: 55 ± 5 %). All mice had free access to water and food pellets. Animals were housed in the cages for at least one week before the start of the experiments

2.1.2.2 Partial sciatic nerve ligation

The partial nerve ligation (PNL) model was first described in mice by Malmberg and Basbaum (Malmberg and Basbaum 1998), and has been shown to be a good model to investigate neuropathic pain. In our experiments, the right sciatic nerve was subjected to a partial ligation to induce neuropathic pain. For this, mice were initially anesthetized in a box with an oxygen/isoflurane mixture (2 – 2.5 % in 95 % O_2). Then, they were fixed on the surgery table while keeping the stream of isoflurane (1,5 – 2 % in 95 % O_2) to maintain anesthesia. The right hind leg was shaved, disinfected with betaisodona (Mundipharma GmbH), and a small incision to the skin was done using a scalpel. Using sharp scissors, the underlying muscle was punctured and the sciatic nerve was found with thin tweezers. Using a medical polypropylene thread (9-0), one half to one third of the nerve was tightly ligated. Afterward, muscle and skin were sutured with polypropylene threads (7-0; 5-0) and the lesion site was disinfected. Sham operation was performed in parallel in the control group mice by exposing the right sciatic nerve then closing the wound without ligation.

2.2 Pain behavioral experiments

2.2.1 Von Frey test

Animals developing neuropathic pain show an increased sensitivity towards normally non noxious mechanical stimuli (Costigan et al. 2009). This mechanical allodynia was assessed with a dynamic plantar aesthesiometer (Ugo Basile Biological Research

Apparatus; for mice: maximum force: 15 g, ramp: 20 s; for rats maximum force: 50 g, ramp: 50 s). It consists of an electronically controlled mobile pressure actuator that can apply a continuously increasing pressure with a metal filament (Von Frey filament) on the paw. The experiments were performed for both animal models.

The behavioral experiments were performed in elevated transparent plexiglass chambers (9 x 9 x 13 cm) with a metal grid floor. In the middle of the plantar surface of the hind paw, the metal filament of the actuator (diameter: 0,5 mm) was applied with increasing force until a clear withdrawal response of the paw was triggered. Paw withdrawal thresholds (PWT) were automatically recorded and given as the withdrawal triggering force in grams. PWTs were calculated as the average of three consecutive tests with at least 3 min between each test to avoid habituation. Animals were not tested while being very active or sleeping. Testing chambers were cleaned with a 70 % ethanol solution between rats or mice.

The animals were habituated to the experimental setup for $\geq$ 1h during three consecutive days before the start of the experiments. After habituation, baseline behavioral measurements were conducted. One day later EAN or PNL was induced to the animals. To assess the development of pain, rats were regularly tested in the behavioral tests on day 1, 3, 6, 8, 10, 13, 15, 17, 21, 24, 28 and 31 after the induction of EAN. For mice, the Von Frey tests were conducted one week after the partial nerve ligation to assess the pain phenotype. Rats and mice were habituated to the chamber for at least 30 min on each day before behavioral tests were performed.

2.3 Tissue preparation

2.3.1 Preparation of single DRG neurons for electrophysiological experiments

Animals were anaesthetized with isoflurane (Abott) and rapidly decapitated. With the help of a forceps, dorsal root ganglia (DRG) from lumbar levels (4-5) were collected in 2 ml Neurobasal Medium A containing B27 supplement (Gibco, Invitrogen, Germany), 100 µg/ ml penicillin and 100 µg/ml streptomycin (Sigma, Germany). L_4- and L_5-DRGs were chosen as they contain cell bodies of sensory neurons innervating the peripheral receptive fields of the hindpaws, and hence contain almost exclusively cell bodies of the sciatic nerve. For the PNL model, DRGs of the operated side were dissected, whereas for the EAN model, DRG of both sides were chosen. First, the dissected neurons were enzymatically digested by adding 0.125% crude collagenase general use type I (Sigma, Germany) in an incubation chamber enriched with carbogen at 37°C for 1.5 h. After centrifugation at 400 rpm for 4 min at room temperature, pellets were resuspended in Neurobasal medium. At room temperature, single neuronal somas were then obtained by a series of triturations. Finally, neurons were plated on 35 mm diameter culture dishes that were coated with poly-$_L$-lysine (Sigma), and stored at 37°C in a humified 5% CO_2 atmosphere. These dishes also served as recoding chamber.

The electrophysiological experiments were performed starting from day 21 till day 30 after EAN induction. For the PNL model the electrophysiological experiments were conducted a week after the operation for two consecutive weeks. Previous studies have

shown that mechanical allodynia persisted for a duration of 70 days following partial ligation of the sciatic nerve (Malmberg and Basbaum 1998).

2.3.2 Preparation of DRG neurons for quantitative real time RT-PCR (PNL-model)

Mice were sacrificed under anesthesia with isoflurane. Dorsal root ganglia (DRG) from lumbar levels (4-5) of the operated side were selected and quickly frozen in liquid nitrogen. The samples were subsequently stored at -80°C.

2.3.3 Preparation of sciatic nerves for histological analysis (EAN-model)

Rats were anaesthetized with isoflurane and rapidly decapitated. Sciatic nerves of both sides were collected in 4% GLA (glutaraldehyde, Serva) in 0.1 M HEPES buffer for fixation. 24 h later the GLA was washed out with 2% sodium azide solution (NaN_3, Merck) and stored at 4 °C until histological analysis started.

2.4 Classification of DRG neurons

Due to the heterogenicity of the DRG neurons (some are heat sensitive, mechano sensitive or polymodal) they were sub-classified on the basis of several criteria. These included cell body size, binding to the plant lectin isolectin B_4 (isolated from the plant Griffonia simplicifolia) (IB_4, life technologies) and the responsiveness to the algogenic compound capsaicin (cap, Sigma-Aldrich).

Neurons were divided into small (<25 µm for mice, <30 µm for rats), medium (30 to 40 µm), and large (>40 µm) based on cell body diameter. Small diameter DRG neurons arise from C- and A-δ fibers that constitute most of nociceptors, whereas DRG neurons with larger cell body diameters are non-nociceptive (Harper and Lawson 1985 b). For this reason we used small DRGs with a cell body diameter <25 µm for mice and < 30 µm for rats for the electrophysiological experiments. The cell body diameter was measured with a calibrated eyepiece reticule.

According to the IB_4-binding ability, unmyelinated C fibers can also be classified in two broad classes. IB_4-negative (IB_4^-) nociceptors represent the peptidergic population. They contain the peptide neurotransmitter substance P as well as the high-affinity tyrosine kinase receptor (TrKA) for nerve growth factor (NGF). IB_4-binding neurons, on the other hand, do not express substance P or TrKA, but express Ret receptors that bind glial cell derived neurotrophic factor (GDNF). L_{4-5} DRG neurons were incubated for 10 min with 2 ml of the external solution containing 12 µg IB_4 conjugated to a fluorescent dye (Alexa Fluor 488). The cells were then visualized using a fluorescent microscope, where only cells showing strong immunofluorescence along the plasma membrane were considered IB_4-positive (IB_4^+) (Fig. 13). IB_4 was stored as stock solution (6 µg/ml) in the external solution.

Furthermore, a subset of small diameter nociceptive DRG neurons express the TRPV1 receptor (transient receptor potential cation channel subfamily V member 1), a polymodal nonselective cation channel that can be directly activated by harmful heat, vanilloid compounds and extracellular protons Hence, this subset of neurons are responsible for processing thermal noxious stimuli. In our experiments, the vanilloid TRPV1 agonist capsaicin was applied to classify small diameter DRG neurons into

capsaicin responsive (cap^+) and unresponsive (cap^-). In case application of 1 µM capsaicin gave rise to a nonselective inward current, these cells were considered as cap^+ (Fig. 13). Capsaicin was applied at the end of the electrophysiological experiment in the voltage clamp mode with a holding potential of -56 mV (not LJP corrected) and was stored as 20 mM stock solution in ethanol and freshly diluted in the external buffer before the recordings.

2.5 Electrophysiology

2.5.1 Shared procedures

A P-97 Flaming/Brown micropipette puller (Sutter Instrument company) was used to pull patch pipettes with a resistance of 3-5 MΩ from borosilicate glass capillaries (outer diameter: 1.5 mm, inner diameter: 0.86 mm; Science products, Germany). The glass pipettes were filled with the intracellular solution. Voltage clamp and current clamp recordings were conducted at room temperature. Voltage and current commands and digitization of membrane voltages and currents were controlled using a Digidata 1322A interface with Clampex 8.2 of the pClamp software package (Molecular Devices), running on a personal computer.

All voltage clamp and current clamp recordings were performed on small sized nociceptive DRG neurons within a maximum of 8 hours after preparation. The culture dishes containing the single neuronal cells were washed several times with the external buffer to wash out the Neurobasal medium. One cell per culture dish was analyzed.

2.5.2 Voltage clamp recordings

Whole-cell recordings were obtained with a seal resistance >1 GΩ in all recordings using Axopatch 200B amplifier (Axon Instruments, Molecular Devices; Ismaning, Germany). Cells with high leakage currents (holding current ≥ 500 pA) and series resistance greater than 12 MΩ were not considered for analysis. Capacitive transients were cancelled before each recording. To improve voltage control, the prediction and compensation circuit was set between 60 and 90 %. Voltage errors were not larger than 3.8 mV or 1.5 mV for Na^+ and Ca^{2+} current measurements respectively. All potentials shown were corrected for liquid junction potentials that were calculated using Clampex 8.2 software. The experiments were performed at room temperature.

Unless otherwise indicated, all chemicals and drugs were obtained from Sigma, Germany.

2.5.3 Determination of passive membrane properties

Passive membrane properties were measured in the voltage clamp mode by analyzing the current response to a 10 mV depolarizing voltage step for 135 ms from a -80 mV holding potential. The current response is made up of a transient RC response formed by the cell capacitance C_m in series with pipette and access resistance (which make up the series resistance R_{series}), and an ohmic or steady state component determined by membrane resistance R_m (Fig. 8). R_m is calculated as $V/\Delta I$, where V is the size of the voltage step and ΔI is the steady state current response. Cell capacitance was determined by quantifying the charge Q required to fully charge the membrane. Q (Q1+Q2) was measured as the total area under the transient current response to the

above mentioned voltage step, where the area of Q1 was quantified manually using Clampfit 9.2 software and Q2 was calculated as $\Delta I * \tau_{fast}$. τ_{fast} is the fast time constant of the transient RC response and was measured via a logarithmic bi-exponential fit on the transient . Cell capacitance C_m was then calculated as Q/V. Series resistance R_{series} was calculated as τ_{fast}/C_m.

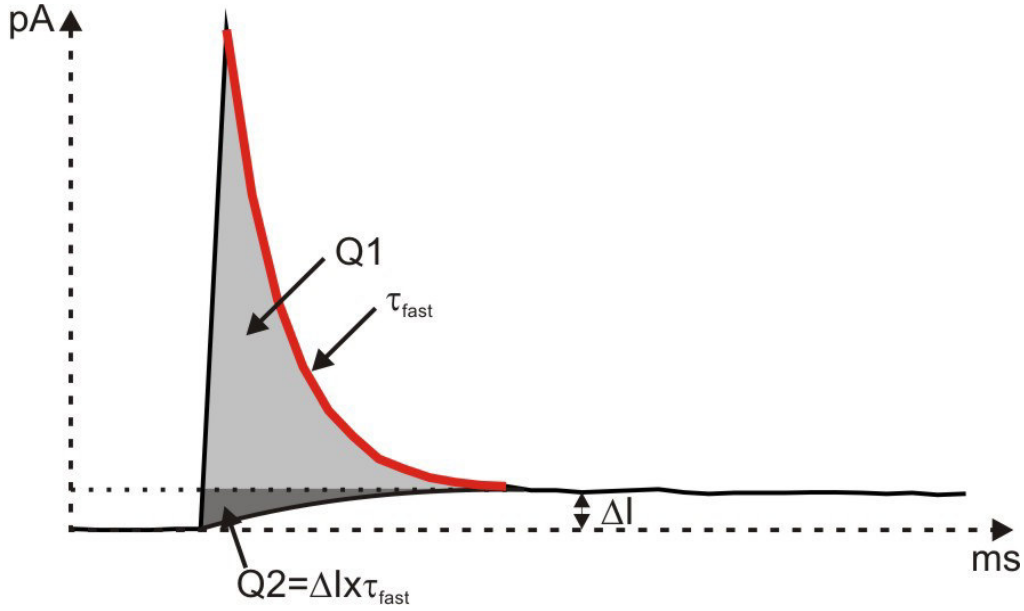

Fig. 8: Calculation of passive membrane properties of DRG neurons. Parameters of the current response to a 10 mV depolarizing voltage step used for calculation of passive membrane properties of DRG neurons. ΔI is the steady state current response, Q (Q1+Q2) is the total area under the transient current response and τ_{fast} is the fast time constant of the transient RC response.

2.5.4 Recording of Na^+ currents

Transient and persistent Na^+ currents were isolated from single DRG neurons using the following solutions: bathing solution (in mM): 25 NaMS (Na methanesulfonate), 110 TEA-Cl (tetraethylammonium-chloride) (Merck), 10 HEPES ((4-(2-hydroxyethyl)-1-piperazineethanesulfonic acid), 2 $CaCl_2$, 3 $MgCl_2$, 0.1 $CdCl_2$ (Fluka), 5 4-AP (4-aminopyridine, ACROS organics), 25 glucose. Osmolarity was adjusted with sucrose to 305 mOsmol/L; pH to 7.4 with NaOH. $CdCl_2$ and 4-aminopyridine were used to block Ca^{2+} and A-type K^+ currents respectively. The intracellular solution contained (in mM): 110 CsF, 10 HEPES-Na, 11 EGTA (ethylene glycol tetraacetic acid), 2 $MgCl_2$, 2 ATP-Na_2. Osmolarity was adjusted with sucrose to 290 mOsmol/L; pH to 7.25 with CsOH. Leakage currents were digitally subtracted using a P/4 protocol. Data were filtered at 10 KHz, and sampled at 10 KHz. The liquid junction potential between intra- and extracellular solution was +13 mV and all values were corrected accordingly.

Cells were held at a membrane potential (V_{hold}) of -120 mV, and Na^+ currents were generated by depolarizing steps for 470 ms to test potentials ranging from -100 to +20 mV in 10 mV increments. Due to the continuous run-up of the transient Na^+ current and a run-down of the persistent Na^+ current in the beginning of the experiment, the

measurement was repeated at an interval of 2 min until the transient current was stable for two successive recordings. Subsequently, 1 µM TTX (Tetrodotoxin) was added to the perfusion, thus allowing the analysis of the TTX-resistant (TTX_R) current. The TTX-sensitive (TTX_S) current was determined by subtraction of TTX_R current waveform from the total current waveform at each test potential. TTX was stored as stock solutions in H_2O, diluted in the bathing solution and delivered using a multichannel, gravity-driven system. To confirm that Na^+ was the major charge carrier in our measurements, the cells were finally perfused with the external solution containing a Na^+ concentration of 3 mM. At this concentration, the reversal potential of Na^+ current is at -35 mV. Indeed, an outward transient Na^+ current was observed by depolarizing test potentials from -30 to +20 mV.

2.5.5 Analysis of voltage clamp Na^+ current recordings

The recorded Na^+ current show two phases in the response with different voltage dependencies and kinetics. This is due to the existence of transient (I_{NaT}) and persistent (I_{NaP}) Na^+ currents. For the current voltage curves, the peak amplitudes of both I_{NaT} and I_{NaP} were measured, where the peak of I_{NaT} was measured at the beginning and the peak of I_{NaP} was analyzed at the end of the depolarizing pulse. Since I_{NaT} and I_{NaP} peak at around -20 mV and -60 mV respectively, the peak transient and persistent Na^+ current was measured at these test potentials.

For the fast Na^+ currents, the steady state voltage dependent activation behavior was analyzed. For this, the peak current amplitudes were converted to Na^+ conductance G_{Na} by means of the following equation:

equation 1 $G_{Na}=I_{Na}/(V-V_{Na})$

where I_{Na} is the peak current amplitude at a given potential (V) and V_{Na} the Na^+ reversal potential, which was found by linear regression of all Na^+ current values at -10 to +10 mV. Conductances were then normalized, averaged and fitted to the following Boltzmann function:

equation 2 $y=((A_1-A_2/1+e^{(V1/2-V)/dx}))+A_2$

where A_1 is the maximum current, A_2 the minimum current, $V_{1/2}$ the voltage of half maximal activation and dx the slope factor.

After activation, the inward transient Na^+ current quickly shuts down even though the potential remains the same. The time course of I_{NaT} decay was evaluated via a double-exponential fit using the following equation:

equation 3 $f(t)= \Sigma A_i e^{-t/\tau i}+C$

where A_i is peak amplitude of current component i, τ is the decay time constant and C amplitude of steady state component (sustained current after full inactivation). The decay time constant τ was evaluated at membrane potential (V_m) = -30 mV, where τ of the fast inactivating current component was analyzed and compared between the groups.

The voltage dependence of steady state inactivation was determined using standard procedure with prepulses of 470 ms duration to voltages ranging from -100 to +20 mV, followed by a 30 ms test pulse to -10 mV. For analysis of the steady state voltage

dependent inactivation of fast Na^+ currents, currents were normalized to the maximum and averaged. Data points were then fitted using *equation 2*.

2.5.6 Recording of the Ca^{2+} current

In these experiments, the capsaicin evoked current response was determined at the beginning of the experiment, as the external solutions for Ca^{2+} current isolation does not allow measurement of the inward current through the TRPV1 receptor. For this, the cap current response was elicited in the following external solution (in mM): 150 NaCl, 5 KCl, 1 $CaCl_2$, 1 $MgCl_2$ and 10 HEPES. The cells were subsequently perfused with the external solution for Ca^{2+} current isolation. The solution contained the following (in mM): 152 TEA-Cl, 10 $BaCl_2$ and 10 HEPES. Osmolarity of the solution was 305 mOsmol/L and did not need further adjustment, whereas the pH was adjusted to 7.4 with TEA-OH (tetraethylammoniumhydroxide). The intracellular solution contained the following (in mM): 135 TEA-OH, 10 EGTA, 40 HEPES and 2 $MgCl_2$. The osmolarity of the solution was 295 mOsmol/L and pH was adjusted to 7.2 using HF. A fluoride (F^-)-based internal solution facilitates run-down of high-voltage activated (HVA) Ca^{2+} current, thus minimizing contamination of T-type Ca^{2+} currents with HVA components. Leakage currents were digitally subtracted using a P/6 or P/8 protocol. Data were filtered at 10 KHz, and sampled at 20 KHz. The liquid junction potential between intra- and extracellular solution was +7 mV and membrane potentials were corrected accordingly.

L_{4-5} DRG neurons were held at -100 mV and total Ca^{2+} current was elicited by a standard voltage clamp protocol, where 200 ms depolarizing voltage steps ranging from -70 to +40 mV in 10 mV increments were applied. Different DRG neurons exhibited various types of Ca^{2+} currents. To isolate the T-type current we used another protocol that involves the application of a series of preconditioning pulses (500 ms duration to voltages ranging from -120 to +30 mV) then measuring the resulting peak amplitude at the second pulse at -30. Subsequently, the cells were perfused with external solution containing 50 µM Ni^{2+}, and the Ni^{2+} resistant Ca^{2+} current was measured via the standard voltage clamp protocol mentioned above. The Ni^{2+} sensitive current component was isolated by digitally subtracting the Ni^{2+} resistant current from the total Ca^{2+}current. 50 µM Ni^{2+} was used to allow the differentiation between the Ni^{2+} sensitive $Ca_V3.2$ (IC_{50} 10 µM) and the 20-fold less Ni^{2+} sensitive $Ca_V3.2$ and 3.3 (Lee, Gomora et al. 1999). To verify recording of Ca^{2+} currents, the cells were perfused at the end of the experiment with external solution containing 50 µM Ni^{2+} and 200 µM Cd^{2+}, which blocks all VGCC. Drugs were prepared as 100 mM stock solution of $NiCl_2$ and $CdCl_2$ in H_2O and freshly diluted to appropriate concentrations at the time of the experiment in the bathing solution and delivered using a multichannel, gravity-driven system. Manually controlled valves were used to switch between the solutions.

2.5.7 Analysis of voltage clamp Ca^{2+} current

Using the standard voltage clamp protocol, different types of Ca^{2+} current were evoked. The T-type current was analyzed by subtracting the peak current response from the current at the end of the depolarizing test potential to avoid contamination with HVA Ca^{2+} current. HVA current was analyzed by measuring the sustained current at the end of the depolarizing pulse. Peak HVA and T-type Ca^{2+} current was measured

at 0 mV and -30 mV respectively. The T-type Ca^{2+} current was also isolated in a different way using the prepulse protocol. Here, the total Ca^{2+} current was recorded from a well hyperpolarized potential of -100 mV. Then, the HVA current was recorded at -40 mV. At this potential the HVA channels are activated, while the T-type channels are inactivated. T-type Ca^{2+} current was then isolated by digitally subtracting the HVA current from the total Ca^{2+} current.

2.5.8 Current clamp recordings

For current clamp recordings in intact DRG neurons, we used the Axopatch 200B amplifier controlled by pCLAMP version 8.2 software. The extracellular solution contained the following (in mM): 150 NaCl, 5 KCl, 2 $CaCl_2$, 1 $MgCl_2$ and 10 HEPES. Osmolarity of the solution was 305 mOsmol/L and did not need further adjustment, whereas the pH was changed to 7.4 with NaOH. The pipette solution used was (in mM): 20 KCl, 120 potassium gluconate, 10 EGTA, 10 HEPES, 2 $MgCl_2$ and 2 ATP-Na_2. Osmolarity of the solution was 290 mOsmol/L and the pH was adjusted to 7.3 via KOH. Data were filtered at 10 KHz, and sampled at 30 KHz. The liquid junction potential determined for these solutions was +14 mV and all values and figures were corrected accordingly.

Whole-cell configuration was obtained in the voltage clamp mode. Here, pipette capacitance was cancelled and passive membrane properties were measured. The membrane potential was then measured by switching to current clamp with no injected current (I=0). Cells with resting membrane potential more positive than -54 mV were excluded. Subsequently, we switched to fast current clamp mode (I-CLAMP FAST). To eliminate the micropipette voltage drop from the recording, bridge balance was carefully compensated. For single action potential (AP) recordings, cells were clamped to a holding potential of -70 mV and an action potential was evoked by 4 ms depolarizing current injections. To analyze the repetitive firing behavior, APs were evoked by repetitive 500 ms current injections increasing from 20 to 1000 pA with increments of 20-40 pA. Subsequently, a series of negative current injections with a step of −10 pA for 500 ms duration was applied to evoke hyperpolarization followed by a set of I_h (hyperpolarization-activated current)-induced depolarizing voltage sags to measure I_h.

2.5.9 Analysis of current clamp recording

Analysis of the parameters of single action potentials elicited by 4 ms current injection was done using Clampfit 9.2. The APs were analyzed at rheobase, which is defined as the minimum amount of depolarizing current that discharged an AP. The following was analyzed (see Fig. 9): repolarizing area: area during the repolarization phase of the action potential (i.e. returning to baseline); AHP area: the full length of the afterhyperpolarization following the action potential was difficult to measure because its approach to the holding potential was so gradual. Therefore, the area of the AHP relative to the holding potential was measured until 250 ms after beginning of the AHP.

Action potentials during prolonged current injection (500ms) change depending on the time and occurrence during the current injection as well as the number of preceding

action potentials. Therefore we analyzed the first action potential elicited during the first 50 ms of current injection, for which the following properties were determined: threshold: determined as the voltage at the time point when the slope of the rising phase of the AP exceeded 10 V/S; maximal amplitude: maximal amplitude of the action potential compared with 0 mV; 10-90% rise time: the time between 10% and 90% percentile of the peak amplitude during the rising phase of the action potential; halfwidth (HW) above threshold: the time between the point to the left and to the right that are 50% of the peak amplitude relative to the threshold. These properties as well as the firing rate were analyzed using an IGOR routine that detected spikes automatically.

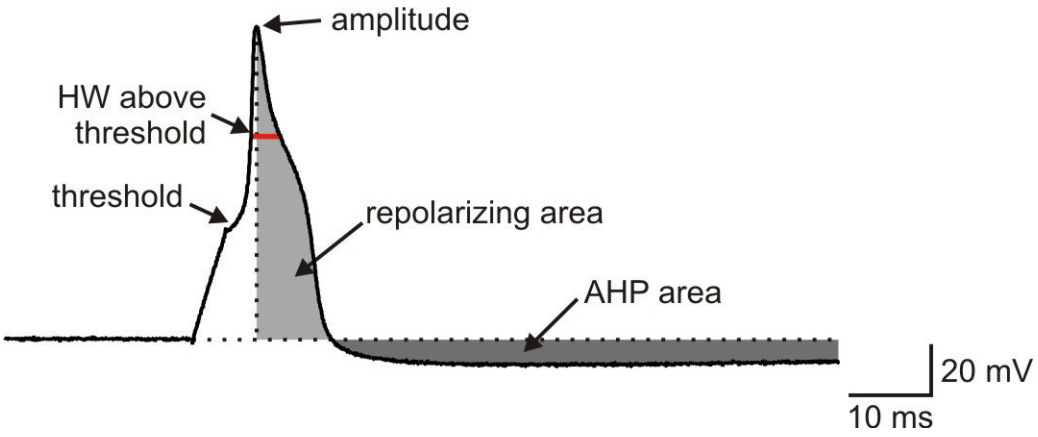

Fig. 9: Different action potential parameters. For the first action potentials elicited by 500 ms or 4 ms current injection, the following parameters were analyzed: repolarizing area, AHP (afterhyperpolarization) area, AP amplitude, AP threshold, HW (halfwidth) relative to threshold and 10-90% rise time.

In addition, the I_h induced depolarizing voltage sags was analyzed by measuring the difference between initial induced hyperpolarizing potential and the steady state potential at the end of the 500 ms current injection.

2.6 Histological analysis: Methylene blue staining of semi thin sections

Resin embedded samples of the sciatic nerve were used for the preparation of semi thin slices. Using the ultramicrotome, 900 nm thick transverse sections were cut. With the help of a glass knife boat, the semi thin sections were mounted on a glass slide containing one drop of distilled water and labeled (with the block number). The sections were dried on a hot plate for 1 hour at 75 °C and subsequently stained at 60 °C for 30-40 seconds by adding few drops of the staining solution (toluidine blue) and then covered. The staining solution (solution C) is composed of a 1:1 mixture of solutions A and B, mentioned in the table below. The stained semi thin sections were examined with a compound light microscope.

Table 2: Methylene blue solution.

Solution A	1g Sodiumborate (Merck) 1 g Methylene blue (Merck) ad 100 ml H_2O
Solution B	1 g Azur II (Merck) ad 100 ml H_2O
Solution C	1:1 mixing of solutions A and B

2.7 Quantitative real-time RT-PCR

2.7.1 Preparation of cDNA

For the RT-PCR analysis of $Ca_V3.2$, 15 wild type mice were ligated and other 15 were sham operated. Lumbar DRGs (L_{4-5}) of the operated side were dissected from the PNL and sham operated mice on day 1, 3, 7, 10 and 14 after surgery. For mRNA isolation, 100 µl lysis binding buffer was added to the DRGs and homogenized using a pistil. Subsequently, mRNA was isolated with a Dynabeads mRNA Direct Micro kit (Invitrogen) according to the manufacturer's protocol. First-strand cDNA was prepared using RevertAid Reverse Transcriptase (Fermentas). The following primers were used: $Ca_V3.2$ forward (5'- ATG TCA TCA CCA TGT CCA TGG A-3'); $Ca_V3.2$ reverse (5'- ACG TAG TTG CAG TAC TTA AGG GCC-3'); synaptophysin forward (5'- TTC AGG ACT CAA CAC CTC GGT -3'); synaptophysin reverse (5'- CAC GAA CCA TAG GTT GCC AAC -3').

2.7.2 Quantitative Real Time RT-PCR (Analysis of mRNA expression)

The principle of Real-time PCR systems is based on the detection and quantification of a fluorescent reporter. The signal of this reporter increases in direct proportion to the amount of PCR product in a reaction. In our experiment, that reporter is the double-strand DNA-specific dye SYBR Green. SYBR Green is able to bind double-stranded DNA, and emits light upon excitation. Thus, as a PCR product increases, the fluorescence also increases.

Transcript quantification was performed by quantitative real time RT-PCR analysis according to the ΔΔCt-method (Fink et al. 1998). To normalize expression, synaptophysin was amplified from all samples. For quantitative RT-PCR a 6.25-µl reaction volume was used containing 3.125 µl of Maxima SYBR Green/Rox qPCR Master Mix (Fermentas), 1.5 µl of diethyl pyrocarbonate H_2O, 1.25 µl of cDNA, and 0.1875 µl of each primer (10 pmol/ml; $Ca_V3.2$). Reactions were performed in triplicate. A preincubation time of 10 min at 94 °C was chosen, after which 40 PCR cycles (20 s at 94 °C, 30 s at 59 °C, and 40 s at 72 °C) were performed on an ABI Prism 9700HT system (PE Applied Biosystems, Foster City, CA). In each cycle, the SYBR Green fluorescence signal was measured.

2.8 Statistical analysis and software

All data are presented as average ± standard error of the mean (SEM).

In the behavioral experiments of the EAN animal model, differences between the three groups of rats (EAN, CFA and ICFA) were determined by two-way ANOVA, considering treatment and time course. In case of significant interactions, the two-way ANOVA was followed by Bonferroni's multiple comparison post test.

Analysis of pain behavior of the PNL animal model was done by comparison of ipsilateral or contralateral side before and after PNL of the same group of mice via paired Student's t-test.

For the electrophysiological data of the EAN animal model, comparison between the three different groups of rats was performed using one-way ANOVA test (parametric test) followed by Tukey's multiple comparison post test. In some cases, where variances were different between the groups, the nonparametric ANOVA Kruskal-Wallis test was used followed by Dunn's multiple comparison test.

Differences between the groups of mice of Ca^{2+} current as well as action potential recordings of mice was analyzed via unpaired Student's t-test. Analysis of differences in mRNA expression was done via unpaired Student's t-test. In case variances were significantly different, an unpaired Student's t-test with Welch's correction has been performed. A chi-squared test has been performed, to analyze differences between the groups with respect to the type of Ca^{2+} current.

For all tests the significance level was set at $p<0.05$. Data analyses were done with Clampfit 9.2 software (Molecular Devices, CA), IGOR (Wavemetrics Inc., Lake Oswego, OR). Graphpad Prism (Graphpad Software, Dan Diego, CA), and Excel 2003 on a WindowsTM based PC-system (Microsoft, Redmond, WA).

3 Results

3.1 Experimental autoimmune neuritis

3.1.1 Clinical course of EAN

EAN clinical scores were assessed immediately before immunization (day 0) and every day until day 31. All rats immunized with P2 antigen + CFA (n=8) developed clinical signs of EAN from day 11 post-immunization onwards. Severity of clinical EAN was mild to moderate. It started with mild paresis of the tail, then developed to slight or strong hind leg paralysis (Fig. 10). None of the rats died or developed complete paralysis. The disease peaked at day 14-17, and rats completely recovered by day 22 post-immunization. Control rats injected with ICFA (n=4) or CFA+BSA (n=7) did not develop any signs of EAN.

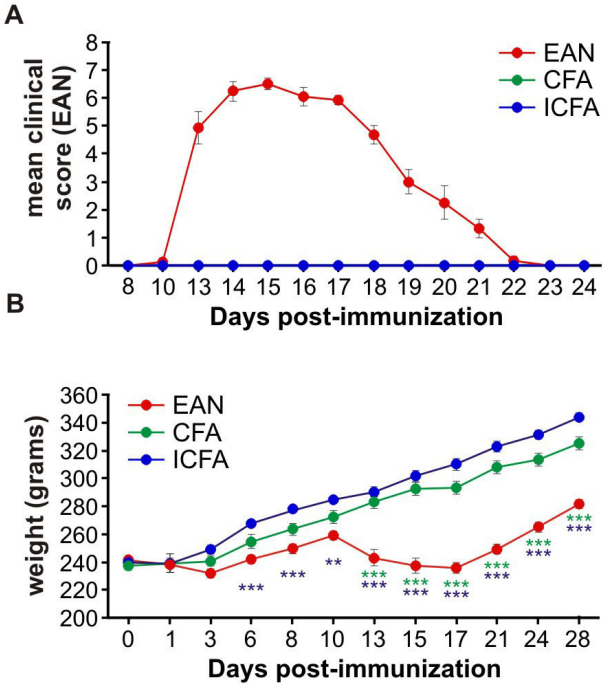

Fig. 10: Clinical scores and body weight of EAN rats. Lewis rats were immunized (day 0) with synthetic neuritogenic P2 peptide plus CFA (n=8). Control rats were immunized with CFA plus BSA (n=7) or saline plus ICFA (n=4). Rats were monitored for clinical signs of EAN (A) and for body weight (B) for 28 days post-immunization. Only rats immunized with P2 developed clinical signs of EAN. A significant weight difference was observed between P2-immunized rats and ICFA-or CFA-immunized controls (two-way ANOVA followed by Bonferroni post test depicted as asterisks, where the blue asterisks represent differences between EAN and ICFA, and the green ones between EAN and CFA).

As a further indicator of the disease, EAN rats began to lose weight at the same time, where clinical signs started to appear (Fig. 10). The weight loss continued throughout the period of maximal illness and paralleled the severity of the disease. There was no weight loss observed in both ICFA- and CFA-control groups (two-way ANOVA showed a significant time and treatment effect on weight loss, $p<0.0001$, $F=52.72$,

df=10 and p<0.0001, F=205.06, df=2 respectively. ANOVA was followed by Bonferroni post test, depicted as asterisks in Fig. 10B, where the blue asterisks represent differences between EAN and ICFA, and the green ones between EAN and CFA).

3.1.2 Histology of the sciatic nerves

To further validate our animal model, a histological analysis of the sciatic nerves was performed to check for typical histological signs of EAN. As mentioned in the introduction, the main target of the autoimmune reaction in EAN is the myelin sheath. To assess the demyelination of the peripheral nerves, methylene blue staining of (semi-thin slices) transverse sections of sciatic nerves of EAN as well as of the two control groups was performed. Sciatic nerves were collected from the rats at disease peak (day 15 post-immunization, mean clinical score of EAN=6.5 ± 0.19). Light microscopy of resin-embedded rat sciatic sections revealed in a considerable number of axons of EAN rats a reduced thickness of myelin sheath as sign for demyelination. In addition, the overall number of axons was clearly reduced (Fig. 11). This reveals that besides demyelination, axonal pathology may play a significant role in the course of EAN. No abnormalities of the sciatic nerves were observed in the two control groups.

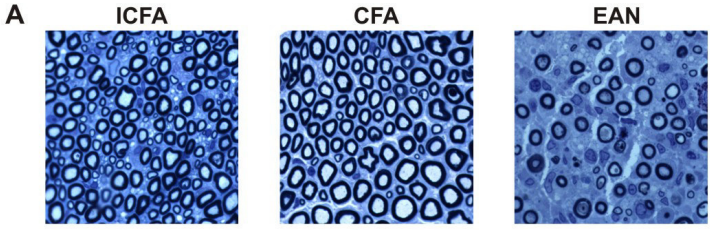

Fig. 11: Demyelination of sciatic nerves of EAN rats. Light microscopic illustrations of sciatic nerve sections stained with methylene blue collected from CFA and ICFA control rats as well as EAN rats at disease peak (day 15). Rats with EAN exhibited evidence of axonal demyelination and reduced axonal density.

3.1.3 Mechanical allodynia during the course of EAN

To examine whether pain responses are altered during EAN, we examined withdrawal thresholds in response to mechanical stimuli in both hindpaws. Since no significant difference was observed between right and left hindpaws, both sides were pooled for each animal. Baseline responses of the rats in the von Frey test were similar in all treatment groups (Fig. 12). On day 1-3, all groups of rats showed a decrease in paw withdrawal latency compared to the basal data, which is presumably due to an unspecific reaction to the injection or to a continuously shortening of response latencies as seen during repeated testing. An obvious decrease in withdrawal response latencies to mechanical stimuli was observed in the EAN group (n=8) starting from day 6 post-immunization, which remained throughout the entire period tested (till day 28) even after disappearance of clinical signs (day 24). There were no differences in withdrawal threshold detected between ICFA- and CFA-injected group (n=4, n=7 respectively) during the entire experiment (two-way ANOVA showed a significant time and treatment effect on withdrawal responses, p<0.0001, F=60.87, df=11 and

p<0.0001, F=86.90, df=2 respectively. Also, a significant interference of the two factors, time and treatment, p=0.013, F=1.84, df=22. ANOVA was followed by Bonferroni post test depicted as asterisks in Fig. 12, where the blue asterisks represent differences between EAN and ICFA, and the green ones between EAN and CFA).

Fig. 12 represents the results of one behavioral experiment, and Fig. 10 shows their corresponding clinical monitoring. However, these experiments were also performed for all animals used for electrophysiological recordings to verify the pain symptoms for each animal, hence allowing for a correlation between pain symptoms and electrophysiological changes. The results of these experiments were not included in this figure.

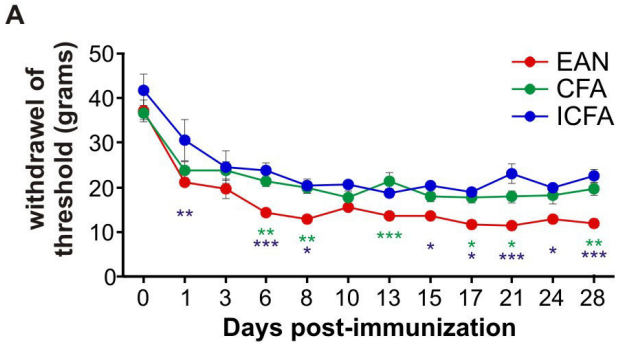

Fig. 12: Pain responses are altered in EAN rats. Mechanical withdrawal thresholds of hindpaws of P2-immunized rats (EAN) and CFA-and ICFA-immunized controls. Withdrawal thresholds of EAN rats were significantly lower than in both control groups from day 6-28 post-immunization (EAN: n=8; CFA: n=7; ICFA: n=4, two-way ANOVA followed by Bonferroni post test depicted as asterisks, where the blue asterisks represent differences between EAN and ICFA, and the green ones between EAN and CFA).

3.1.4 DRG neuron classification

For electrophysiological experiments DRG neurons were dissociated from $L_{4\text{-}5}$ DRG-ganglia on day 17-30 by a combination of enzymatical und mechanical methods (2.3.1). As nociceptive DRG neurons can be distinguished by their smaller cell diameter from other, non-nociceptive DRG neurons, only small DRG neurons (diameter < 30 µM) were used for this study (Harper and Lawson 1985 b).

To further detect possible nociceptor subclass specific differences, each cell was analyzed for its responsiveness to the TRPV1 receptor agonist capsaicin as well as the IB_4-binding capacity. The polymodal nonselective cation channel TRPV1 is activated by harmful heat, extracellular protons and vanilloid compounds (Snider and McMahon 1998; McCleskey and Gold 1999; Petruska et al. 2000). It is an important selective marker of nociceptive function of DRG cells (Caterina and Julius 2001), and the majority of small sized sensory neurons express this receptor. In the voltage clamp mode of the whole-cell configuration, 1 µM capsaicin gave rise to a nonselective inward current in the majority of cells (Fig. 13 A). The percentage of $caps^+$ cells (100% of ICFA, 88.5 % of CFA, 82 % of EAN) as well as the magnitude of the

capsaicin-induced current (ICFA: -3.5 nA ± 0.76, n=15,CFA: -2.4 nA ± 0.4, n=14, EAN: -2.5 nA ±0.3, n=28) (Fig. 13 A) was not significantly different between groups.

Furthermore, nociceptors can be classified according to their ability to bind the glycoprotein IB_4 from the plant Griffonia simplicifolia. IB_4^- nociceptors represent the peptidergic population. They contain peptide neurotransmitters substance P and are able to respond to NGF by expressing TrKA, the high-affinity tyrosine kinase receptor for nerve growth factor (NGF). IB_4^+ neurons, on the other hand, do not express substance P or TrKA, but express Ret receptors that bind glial cell derived neuropathic factor (GDNF). To check for the IB_4-binding capacity, DRG neurons were incubated with external solution containing fluorescent-dye-labeled IB_4. Cells showing an intense green fluorescence along the outer cell membrane are considered IB_4^+ (Fig. 13 B).

Classification of nociceptors according to their IB_4-binding capacity revealed that the majority of small DRG neurons were IB_4^+ (73% of ICFA, 71% of CFA, 88% of EAN). The percentage of IB_4^+ cells was in agreement with previous findings (e.g. 89% $IB4^+$, (Fang et al. 2006) and was not different between groups.

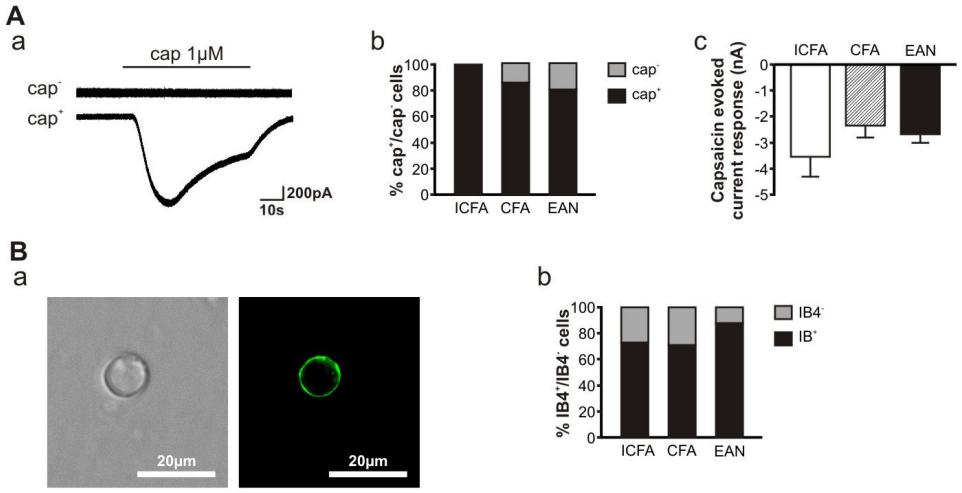

Fig. 13: Classification of DRG neurons according to capsaicin-evoked current response and IB_4-binding. (A) Capsaicin evoked current response in small DRG neurons. (Aa) Application of 1 µM capsaicin in the voltage clamp mode gave rise to a nonselective inward current in a subset of cells. Representative currents from a non-responsive (cap^-) and a responsive (cap^+) control cell are shown (upper trace and lower trace, respectively). (Ab) Histograms indicate the percentages of cap^+ and cap^- cells in the different experimental groups. There was no statistically significant difference between percentages of cells responding to capsaicin in the ICFA- (100%, n=16), CFA- (88.5%, n=19) and EAN-group (82%, n=55). (Ac) The maximal capsaicin-induced current amplitude of cap^+ cells was not significantly different between experimental groups. (B) The majority of small sized DRG cells were IB_4^+. (Ba) Microphotograph of acutely dissociated DRG cell from a control rat showing a bright-field image on the left and a fluorescent image on the right. (Bb) Histograms show that the majority of small sized DRG cells in all experimental groups were IB_4^+ (ICFA 73%, n= 15, CFA 71%, n=14, EAN 88%, n= 34).

Based on the large overlap between capsaicin-responsiveness and IB_4-binding capacity found in the small DRG neurons of the three different groups (ICFA: 75% of cap^+ are IB_4^+, 100% of $IB4^+$ are cap^+; CFA: 64% of cap^+ are IB_4^+, 90% of IB_4^+ are cap^+; EAN: 85% of cap^+ are IB_4^+, 79% of IB_4^+ are cap^+), we classified the neurons for the following electrophysiological experiments according to their capsaicin-responsiveness.

3.1.5 Passive membrane properties

After obtaining the whole-cell configuration we first analyzed the passive membrane properties. In cap^+ neurons, the resting membrane potential as well as the input resistance (ICFA: n=20, CFA: n=17, EAN: n=45) were similar between groups (one-way ANOVA, p=0.24, F=1.47, df=80; one-way ANOVA, p=0.40, F=0.94, df=81 respectively). A small, but significant difference was found in the capacity of neurons between the EAN group and the ICFA control group (one-way ANOVA, p=0.036, F=3.47, df=81 followed by Tukey's multiple comparison test depicted as asterisk in Fig. 14).

It should be noted that the passive membrane properties represented in Fig. 14 are measured before current clamp recordings (AP measurements). Since the number of cap^- neurons of both control groups were too small (ICFA: n=0, CFA: n=2), we could not analyse differences in passive membrane properties in this group of neurons.

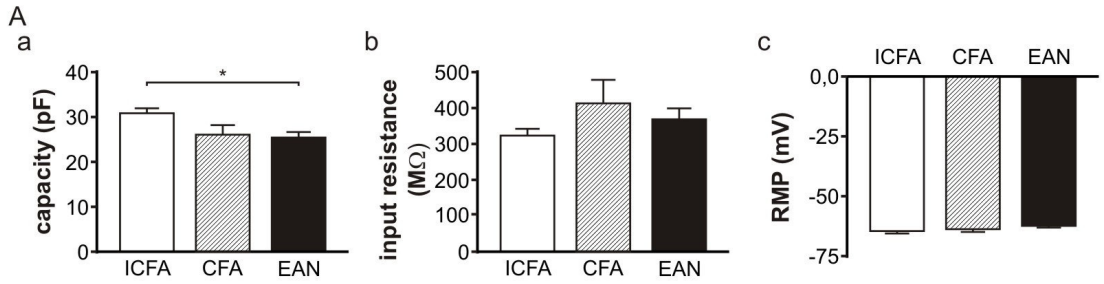

Fig. 14: Passive membrane properties of small cap^+ DRG neurons. There were no significant differences between cap^+ EAN cells and cap^+ ICFA or CFA cells with respect to the input resistance (b) and resting membrane potential (c). A small but significant difference was found in the capacity (a) between ICFA and EAN cells (ICFA: n=20, CFA: n=17, EAN: n=45) (one-way ANOVA followed by Tukey's multiple comparison test depicted as asterisk).

3.1.6 EAN is associated with changes in AP waveform and repetitive firing properties of cap^+ small sensory DRG neurons

As the behavioral pain tests verified a significant neuropathic pain phenotype in EAN rats, we next analyzed nociceptive DRG neurons of EAN rats for changes in their electrophysiological properties that might be correlated to severe pain. It is known from other animal models of neuropathic pain that neuropathic pain behavior is associated with a hyperexcitability of nociceptive DRG neurons. Therefore, we first performed an analysis of single action potential parameters and subsequently evaluated the repetitive firing capacity.

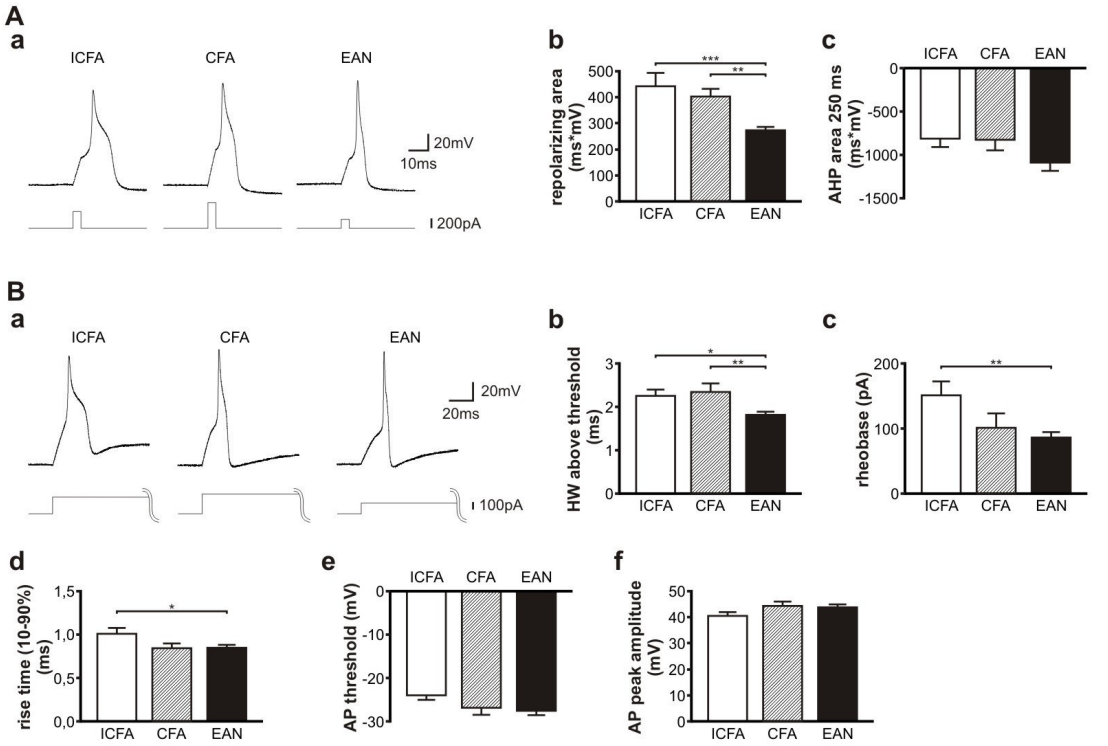

Fig. 15: The repolarization phase is reduced in cap$^+$ nociceptors from EAN rats. (Aa) Examples of APs evoked in cap$^+$ DRG neurons by injection of 4 ms depolarizing current commands of increasing amplitude. Sample recordings are depicted for cap$^+$ ICFA, CFA and EAN cells. (Ab) Histograms showing that the area of repolarizing phase of the AP is significantly reduced in cap$^+$ EAN DRG cells compared to cap$^+$ ICFA- and CFA controls. (Ac) Histograms showing no significant differences with respect to the AHP area in cap$^+$ nociceptors of EAN rats compared to ICFA- and CFA controls. (Ba) Examples of the first AP evoked in cap$^+$ DRG neurons by injection of 500 ms depolarizing current commands of increasing amplitude. Sample recordings are depicted for ICFA, CFA and EAN cells. (Bb) The AP duration (HW relative to threshold) was significantly shorter in cap$^+$ nociceptive neurons of EAN rats compared to the control groups. (Bc) Rheobase of AP firing was lowest in EAN group. A significant difference was found compared to the ICFA control group. (Bd) Rise time (10-90%) was significantly different in EAN group compared to ICFA group. (Be-f) Histograms showing no significant differences with respect to the (Be) AP threshold and (Bf) AP peak amplitude in cap$^+$ nociceptors of EAN rats compared to ICFA-and CFA controls. The number of cells were 20, 17 and 45 for ICFA, CFA and EAN rats respectively. Statistical differences were detected using one-way ANOVA followed by Tukey's multiple comparison test depicted as asterisks in the figure.

DRG cells of the three treatment groups generated overshooting action potentials in response to brief 4 ms current injections (Fig. 15 A) of increasing amplitude. DRG neurons of both control groups exhibited wide action potentials with an inflection in the falling phase. The presence of an inflection ("shoulder") in the repolarizing phase of the action potential is a typical characteristic of small DRG neurons (Harper and Lawson 1985 a; Renganathan et al. 2001). In cap$^+$ cells of EAN rats, however, this inflection, measured as repolarizing area of the action potentials (see Materials and Methods 2.5.9, Fig. 9), was significantly smaller compared to both CFA and ICFA

cap$^+$ control groups (one-way ANOVA p<0.0001, F=12.93, df=77 followed by Tukey's multiple comparison test depicted as asterisks in Fig. 15 Ab). This result was confirmed by analyzing the first action potential evoked by prolonged depolarizing current injections (500 ms, Fig. 15 B). Here, the halfwidth of cap$^+$ cells of the EAN group was significantly reduced compared to the ICFA- and CFA- group (one-way ANOVA p=0.0027, F=6.40, df=78 followed by Tukey's multiple comparison test depicted as asterisks in Fig. 15 Bb). There was no difference between CFA und ICFA control groups. Small but significant changes has been also observed in the rise time (10-90%) of these first evoked action potentials between cap$^+$ neurons of EAN and ICFA rats (one-way ANOVA p=0.046, F=3.22, df=76 followed by Tukey's multiple comparison test depicted as asterisk in Fig. 15 Bd). Furthermore, the mean value of the rheobase of first elicited AP was smallest in EAN DRG cells, and a significant difference was shown compared to the ICFA control group (one-way ANOVA p=0.0092, F=5.03, df=71 followed by Tukey's multiple comparison test depicted as asterisks in Fig. 15 Bc). There was no difference in the action potential threshold (one-way ANOVA p=0.11, F=2.28, df=77), action potential amplitude (one-way ANOVA p=0.18, F=1.78, df=75) and AHP area (250 ms) (one-way ANOVA p=0.11, F=2.25, df=79) between the different treatment groups. The number of cells used for the analysis of action potential morphology were 20, 17 and 45 for ICFA, CFA and EAN rats respectively.

Since none of the analyzed neurons of the ICFA treated group and only two of the CFA treated group were found to be insensitive to 1 µM capsaicin, we could not detect potential changes of AP parameters between EAN rats and the control groups in cap$^-$ cells. However, 10 neurons of the EAN group did not show an inward current in response to capsaicin. The mean values of the AP parameters of cap$^-$ neurons of P2-treated group were as follows: repolarizing area: 422 ms*mV ± 66; HW relative to threshold: 2.6 mV ± 0.2, rheobase: 148 pA ± 33, amplitude of (AHP): -10.7 mV ± 1.5; AHP area (250 ms): -1276 ms*mV ± 194, AP threshold: -25.9 mV ± 2.2, AP amplitude: 42.9 mV ± 3.02 and rise time (10-90%): 0.56 ms ± 0.06.

As we found differences in the AP morphology of cap$^+$ EAN cells, we analyzed whether the repetitive firing behavior of cap$^+$ DRG neurons is also altered in EAN rats. We observed a high variability of firing behavior in response to 500 ms current injections among the cells of the same treatment group. However, analysis of the maximum firing frequency of nociceptive cap$^+$ neurons revealed that this was significantly increased in EAN rats (n=33) compared to the ICFA control group (n=10), whereas the increase did not reach statistical significance compared to the CFA group (n=11) (one-way ANOVA p=0.0032, F=6.45, df=52 followed by Tukey's multiple comparison test depicted as asterisks in Fig. 16 B). The effect of EAN on repetitive discharge is demonstrated more clearly by studying the relationship between the HW (relative to threshold) of the action potential and the maximum firing frequency. Fig. 16 Bb shows that cap$^+$ DRG neurons of EAN rats have the shortest action potential duration, as previously shown (Fig. 15 Bb), and the highest maximum firing rate compared to both controls. This implies, that the shorter the action potential duration, the higher the firing frequency of a cell. In summary, the above mentioned

data reveal, that cap$^+$ DRG neurons of EAN rats exhibit signs of an increased excitability.

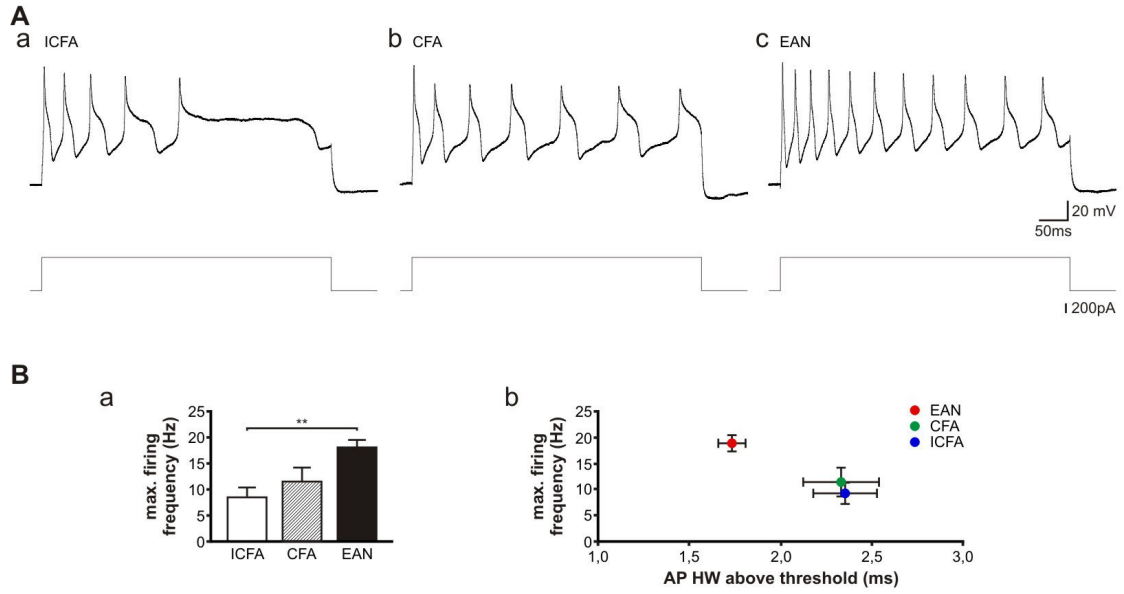

Fig. 16: The maximum firing frequency is increased in cap$^+$ nociceptors from EAN rats. (A) Repetitive firing of DRG neurons elicited by injection of 500 ms depolarizing current commands of increasing amplitude (here shown for 680 pA). Sample recordings are depicted for cap$^+$ ICFA, CFA and EAN cells. (Ba) Histogram showing that the firing frequency of cap$^+$ EAN DRG cells was significantly increased compared to cap$^+$ ICFA control neurons (one-way ANOVA followed by Tukey's multiple comparison test depicted as asterisks). (Bb) Relationship of AP duration (HW relative to threshold) and maximum firing rate shows that in cap$^+$ cells of EAN rats, the short AP duration is associated with an increased firing frequency compared to ICFA- and CFA-controls.

In addition, the I_h (hyperpolarization-activated current)-induced depolarizing voltage sags were analyzed in cap$^+$ neurons of the three treatment groups. For this, a series of negative current injections with increasing steps of −10 pA for 500 ms duration were applied to the neurons. The results are summarized in Fig. 17. No difference was observed between EAN and ICFA or CFA controls with respect to the I_h induced depolarizing sags (ICFA: n=16, CFA: n=16, EAN: n=16).

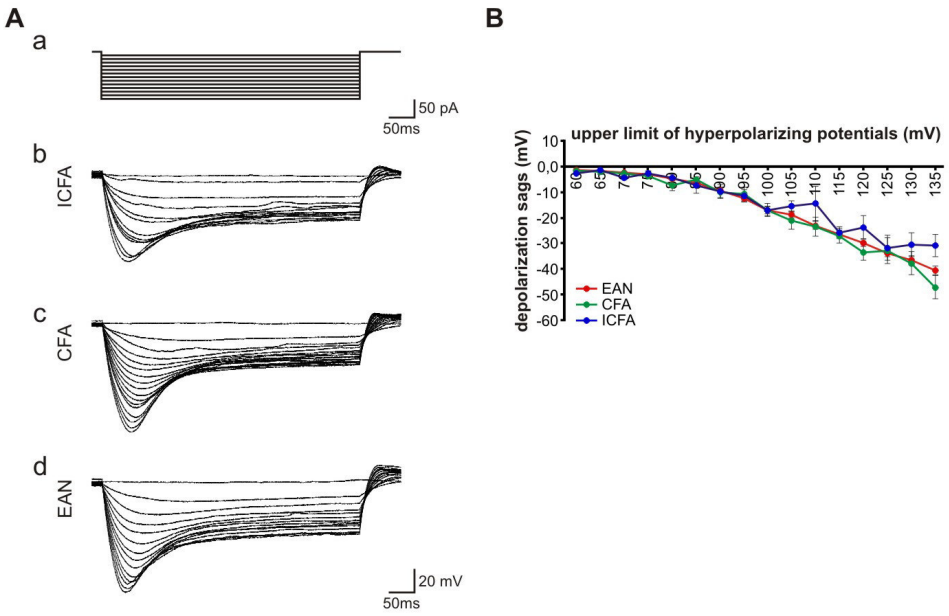

Fig. 17: I_h induced depolarizing voltage sags are not altered in EAN rats. (A) Representative traces of membrane potentials of (Ab) ICFA, (Ac) CFA and (Ad) EAN cells that were elicited by a series of negative current injections (Aa). (B) Relationship between the voltage sags and the corresponding hyperpolarizing membrane potentials of ICFA, CFA and EAN DRG neurons.

3.1.7 Impact of EAN on transient Na^+ currents in DRG neurons

The described changes in the action potential morphology and repetitive firing behavior of cap^+ neurons implies that EAN might be associated with changes in ionic currents in the same subgroup of neurons. Na^+ channels play an essential role in regulating the discharge behavior of excitable cells. Furthermore, the characteristic action potential configuration of nociceptive DRG neurons with the inflection in the falling phase is associated with the expression of specific Na^+ channels subtypes as $Na_V1.8$ and $Na_V1.9$, and to a lower extent with voltage gated Ca^{2+} channels (Blair and Bean 2002). Hence, we sought to determine the potential basis for the difference in AP duration and especially the "smaller shoulder" by examining the properties of voltage gated Na^+ currents.

In initial experiments, we found that capsaicin application affected the I_{NaP} current amplitude. Fig. 18 A shows the persistent Na^+ current of control DRG neurons measured before (n=39) and after (n=7) capsaicin application revealing a significant decrease in I_{NaP} when measured after capsaicin wash (unpaired t-test with Welch's correction, p=0.0009, t=3.75, df=26). For this, capsaicin was applied at the end of the experiments and cells were divided according to their capsaicin responsiveness into the cap^+ and cap^- group.

In contrast to the current clamp recordings, more nociceptive neurons were found to be insensitive to capsaicin in the three different treatment groups after recording of Na^+ currents. Analysis of the cumulative probability distribution of capsaicin evoked response measured before (n=8) and after (n=51) Na^+ current measurement is

presented in Fig. 18 B. The analysis revealed a reduced capsaicin induced current response after Na^+ current measurement when compared to the responses before the recordings. This reveals an impact of the preceding measurement on the capsaicin responsiveness. Therefore, the cap^- group might contain cells that were actually cap^+. However, this should not represent a problem for the analysis of the relevant subset of cap^+ DRG neurons as this group might be a little smaller, but contain no false classified cells.

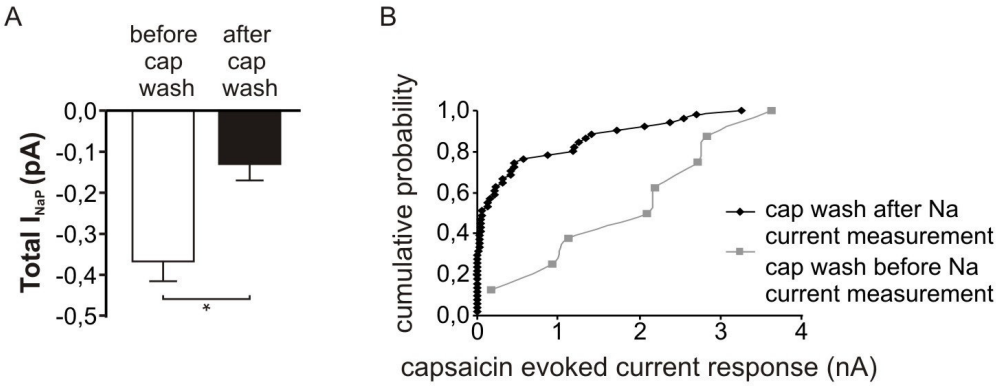

Fig. 18: I_{NaP} is altered following capsaicin application. (A) Comparison of the persistent Na^+ current of control DRG neurons (ICFA, CFA) when measured before (n=39) and after (n=7) capsaicin wash showing a significant reduction of I_{NaP} when measured after capsaicin application (unpaired t-test). (B) Cumulative probability distribution of capsaicin evoked response of control DRG neurons (ICFA, CFA or non-injected) before (n=8) and after (n=51) Na^+ current measurement showing a reduction of capsaicin induced current when analyzed after Na^+ current measurement.

For the voltage clamp recordings of Na^+ currents in nociceptice neurons, cells were held at -120 mV and subjected to depolarizing voltage steps of increasing amplitude. Representative traces of the total transient Na^+ current (I_{NaT}) evoked by increasing voltage steps in a cap^+ control neuron (CFA) are shown in Fig. 19 A. From this data we constructed current voltage curves (Fig. 19 B), where no changes in the peak magnitude of the total Na^+ current were observed among the different treatment groups (one-way ANOVA p=0.11, F=2.29, df=48) (ICFA: n=13; CFA: n=21; EAN: -n=15) (Fig. 19 Ca).

Since small nociceptive DRG neurons express TTX-sensitive Na^+ channels (Black et al. 1996; Sangameswaran et al. 1997) in combination with TTX-resistant $Na_V1.8$ and $Na_V1.9$ channels (Amaya et al. 2000; Fjell et al. 2000), we further examined the impact of EAN on the composition of TTX_S and TTX_R Na^+ currents. Application of 1 µM TTX allowed the pharmacological separation of total I_{NaT} into a TTX_R current component. TTX_S Na^+ current was obtained by digitally subtracting the TTX_R current from the total Na^+ current. Fig. 19 A shows representative traces of the TTX_S and TTX_R Na^+ currents of the same cap^+ CFA control neuron. Analysis of the current voltage curves and the peak amplitudes revealed a clear up-regulation of the TTX_S Na^+ current of EAN nociceptive neurons (n=15) compared to ICFA and CFA control cells (n=12; n=21) (one-way ANOVA $p<0.0001$, F=13.32, df=47 followed by Tukey's multiple comparison test depicted as asterisks Fig. 19 Cc) at -20 mV. One-way ANOVA also showed a significant difference with respect to the TTX_R peak current

responses at -20 mV (p=0.0081, F=5.37, df=47). Further analysis using Tukey's multiple comparison test showed a significant reduction of TTX_R Na^+ current of EAN cells compared to the ICFA control group, whereas the difference to the CFA group did not reach statistical significance (Fig. 19 Cb).

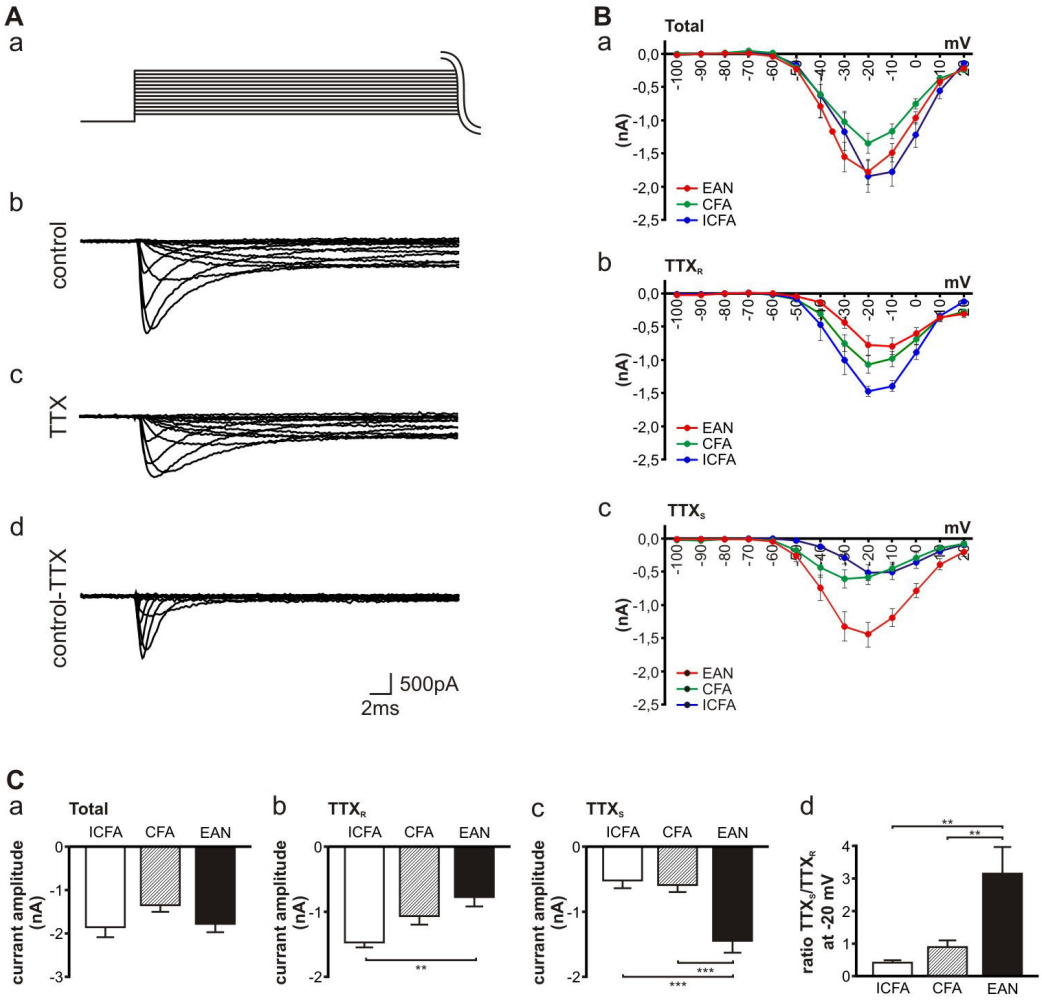

Fig. 19: Fast Na^+ currents are altered in EAN rats. (A) Representative current traces recorded from a cap^+ CFA control cell. Total fast Na^+ currents (I_{NaT}) (Ab) were elicited by a standard voltage clamp protocol (Aa). By application of 1 µM TTX, total I_{NaT} was pharmacologically separated into a TTX_R current component (Ac), and by subtracting the TTX_R from the total Na^+ current, into a TTX_S current component (Ad). (B) current-voltage relationship for (a) total, (b) TTX_R and (c) TTX_S I_{NaT}. Data are shown for cap^+ EAN, cap^+ ICFA and cap^+ CFA cells. (C) Histograms showing total, TTX_R and TTX_S peak current densities at -20 mV of ICFA, CFA and EAN DRG neurons. (a) The total Na^+ current was not altered in EAN rats. (b) TTX_R Na^+ current was smallest in EAN DRG cells. A significant difference was observed compared to the ICFA control group. (c) The TTX_S current was significantly increased in DRG cells of EAN rats compared to both ICFA-and CFA controls. (d) Ratio of TTX_S to TTX_R currents calculated at -20 mV test potential. The ratio is significantly higher in EAN neurons compared to ICFA-and CFA controls. For statistical analysis, we used one-way ANOVA followed by Tukey's multiple comparison test depicted as asterisks.

In summary, EAN caused an up-regulation of the fast TTX_S and a down-regulation of the fast TTX_R Na^+ current (in comparison to ICFA control group), though the total fast Na^+ current of EAN nociceptive neurons remained unaffected. This hypothesis was confirmed by analyzing the ratio of TTX_S to TTX_R Na^+ current that proved to be significantly higher in the EAN group compared to the ICFA as well as the CFA control group (one-way ANOVA p=0.0006, F=8.63, df=49 followed by Tukey's multiple comparison test depicted as asterisks in Fig. 19 Cd).

From the current responses at each test potential, I_{NaT} activation curves of TTX_R Na^+ current were constructed for the different treatment groups by fitting with a Boltzmann function (see Materials and Methods 2.5.5). An activation curve of TTX_S Na^+ current was constructed only for neurons of the EAN group (V_{50} = -32.62 mV ± 2.27; slope factor = 5.4 ± 0.55, n=13) as the TTX_S Na^+ current component of both ICFA and CFA controls were too small. The averaged normalized data and activation curve for each group of neurons are provided in figure (Fig. 20), where the voltage dependence as well as the steepness of the activation curves of TTX_R Na^+ current were not different between the groups (ICFA: n=10; CFA: n= 20; EAN: n=15) (one-way ANOVA p=0.63, F=0.47, df=44 and p=0.07, F=2.80, df=44 respectively).

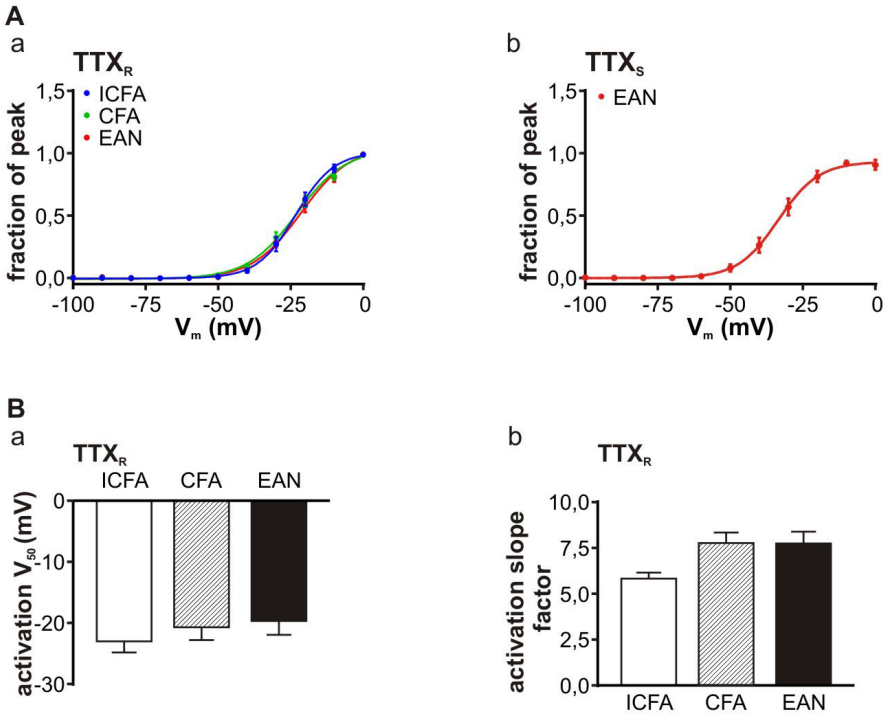

Fig. 20: Voltage dependence of steady state activation of TTX_R I_{NaT} is not altered in EAN DRGs. (Aa) Steady state activation profiles of I_{NaT} TTX_R for EAN, CFA and ICFA rats, and of I_{NaT} TTX_S for EAN group (Ab). Data are shown for cap^+ cells. Boltzmann equations reconstructed from fitted parameters of each group are shown as solid lines superimposed on the data points. There were no differences in the voltage dependence of activation of I_{NaT} TTX_R between the three groups. (B) Voltage of half maximal activation (a) and slope factor of steady state activation (b).

Furthermore, we determined the decay time constant (τ_{Decay}) of total, TTX_S and TTX_R transient Na^+ current elicited at a test potential of -30 mV. As shown previously (Blair

and Bean 2002), the currents carried by TTX_R Na^+ channels displayed approximately fivefold slower inactivation kinetics compared with TTX_S Na^+ currents. Statistical analysis revealed that τ_{Decay} of TTX_S and of TTX_R Na^+ currents were similar in the three groups of neurons (Fig. 21), suggesting that these currents were mediated by the same ion channels in the different groups. The decay time constant of the total transient Na^+ current, on the other hand, was significantly smaller in neurons of the EAN group (n=12) compared to the ICFA and CFA control groups (n=10, n=13, respectively) (because of differences in variances between the groups, the nonparametric ANOVA Kruskal-Wallis test was used p=0.001 followed by Dunn's multiple comparison test depicted as asterisks in Fig. 21a). This result confirms our finding of a significant up-regulation of fast TTX_S Na^+ currents in EAN cells and reflects its relevant impact on the inactivation kinetics of the total Na^+ current.

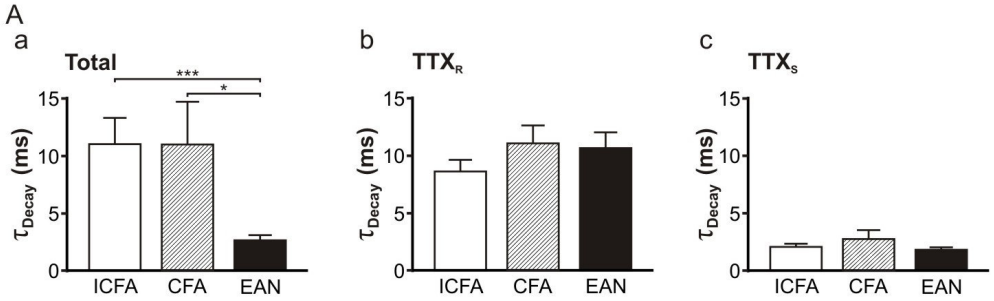

Fig. 21: The decay time constant (τ_{Decay}) of total, TTX_R and TTX_S transient Na^+ currents. Data are shown for cap$^+$ DRG neurons of ICFA, CFA and EAN rats. τ_{Decay} was analyzed for currents elicited at a test potential of -30 mV. (a) Histograms showing that τ_{Decay} of total I_{NaT} was significantly smaller in EAN neurons than in both control groups (ANOVA Kruskal-Wallis test followed by Dunn's multiple comparison test depicted as asterisks). τ_{Decay} analyzed for TTX_R (b) and TTX_S (c) I_{NaT} was not altered among the different treatment groups.

We also compared the three different groups of neurons with respect to the steady state inactivation of TTX_R I_{NaT}. Representative families of I_{NaT} traces evoked by a depolarizing step to -10 mV preceded by prepulses to various potentials in a control neuron (CFA) are shown in Fig. 22 A. From these data we constructed TTX_R I_{NaT} steady state inactivation curves for each of the tested neurons by fitting with a Boltzmann function. The averaged data for each group of neurons is provided in Fig. 22 B. The steady state inactivation as well as the slope factor was similar in the three groups of neurons (one-way ANOVA p=0.36, F=1.05, df=44 and p=0.52, F=0.67, df=44 respectively) (ICFA: n=11; CFA: n= 19; EAN: n=15). We were only able to analyze the steady state inactivation of the TTX_S Na^+ current for EAN neurons, as the TTX_S Na^+ current component of both ICFA and CFA controls were too small. Comparing the properties of TTX_S and TTX_R currents of EAN neurons revealed the differences in their voltage dependent activation and inactivation that have been previously described (Roy and Narahashi 1992; Elliott and Elliott 1993). The half maximal voltage of activation of TTX_S current was more hyperpolarized compared to TTX_R current ($V_{1/2}$ of TTX_S: -32.6 mV ± 2.3, $V_{1/2}$ of TTX_R: -19.7 mV ± 2.3). The difference in the voltage dependence of inactivation was even larger, with the midpoint

for TTX_S current shifted by ~30 mV in the hyperpolarized direction ($V_{1/2}$ of TTX_s: -77.3 mV ± 1.9, $V_{1/2}$ of TTX_R: -43.8 mV ± 1.5).

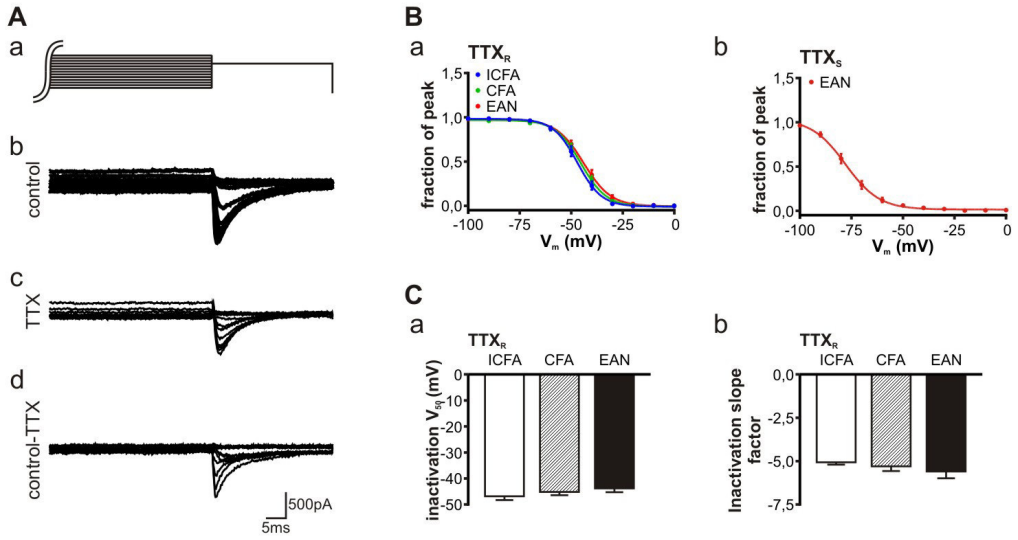

Fig. 22: Voltage dependence of steady state inactivation of TTX_R I_{NaT} is not altered in EAN DRGs. (A) The voltage dependence of steady state inactivation obtained by a depolarizing step to -10 mV preceded by prepulses to various potentials in a control neuron (CFA). The total Na^+ currents (Ab) were pharmacologically divided into a TTX_R component (Ac) and into a TTX_S current component (Ad). (B) Steady state inacitvation profiles of I_{NaT} TTX_R for EAN, CFA and ICFA rats (a), and of I_{NaT} TTX_S for the EAN group (b). Data are shown for cap^+ cells. There were no differences in the voltage dependence of inactivation of I_{NaT} TTX_R between the three groups. (C) Voltage of half maximal inactivation (a) and slope factor of steady state inactivation (b).

Total, TTX_S and TTX_R transient Na^+ current were also analyzed in cap^- DRG neurons of ICFA, CFA and EAN animal groups. Representative traces of the different types of Na^+ currents (I_{NaT}) of a cap^- control neuron (CFA) are shown in Fig. 23 A. The corresponding current voltage curves and analysis of peak current amplitudes revealed no changes in the magnitude of the total Na^+ current among the different treatment groups. Consistent with the cap^+ cells, cap^- cells of the EAN group tended to display increased TTX_S currents and decreased TTX_R transient Na^+ currents (ICFA: n=6; CFA: -n= 5; EAN: n=5) (Fig. 23 C). Statistical tests, however, failed to show significant changes between EAN neurons and the two different control groups (one-way ANOVA p=0.70, F=0.38, df=15 for TTX_R and p=0.09, F=2.84, df=15 for TTX_S).

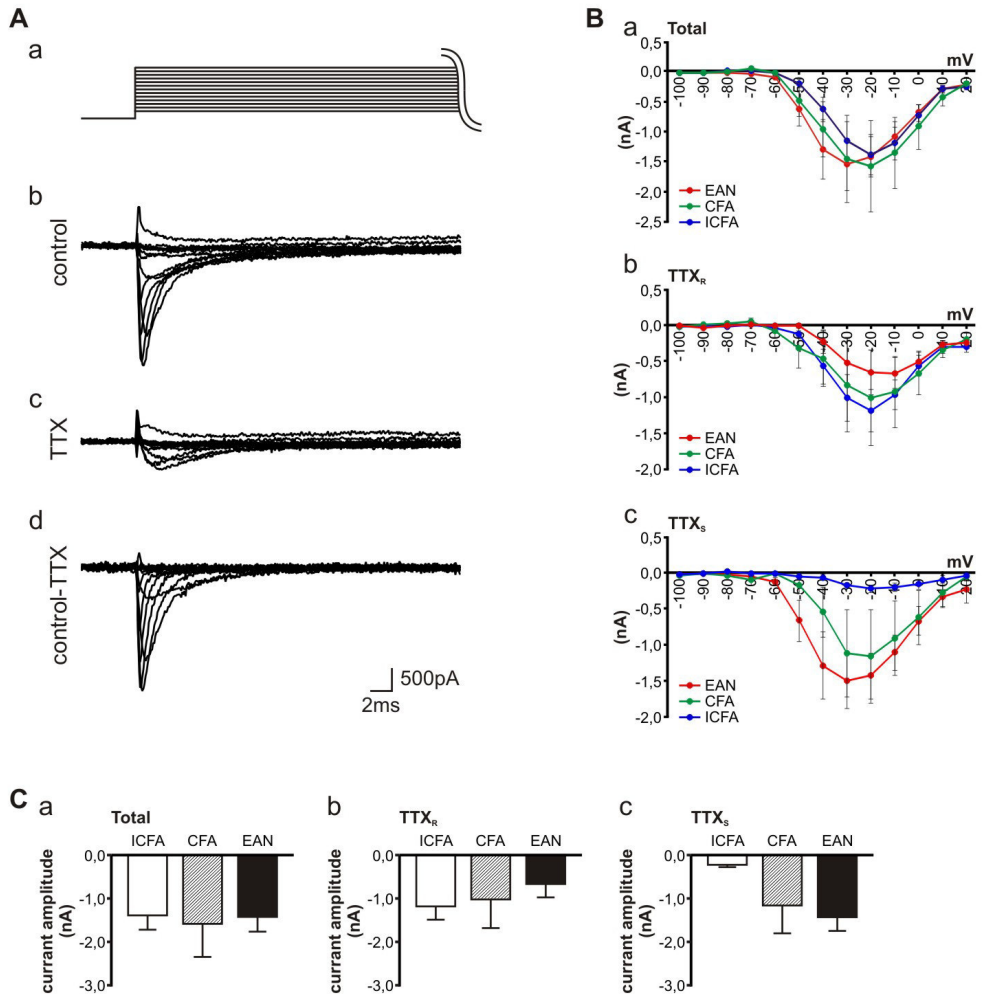

Fig. 23: Fast Na^+ currents are not altered in cap$^-$ cells of EAN rats. (A) Representative current traces recorded from a cap$^-$ control (CFA) cell. Total fast Na^+ currents (I_{NaT}) (Ab) were elicited by a standard voltage clamp protocol (Aa). By application of 1 µM TTX, total I_{NaT} was pharmacologically separated into a TTX_R current component (Ac), and by subtracting the TTX_R from the total Na^+ current, into a TTX_S current component (Ad). (B) Current voltage relationship for (a) total, (b) TTX_R and (c) TTX_S I_{NaT}. Data are shown for cap$^-$ EAN, cap$^-$ ICFA and cap$^-$ CFA cells. (C) Histograms showing total, TTX_R and TTX_S peak current densities at -20 mV of ICFA, CFA and EAN DRG neurons. (a) Total, (b) TTX_R and (c) TTX_S Na^+ current were not significantly altered in EAN rats.

3.1.8 Impact of EAN on persistent Na^+ currents in DRG neurons

Numerous studies have shown that DRG neurons express multiple different Na^+ channels (Kostyuk, Veselovsky et al. 1981; Caffrey, Eng et al. 1992), giving rise to transient (I_{NaT}) as well as persistent Na^+ currents (I_{NaP}). $Na_V1.3$ and Na_V 1.6 can produce TTX-sensitive I_{NaP} in DRG neurons. Na_V 1.9 and Nav1.8, on the other hand, give rise to TTX-resistant I_{NaP}, that can contribute to the long AP duration in small DRG neurons (Fang, Djouhri et al. 2006).

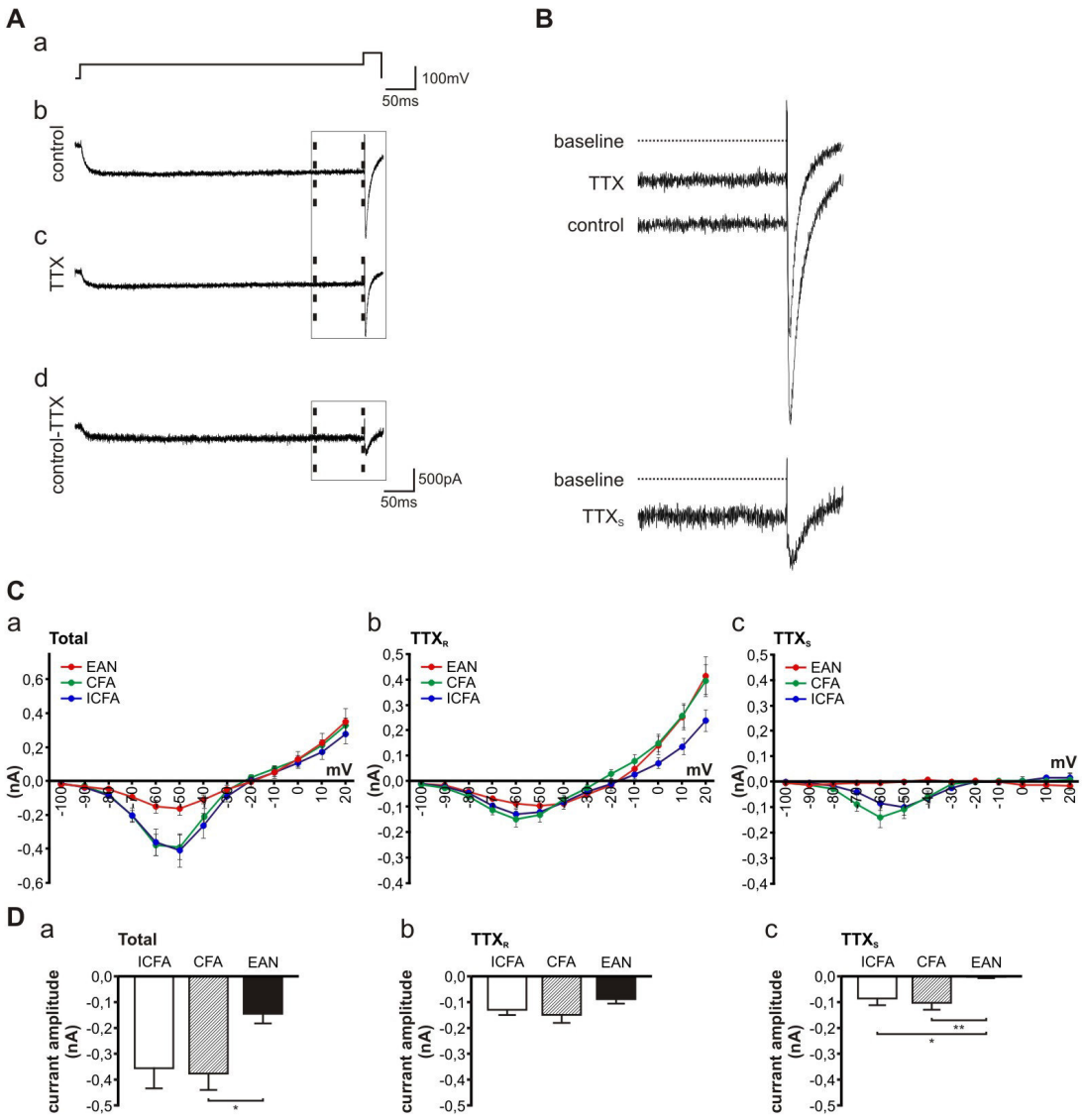

Fig. 24: I_{NaP} is reduced in DRG neurons of EAN rats. Peak persistent Na^+ currents were measured at the end of the 480 ms depolarizing voltage step of the same pulse protocol used for transient Na^+ currents. Representative current traces at -60 mV are shown for a cap^+ control (ICFA) cell (A). Total persistent Na^+ currents (b) were pharmacologically divided into TTX_R (c) and TTX_S (d) current components. (B) Magnification of the inset in (A). (C) Current voltage relationship for (a) total, (b) TTX_R and (c) TTX_S I_{NaP}. Data are shown for cap^+ EAN, ICFA and CFA cells. (D) Histograms showing total, TTX_R and TTX_S peak current densities at -60 mV of ICFA, CFA and EAN DRG neurons. (a) Cap^+ cells of EAN rats revealed a decrease in peak persistent Na^+ current compared to cap^+ control cells. This was due to a significant reduction of TTX_S I_{NaP}.

In our recordings, a persistent Na^+ current could in fact be observed at the end of the prolonged command potential in cap^+ as well as in cap^- DRG neurons. A representative trace of the total persistent Na^+ current (I_{NaP}) evoked by a -60 mV voltage step in a cap^+ control neuron (ICFA) is shown in Fig. 24 A. I_{NaP} could also be pharmacologically separated into TTX_S and TTX_R components. According to previous

studies (Baker and Bostock 1997) the current voltage curves show that the persistent Na^+ current activated at a quite hyperpolarized potential of -80 mV and reached a peak at -60 mV. Comparison of the three different treatment groups revealed a decrease in the peak current amplitude of the total persistent Na^+ current of cap^+ EAN neurons (n=15), that was significant compared to the CFA control group (n=21), but not to the ICFA control group (n=16) (one-way ANOVA p=0.03, F=3.77, df=51 followed by Tukey's multiple comparison test depicted as asterisks in Fig. 24 Da). Studying of the TTX_S and TTX_R current components showed that the decrease in the persistent Na^+ current in EAN neurons could be mainly explained by a reduction of I_{NaP} TTX_S. A significant reduction of the persistent TTX_S Na^+ current component of the EAN neurons (n=15) compared to ICFA (n=16) and CFA (n=21) was observed (since peak current response of EAN neurons was almost 0 pA, and variances were significantly different between the groups, the nonparametric ANOVA Kruskal-Wallis test was used p=0.0026 followed by Dunn's multiple comparison test depicted as asterisks in Fig. 24 Dc), where no changes could be detected for the TTX_R I_{NaP} (nonparametric ANOVA Kruskal-Wallis test p=0.23).

In addition, we measured the total, TTX_S and TTX_R persistent Na^+ current in cap^- DRG neurons of ICFA, CFA and EAN animal groups. There was a tendency of reduced I_{NaP} in EAN neurons, however, no significant changes in the peak current density (-60 mV) of the different persistent Na^+ current components was detected among the different treatment groups (Fig. 25) (ICFA n=8, CFA n=7, EAN n=7) (nonparametric ANOVA Kruskal-Wallis test p=0.14 for TTX_R I_{NAP} and p=0.67 for TTX_S I_{NaP}).

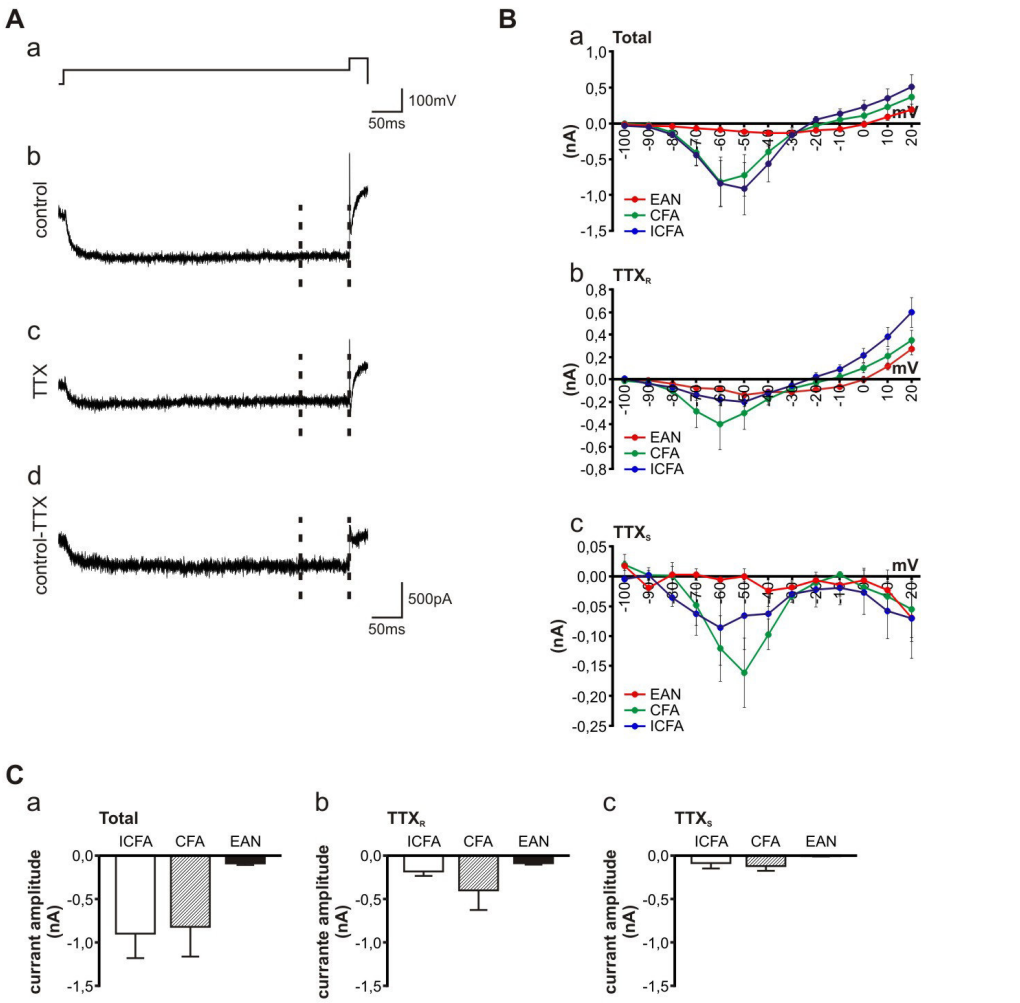

Fig. 25: I_{NaP} is not altered in cap$^-$ DRG neurons of EAN rats. Peak persistent Na^+ currents were measured at the end of the 480 ms depolarizing voltage step of the same pulse protocol used for transient Na^+ currents. Representative current traces at -60 mV are shown for a cap$^-$ control (ICFA) cell (A). Total persistent Na^+ currents (b) were pharmacologically divided into TTX_R (c) and TTX_S (d) current components. (B) Current voltage relationship for (a) total, (b) TTX_R and (c) TTX_S I_{NaP}. Data are shown for cap$^-$ EAN, ICFA and CFA cells. (C) Histograms showing that (a) total, (b) TTX_R and (c) TTX_S peak current densities at -60 mV of ICFA, CFA and EAN DRG neurons are not significantly different.

3.2 Partial sciatic nerve ligation

In the second part of this study we used partial sciatic nerve ligation (PNL) as animal model of neuropathic pain due to nerve trauma. Here, the sciatic nerve of female wild type (wt) as well as female $Ca_V3.2$ knock-out (KO) mice was partially ligated to study the function of T-type Ca^{2+} currents in supporting neuropathic pain.

3.2.1 Pain hypersensitivity in wild type mice after PNL

Since painful responses towards innocuous mechanical stimuli (mechanical allodynia) can indicate the development of neuropathic pain (Costigan, Scholz et al. 2009), PNL-mice (mice subjected to partial ligation of the sciatic nerve, see Materials and Methods 2.1.2) as well as sham operated mice were tested in the von Frey test for mechanical

allodynia. Baseline responses were similar in PNL- and sham-operated mice. The partial ligation of the right sciatic nerve induced mechanical allodynia in the ipsilateral hind paws, revealed by significantly decreased mechanical withdrawal thresholds a week after PNL compared to the basal value in the von Frey test (paired t-test, p=0.0007, t=5.72, df=7, n=8) (Fig. 26). The mechanical withdrawal responses in sham-operated mice remained unaffected (p=4.41, t=0.90, df=5, n=6).

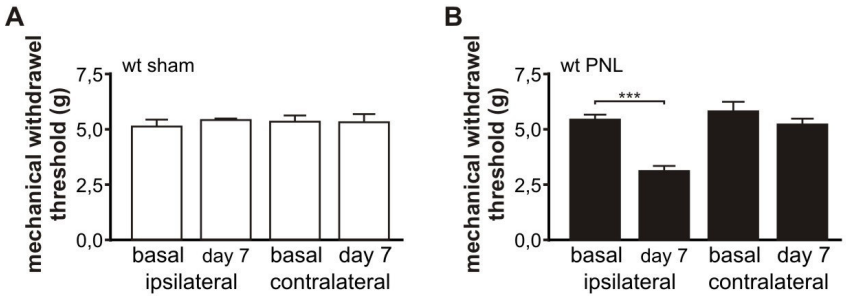

Fig. 26: Mechanical allodynia in PNL mice. The presence of PNL induced mechanical allodynia for animals used in the voltage clamp recordings was confirmed by the von Frey Filament test. Our results show a significant reduction of the paw withdrawal threshold (PWT) of the right side (ipsilateral, ligated) 7 days after surgery compared to the basal data measured before surgery. In contrast, PWTs of the left side (contralateral, non ligated) were not affected (B). Sham treatment did not affect the PWTs 7 days after surgery (A).

3.2.2 Up-regulation of T-type Ca^{2+} current in a subpopulation of nociceptive DRG neurons after PNL

Changes in T-type Ca^{2+} currents upon nerve injury has been quite controversial. T-type Ca^{2+} current has been shown to increase in small nociceptive DRG neurons of animal models of neuropathic pain due to chronic constrictive injury (CCI) and diabetic neuropathy (Jagodic, Pathirathna et al. 2007; Jagodic, Pathirathna et al. 2008). Other studies, however, reported a loss of the T-type current in DRG cells of animals after CCI (Hogan, McCallum et al. 2000). Due to these opposing results, we wanted to clarify the contribution of T-type currents of DRG neurons to the pathophysiology of neuropathic pain. For this, total Ca^{2+} currents were first recorded from small nociceptive DRG cells via a standard pulse protocol with voltage steps from -70 mV to +40 mV (10 mV increments). The total Ca^{2+} current can be divided into two main groups. The T-type Ca^{2+} currents activate by subthreshold membrane depolarization above -60 mV and display fast and almost complete inactivation. The HVA Ca^{2+} currents, on the other hand, show very slow inactivation (sustained current) during depolarizing test potentials. According to this, three different populations of DRG neurons were detected: a) cells rich in T-type (inactivating) Ca^{2+} current, b) cells with mixed HVA and T-type Ca^{2+} currents and c) cells exclusively with HVA Ca^{2+} current (Fig. 27).

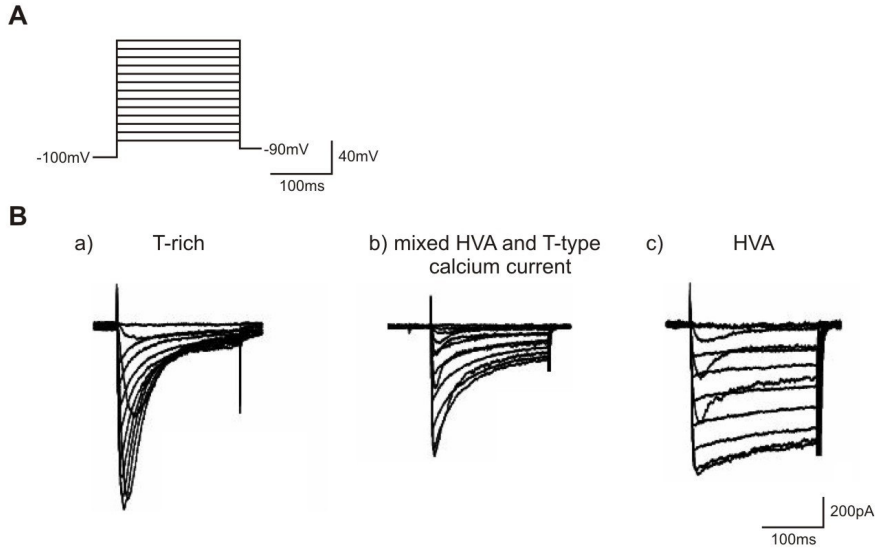

Fig. 27: Various types of Ca^{2+} currents in small sized DRG neurons. (A) Total Ca^{2+} currents were evoked in small (15 – 25 µm) nociceptive L_{4-5} DRG cells by using a standard pulse protocol with voltage steps from -70 mV to +40 mV (10 mV increments). (B) Different DRG neurons exhibited various types of Ca^{2+} currents: a) Example of a cell rich in T-type (inactivating) Ca^{2+} current, b) example of a cell with mixed HVA and T-type Ca^{2+} currents (note both inactivating and sustained component), c) example of a cell with a rather non-inactivating (sustained) HVA Ca^{2+} current.

In the next step we analyzed the HVA and T-type currents. The T-type Ca^{2+} current was quantified by subtracting the sustained current at the end of the depolarizing pulse from the peak current response at -30 mV, as T-type currents peak at this test potential (wt sham: n=13; wt PNL: n=20) (Fig. 28 A). For a more accurate analysis, the T-type current was isolated using a pre-pulse protocol (Fig. 28 B) (see Materials and Methods 2.5.7) (wt sham: n=6; wt PNL: n=16). With both methods, a significant increase in the T-type Ca^{2+} current in cap^+ DRG cells was found after PNL (unpaired t-test with Welch's correction p=0.0002, t=4.34, df=26; p= 0.0056, t=3.16, df=17 respectively) (Fig. 28 C,D). For cap^- neurons, on the other hand, the increase was not significant (wt sham: n=13; wt PNL: n=9) or (wt sham: n=9; wt PNL: n=5) (unpaired t-test p=0.50, t=2.08, df=20; p= 0.12, t=1.67, df=12 respectively).

Furthermore, a group of DRG cells with a high density of T-type current, called "T-rich cells", were only seen in cap^- cells under control conditions. Following nerve injury, T-rich cells have been observed in both the cap^+ as well as the cap^- groups (Table 3), but analysis of the distribution of "T-rich cells" cells by chi-squared test showed no differences between the groups.

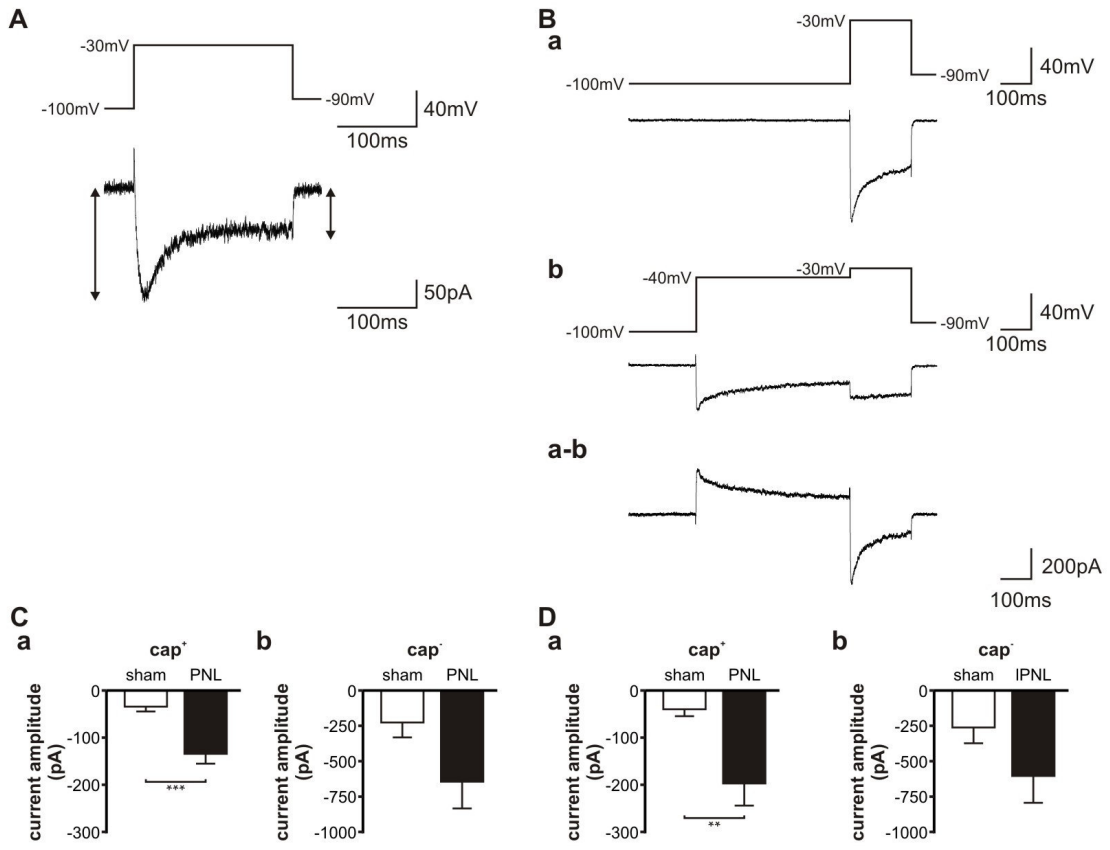

Fig. 28: The T-type Ca^{2+} current is up-regulated in PNL mice. The figure shows representative current traces recorded from a PNL cap^+ cell. The current was measured via two different pulse protocols. (A) Via a standard pulse protocol with voltage steps from -70 mV to +40 mV (10 mV increments), the T-type Ca^{2+} current was quantified by subtracting the sustained current at the end of the depolarizing pulse from the peak current response. Peak T-type current was measured at -30mV. (B) The second protocol used a preconditioning prepulse to isolate the T-type current based on the more hyperpolarized steady state inactivation of T-type Ca^{2+} current compared to HVA currents (see Materials and Methods 2.5.7). (C, D) With both methods we found a significant increase in the T-type Ca^{2+} current in small DRG cells after PNL. This increase was only seen in cap^+ cells. Statistical analysis were done using unpaired t-test.

Table 3: Subdivision of cap^+ and cap^- DRG neurons into "T-rich" cells and cells with mixed HVA and T-type Ca^{2+} current.

	cap^- sham	cap^+ sham	cap^- PNL	cap^+ PNL
"T-rich"	4	0	5	4
HVA or mixed HVA and T-type	14	13	9	22

Previous studies have shown a significant reduction of HVA Ca^{2+} current following axotomy (Abdulla and Smith 2001 b) and CFA induced inflammation (Lu et al. 2010). In this study, we also analyzed potential changes in HVA currents after PNL. The current was isolated by measuring the sustained current at the end of the depolarizing pulse at 0 mV, since HVA currents reach their peak at this test potential. Our results show, however, no significant changes in HVA Ca^{2+} current elicited at 0 mV after PNL in both cap^+ (wt sham: n=13; wt PNL: n=21) (unpaired t-test with Welch's correction p=0.061, t=2.01, df=17) and cap^- cells (wt sham: n=14; wt PNL: n=9) (unpaired t-test p=0.86, t=0.17, df=21) (Fig. 29).

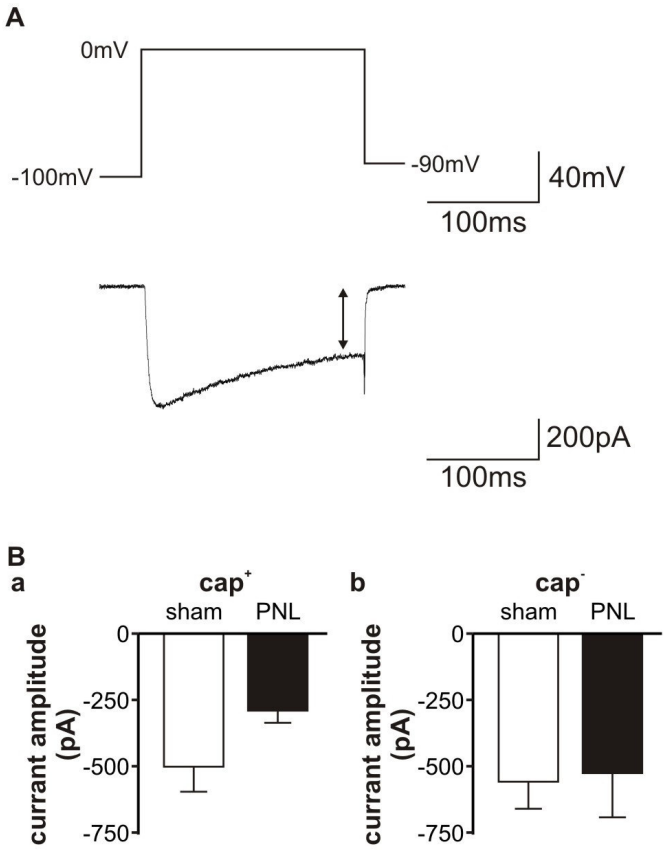

Fig. 29: The HVA Ca^{2+} current is not altered in DRG neurons of PNL mice. (A) Representative current trace recorded from a cap^+ control cell. The HVA current was analyzed by measuring the sustained current at the end of the depolarizing pulse to 0 mV. (B) There were no significant differences in the HVA current magnitude in small DRG neurons of PNL mice compared to sham operated animals.

Furthermore, we wanted to detect which of the three T-type channel isoforms underlies the current up-regulation in cap^+ cells after PNL. Due to the lack of specific blockers, we analyzed the sensitivity of the increased T-type current to Ni^{2+}. Only $Ca_V3.2$ channels are highly nickel sensitive (IC_{50} ~ 10 µM), while $Ca_V3.1$ and $Ca_V3.2$ are 20-fold less sensitive (Lee, Gomora et al. 1999). For this, DRG neurons of PNL and sham-operated mice were depolarized to voltage steps from -70 mV to +40 mV (10 mV increments) before and during application of 50 µM Ni^{2+}, and the T-type current was isolated as mentioned above from the Ni^{2+} sensitive as well as the Ni^{2+} resistant current components.

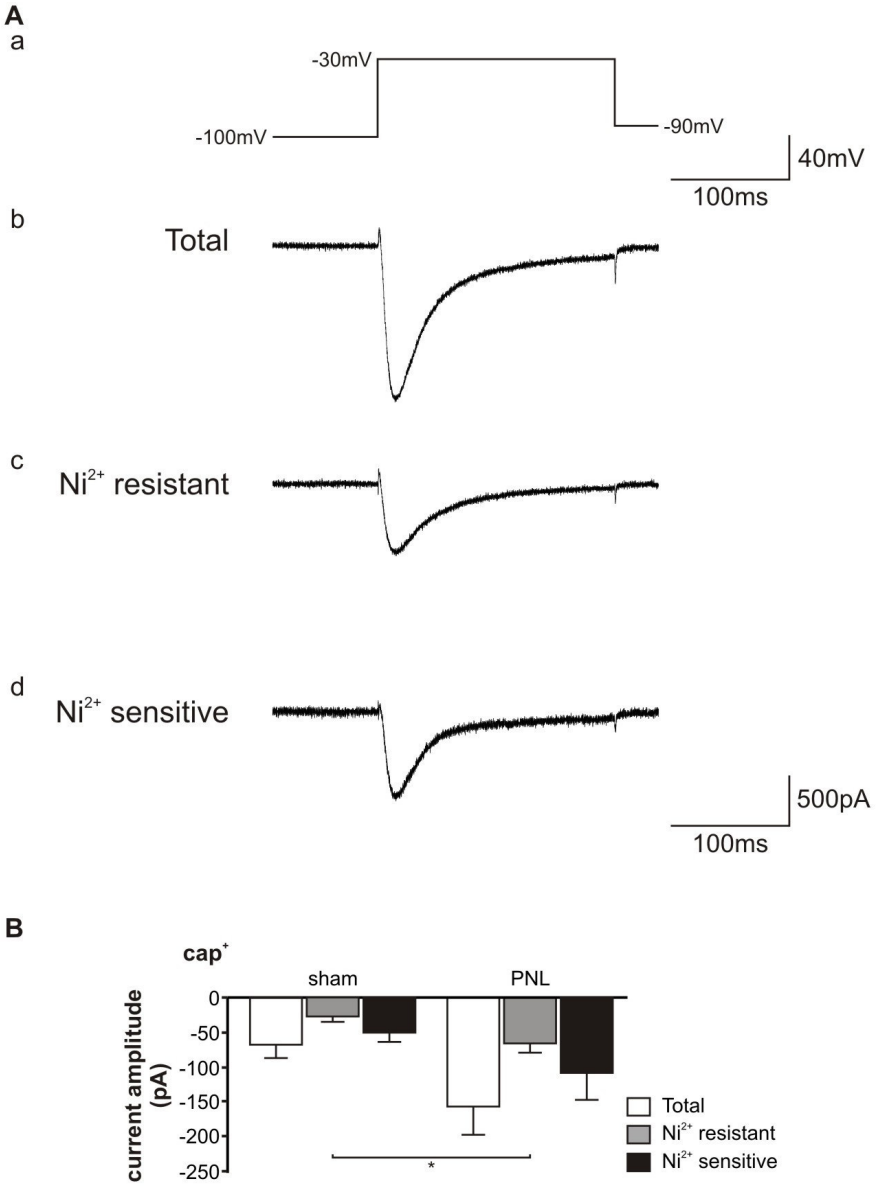

Fig. 30: The Ni^{2+} resistant T-type Ca^{2+} current is increased in PNL mice. (A) Representative current traces recorded from a PNL cap^+ cell. The total Ca^{2+} current was elicited by a standard voltage clamp protocol (Aa). By application of 50 µM Ni^{2+}, the total Ca^{2+} current (Ab) was pharmacologically separated into a Ni^{2+} resistant current component (Ac), and by subtracting the total Ca^{2+} current from the Ni^{2+} resistant current, into a Ni^{2+} sensitive current component (Ad). The Ni^{2+} sensitive/resistant T-type Ca^{2+} current were quantified by subtracting the sustained current at the end of the depolarizing pulse from the peak current response at -30 mV. (B) Histograms showing total, Ni^{2+} resistant and Ni^{2+} sensitive peak current densities at -30 mV of sham- and PNL-DRG neurons, where the Ni^{2+} resistant current component was significantly increased following PNL. Significant differences were detected via unpaired t-test.

Our results show, that Ni^{2+} blocked 74 % of the T-type current in DRG cells from control mice, and 69 % in DRG cells from PNL mice revealing the main T-type Ca^{2+} current component to be Ni^{2+} sensitive (Fig. 30). Nevertheless, we further compared

the Ni^{2+} sensitive (sham: n=10; PNL: n=13) and Ni^{2+} resistant (sham: n=10; PNL: n=14) T-type current components between sham operated and PNL mice. The analysis revealed a significant increase in the Ni^{2+} resistant current component after PNL (unpaired t-test with Welch's correction, p=0.028, t=2.41, df=17) (Fig. 30 B), whereas the Ni^{2+} sensitive component was unchanged (unpaired t-test with Welch's correction p=0.18, t=1.42, df=15). These data suggest that the up-regulation of T-Type Ca^{2+} currents in nociceptive cap^+ DRG neurons after PNL is mediated by an increase in one or both of the Ni^{2+} insensitive T-type subunits ($Ca_V3.1$ or $Ca_V3.3$).

3.2.3 $Ca_V3.2$ KO mice display normal neuropathic pain behavior after PNL

Our previous experiments revealed an up-regulation of the T-type Ca^{2+} current following PNL. This increase was due to an increase of the Ni^{2+} insensitive current component ($Ca_V3.1$ or $Ca_V3.3$). This stands in contrast to other studies, who suggested a role of the Ni^{2+} sensitive T-type Ca^{2+} isoform $Ca_V3.2$ in contributing to neuropathic pain (Bourinet, Alloui et al. 2005). In addition, $Ca_V3.2$ is the most abundant isoform of T-type Ca^{2+} channels in small DRG neurons (Talley, Cribbs et al. 1999). To verify our results and determine the role of the $Ca_V3.2$ Ca^{2+} channel isoform in supporting neuropathic pain, pain behavioral experiments were repeated in PNL and sham-operated $Ca_V3.2$ KO mice. As for the wt mice, the partial ligation of the right sciatic nerve induced mechanical allodynia (paired t-test, p=0.0001, t=8.30, df=7, n=8) (Fig. 31) in the ipsilateral hind paw of female $Ca_V3.2$ KO mice. The sham operation had no effect on the mechanical withdrawal responses (paired t-test, p=0.20, t=1.46, df=6, n=7).

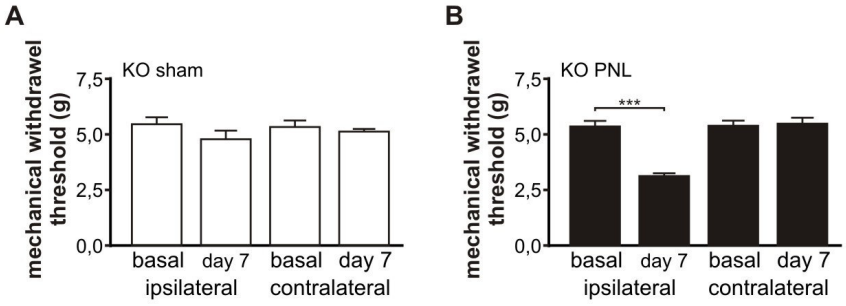

Fig. 31: Mechanical allodynia in $Ca_V3.2$ KO mice following PNL. The diagrams show a significant reduction of the paw withdrawal threshold (PWT) of the right side (ipsilateral, ligated) 7 days after surgery compared to the basal data measured before surgery in $Ca_V3.2$ KO mice subjected to PNL of the right sciatic nerve. In contrast, PWTs of the left side (contralateral, non ligated) were not affected (B). Sham treatment did not affect the PWTs 7 days after surgery in $Ca_V3.2$ KO mice (A). Significant differences were detected via a paired t-test.

3.2.4 The T-type Ca^{2+} current is up-regulated in $Ca_V3.2$ KO mice after PNL

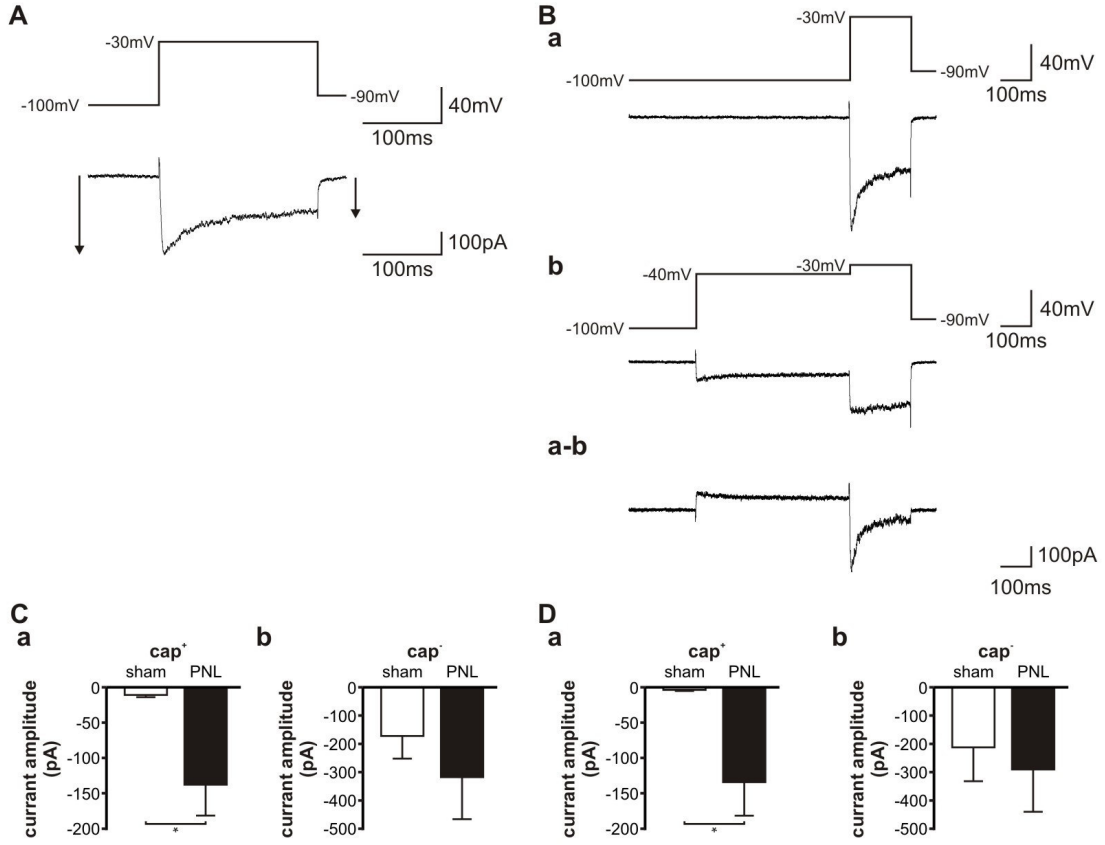

Fig. 32: T-type current is up-regulated in cap$^+$ neurons of $Ca_V3.2$ KO mice following PNL. The figure shows representative current traces recorded from a PNL cap$^+$ cell of $Ca_V3.2$ KO mice. The current was measured via two different pulse protocols. (A) Via a standard pulse protocol with voltage steps from -70 mV to +40 mV (10 mV increments), the T-type Ca^{2+} current was quantified by subtracting the sustained current at the end of the depolarizing pulse from the peak current response. Peak T-type current was measured at -30mV. (B) The second protocol used a preconditioning prepulse to isolate the T-type current based on the more hyperpolarized steady state inactivation of T-type Ca^{2+} current compared to HVA currents (see Materials and Methods 2.5.7). (C, D) Our results show a significant increase in the T-type current after PNL despite the lack of $Ca_V3.2$. This difference was observed using both quantification methods and only in cap$^+$ cells. Significant differences were detected via a paired t-test.

In the next step, we wanted to verify the hypothesis, that the T-type Ca^{2+} current up-regulation in cap$^+$ DRG-neurons after PNL is mediated by a Ni^{2+} insensitive T-type subunit. For this, Ca^{2+} current recordings were repeated in DRG cells of PNL and sham-operated $Ca_V3.2$ KO mice and the T-type current was quantified in the two different ways as described above. The T-type Ca^{2+} current amplitude of cap$^+$ DRG neurons was found to be quite small in untreated (sham operated) $Ca_V3.2$ KO mice (-10.6 pA ± 3.3, n=12 Fig. 32C or -3.8 pA ± 1.3, n=6 Fig. 32D) compared to wt mice (-39.7 pA ± 14.7 Fig. 28C), confirming the fact, that $Ca_V3.2$ is the predominant isoform of T-type channels in untreated nociceptive DRG neurons. After PNL (n=11),

however, a significant up-regulation of the T-type current was observed in cap$^+$ DRG cells (unpaired t-test with Welch's correction p=0.016, t=2.91, df=10 or p=0.021, t=2.75, df=10). For cap$^-$ neurons, no changes in T-type current densities were found in PNL KO mice (n=4) compared to untreated KO animals (n=7 or -n=4) (unpaired t-test p=0.37, t=0.95, df=9) (Fig. 32 C,D). However, the number of cap$^-$ cells were small and a higher number of cells might be needed to detect potential changes. Furthermore, no significant changes were found in HVA Ca^{2+} currents after PNL in both cap$^+$ (KO sham: n=11; KO PNL: n=10) (unpaired t-test p=0.49, t=0.70, df=19) and cap$^-$ cells (KO sham: n=6; KO PNL: n=4) (unpaired t-test with Welch's correction p=0.14, t=1.71, df=6) (Fig. 33).

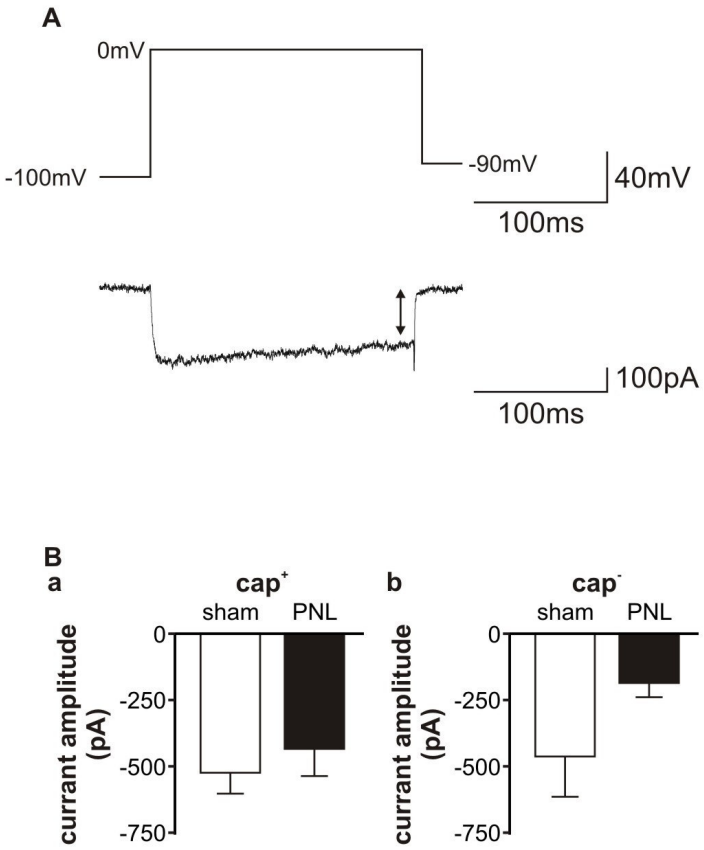

Fig. 33: The HVA Ca^{2+} current is not altered in DRG neurons of Cav3.2 KO mice following PNL. (A) Representative current trace recorded from a cap$^+$ control cell of Cav3.2 KO mice. The HVA current was analyzed by measuring the sustained current at the end of the depolarizing pulse to 0 mV. (B) There were no significant differences in the HVA current magnitude of small DRG neurons of Cav3.2 KO PNL mice compared to the KO sham operated animals.

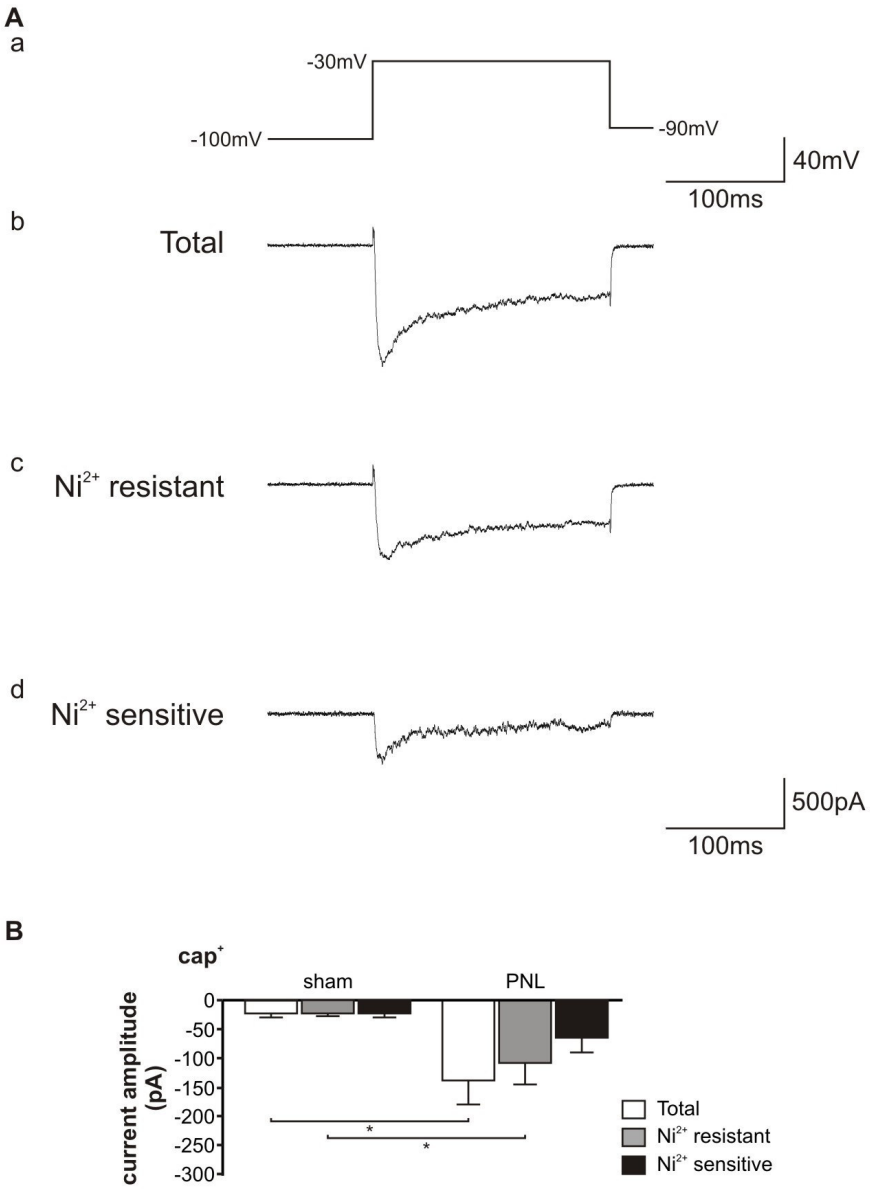

Fig. 34: The Ni^{2+} resistant T-type Ca^{2+} current of cap^+ cells is increased in $Ca_V3.2$ KO mice following PNL. (A) Representative current traces recorded from a PNL cap^+ cell of $Ca_V3.2$ KO mice. The total Ca^{2+} current was elicited by a standard voltage-clamp protocol (Aa). By application of 50 µM Ni^{2+}, the total Ca^{2+} current (Ab) was pharmacologically separated into a Ni^{2+} resistant current component (Ac), and by subtracting the total Ca^{2+} current from the Ni^{2+} resistant current, into a Ni^{2+} sensitive current component (Ad). The Ni^{2+} sensitive and resistant T-type Ca^{2+} currents were quantified by subtracting the sustained current at the end of the depolarizing pulse from the peak current response at -30 mV. (B) Histograms showing total, Ni^{2+} resistant and Ni^{2+} sensitive peak current densities at -30 mV of sham- and PNL-cap^+ DRG neurons of $Ca_V3.2$ KO mice. The Ni^{2+} resistant current component was significantly increased following PNL (unpaired t-test).

Furthermore, we wanted to detect which of the three T-type channel isoforms underlies the current up-regulation in cap^+ cells after PNL of $Ca_V3.2$ KO mice. Hence, we analyzed the sensitivity of the increased T-type current to Ni^{2+} as previously described

and isolated the Ni^{2+} sensitive and the Ni^{2+} resistant T-type current components. A comparison of the Ni^{2+} sensitive and Ni^{2+} resistant T-type current components between sham-operated and PNL $Ca_V3.2$ KO mice (KO sham: n=9; KO PNL: n=8), showed a significant increase in the Ni^{2+} resistant current component after PNL (unpaired t-test with Welch's correction p=0.046, t=2.43, df=7), whereas there was no difference in the Ni^{2+} sensitive current component (unpaired t-test with Welch's correction p=0.13, t=1.71, df=7) (Fig. 34). These data confirm that the up-regulation of T-type Ca^{2+} currents in nociceptive cap^+ DRG neurons after PNL is mediated by a Ni^{2+} insensitive T-type subunit ($Ca_V3.1$ or $Ca_V3.3$).

To answer the question whether $Ca_V3.2$ KO mice differ in pain behavior from wt mice, we compared the mechanical withdrawel responses obtained in the von Frey test of the ipsilateral hind paw of both groups 7 days following PNL. The partial ligation of the right sciatic nerve induced mechanical allodynia in $Ca_V3.2$ KO mice (n=8) and wt mice (n=8) to the same extent as seen in Fig. 35, which was also confirmed by the lack of significant differences between both groups (unpaired t-test, p=0.97, t=0.035, df=14). Also, a comparison of the increased T-type Ca^{2+} current observed following PNL in both wt and $Ca_V3.2$ KO mice revealed no significant differences between both groups (unpaired t-test with Welch's correction p=0.94, t=0.071, df=14) (Fig. 35). This implies that most probably the increased T-type current observed in $Ca_V3.2$ KO mice and their wt littermates following nerve injury is mediated by the same T-type channel isoform/isoforms and is not due to $Ca_V3.2$.

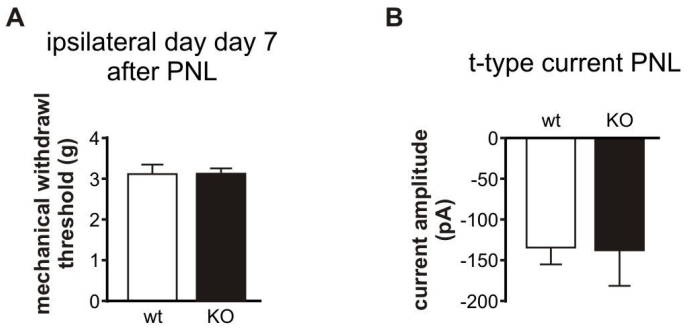

Fig. 35: Mechanical allodynia and T-type current are not different between wt and $Ca_V3.2$ KO mice following PNL. (A) Mechanical withdrawal responses of the ipsilateral hind paw of wt and $Ca_V3.2$ KO mice are similar 7 days following PNL. (B) The increase in T-type Ca^{2+} current following PNL is similar in both wt and $Ca_V3.2$ KO mice.

3.2.5 $Ca_V3.2$ T-type Ca^{2+} channel expression following PNL

So far, our results suggested that neuropathic pain resulting from peripheral nerve injury is paralleled by an increase of the T-type Ca^{2+} current in nociceptive cap^+ DRG neurons. Pharmacological analysis implied that this effect is not mediated by the $Ca_V3.2$ isoform, which is highly expressed in wild-type nociceptive DRG neurons, but by a Ni^{2+} insensitive T-type subunit ($Ca_V3.1$ or $Ca_V3.3$). These results were confirmed by analyzing the expression of the mRNA for the $Ca_V3.2$ T-Type channel isoform in L_{4-5} DRG neurons following PNL by SYBR green qRT-PCR. We compared the

mRNA expression at five time points (*1 d*, 3 *d*, *7 d*, *10 d*, *14 d*) following partial nerve ligation to time matched tissue acquired from sham control mice. As internal control we used expression data obtained for the neuron specific protein synaptophysin (SYP). The results are presented in Fig. 36 showing that at all time points in tissue collected after PNL the $Ca_V3.2$ T-type Ca^{2+} channel mRNA expression was not significantly different compared to expression in sham controls. This data show that the mRNA expression of the $Ca_V3.2$ channel α-subunit remains stable during 14 days following nerve injury, thus, confirming our hypothesis, that the T-type current increase is mediated by a Ni^{2+} insensitive subunit.

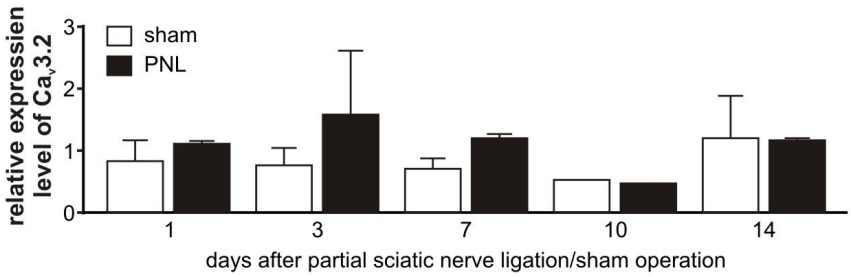

Fig. 36: $Ca_V3.2$ T-type Ca^{2+} channel expression is not altered in PNL mice. Lumbar DRGs (L_{4-5}) were dissected from PNL and sham mice 1, 3, 7, 10 and 14 days after surgery. The mRNA expression of the $Ca_V3.2$ T-type channel isoform was analyzed by qRT-PCR (performed in triplicate) using SYBR Green Master Mix reagents. The experiment shows no difference in the $Ca_V3.2$ expression level in the PNL mice compared to the sham animals at any time after surgery.

3.2.6 Reduced threshold of AP firing in a subpopulation of nociceptive DRG neurons after PNL

In a variety of animal models of chronic pain, the hyperexcitability of primary afferent nociceptors has been linked to the alteration of ion channel expression (Wood 2000; Cervero and Laird 2003). Furthermore, in an animal model of streptozotocin-induced diabetic neuropathy, the hyperexcitability observed in medium sized DRG neurons was paralleled by an increase in T-type currents (Jagodic, Pathirathna et al. 2007). For this, we performed current clamp experiments to determine possible differences in the electrophysiological properties of action potentials between DRG neurons of PNL and control mice that might be correlated to the observed increase in the T-type Ca^{2+} current after PNL. DRG cells of PNL and control mice generated overshooting action potentials with the characteristic inflection in the falling phase, which are followed by a long lasting afterhyperpolarization (AHP, Fig. 37 A). In cap^+ cells, analysis of action potential parameters revealed a significant reduction of the AP threshold in PNL animals (n=8) compared to control cells (n=8) (unpaired t-test, p=0.0281, t=2.448, df=14) (Fig. 37 B). Other action potential parameters did not vary significantly between PNL and control animals (Fig. 37 A,B). Also, none of the cells of the control or the PNL group showed an afterdepolarizing potential (ADP).

In cap^- cells the AP amplitude was increased after PNL (unpaired t-test, p=0.0377, t=2.656, df=6) (Fig. 38, control: n=4; PNL: n=4), but the significance is doubtful due

to the small number of cells. Other action potential parameters did not vary significantly between PNL and control animals.

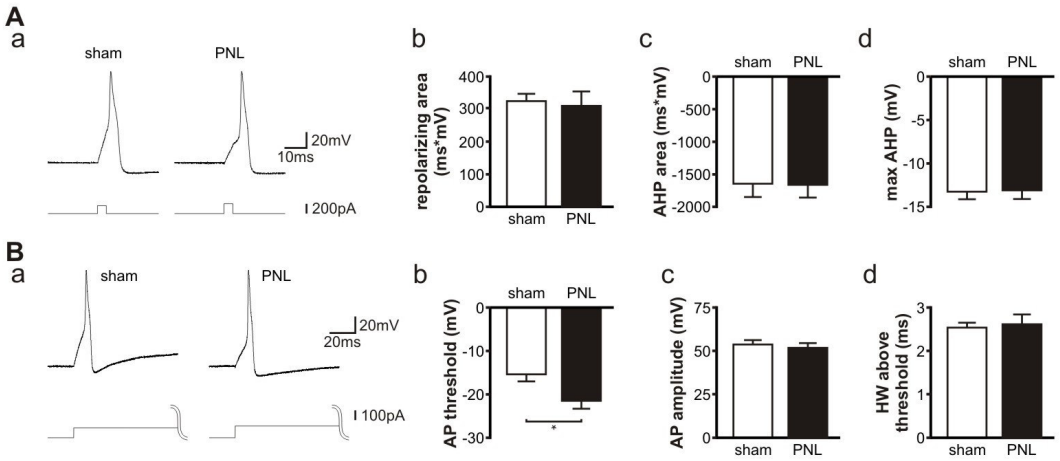

Fig. 37: The action potential threshold is reduced in cap$^+$ nociceptors from wt PNL mice. (Aa) Examples of APs evoked in DRG neurons of sham and PNL-operated mice by injection of 4 ms depolarizing current commands of increasing amplitude. (Ab-d) Comparison of the repolarizing area, AHP area and max. AHP showed no differences between PNL DRG neurons and control neurons. (Ba) Examples of the first AP evoked in cap$^+$ DRG neurons of sham and PNL-operated mice by injection of 500 ms depolarizing current command of increasing amplitude. (Bb) Histograms showing that the AP threshold is significantly reduced in cap$^+$ PNL DRG cells compared to cap$^+$ controls. (Bc-d) Other action potential parameters were not altered.

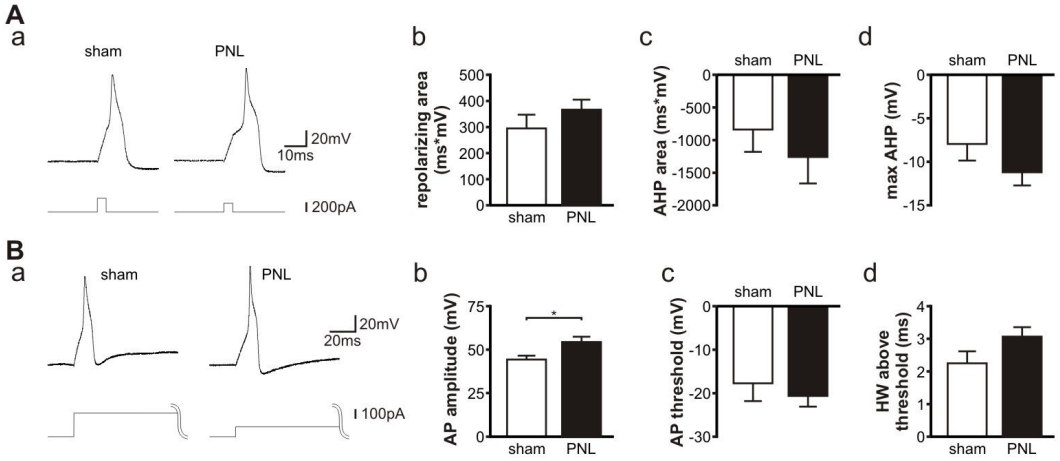

Fig. 38: The action potential amplitude is increased in cap$^-$ nociceptors from wt PNL mice. (Aa) Examples of APs evoked in cap$^-$ DRG neurons of sham and PNL-operated mice by injection of 4 ms depolarizing current command. (Ab-d) Comparison of the repolarizing area, AHP area and max. AHP showed no differences between PNL DRG neurons and control neurons. (Ba) Examples of the first AP evoked in cap$^-$ DRG neurons of sham and PNL-operated mice by injection of 500 ms depolarizing current commands of increasing amplitude. (Bb) Histograms showing that the AP amplitude is significantly increased in cap$^-$ PNL DRG cells compared to cap$^-$ control cells. The result is doubtful due to the small number of analyzed cells. (Bc-d) Other Action potential parameters were not altered.

In summary, the increase of the Ni^{2+} resistant T-type current component in cap^+ DRG neurons after PNL is associated with a lowering of the AP threshold in the same subgroup of cells. The reduced AP threshold is likely to contribute to a hyperexcitability of cells of this group and may be associated to neuropathic pain behavior.

The difference in AP parameters observed between DRG cells of PNL and sham-operated mice was not explained by treatment differences in cell capacitance (C_m), input resistance (R_{in}), or resting potential (RMP) for cap^+ cells or cap^- cells (Fig. 39).

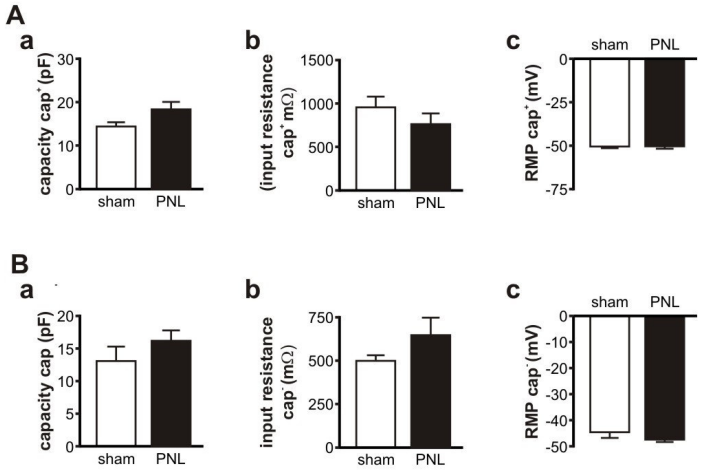

Fig. 39: Passive membrane properties of small cap^+ and cap^- DRG neurons. There were no significant differences between PNL and control cap^+ DRG neurons (A) or cap^- DRG neurons (B) with respect to the capacitance, input resistance and resting membrane potential.

4 Discussion

4.1 Experimental autoimmune neuritis

Abnormal sensory phenomena including spontaneous pain, hyperalgesia, and allodynia are associated with human peripheral demyelinating neuropathies such as GBS. 54-84% of patients with GBS suffer moderate to severe pain (Asbury 1990). The mechanism underlying pain symptoms in GBS is not yet understood (Rasminsky 1981; Carter et al. 1998). We used EAN, an animal model of GBS (Hahn 1996), to study possible mechanisms underlying pain hypersensitivity.

4.1.1 Clinical and pathological features of EAN

EAN rats developed mild to modest motor deficits, which were accompanied by weight loss and followed by spontaneous recovery. Histological analysis of the sciatic nerves showed significant demyelination and axonal loss at peak severity, indicating that demyelination as well as axonal pathology might play a role in the observed disability. Furthermore, behavioral testing of neuropathic pain behavior demonstrated that animals with active EAN developed significant mechanical allodynia. The onset of increased pain responses preceded the onset of motor deficits and remained till the end of the experiments (day 28 post-immunization), even after other clinical signs had disappeared. An increased nociceptive sensitivity either with the same onset as motor deficits (Moalem-Taylor et al. 2007) or before the onset of neurological signs (Luongo et al. 2008; Zhang et al. 2008) was demonstrated in previous studies. However, in these studies pain symptoms recovered completely with regression of motor deficits or later on (Moalem-Taylor, Allbutt et al. 2007; Zhang, Zhang et al. 2008). As we did not perform mechanical pain testing longer than day 32 we cannot exclude the possibility that EAN rats in our experiments could have also recovered later on. Nevertheless, a recent prospective cohort study in 156 patients with GBS reported that not only approximately 2/3 of patients suffer moderate to severe pain in the acute phase, but 1/3 experienced pain before the onset of weakness and 1/3 reported maintenance of pain after 1 year, resembling the results of our study (Ruts, Drenthen et al. 2010). Since the EAN animals experienced motor deficits, this may have impacted their ability to produce a withdrawal response. However, we have not observed a significant increase in mechanical thresholds at disease peak (Fig. 12, day 14-17). The clinical and pathological alterations observed in our animal model are characteristic for EAN and in agreement with previous studies (Hahn 1996; Bechtold et al. 2005; Moalem-Taylor, Allbutt et al. 2007; Meyer zu Horste, Hu et al. 2008), that described close similarities between EAN and AIDP making EAN a good model for studying the mechanisms underlying pain in GBS.

As pain symptoms follow a different time course and display a lack of recovery in contrast to motor deficits it is unlikely that both underlie the same pathophysiological mechanism. Several mechanisms could explain the increased pain sensitivity in EAN animals. A previous study showed that focal lysolecithin-induced demyelination of peripheral afferents led to neuropathic pain due to spontaneous action potentials in afferents and central sensitization of sensory processing (Wallace et al. 2003). Axonal degeneration has also been associated with pain. Another study could show, that

delaying Wallerian degeneration attenuated neuropathic pain behavior in mice (Ramer et al. 1997). Also, degeneration of myelinated efferent fibers induced spontaneous activity in uninjured C-fiber afferents as well as mechanical hyperalgesia in animals (Wu et al. 2002). In our experiments, pain sensitivity was observed early in the disease (day 6 post-immunization) before the start of motor deficits and therefore before severe demyelination or axonal degeneration was expected to take place, keeping it unlikely that allodynia resulted from EAN-induced structural changes in peripheral nerves. However, since our histological analysis were performed at peak severity (day 15 post-immunization), we cannot exclude the probability that structural changes might have occurred early in the disease. Nevertheless, a previous study found no histological changes of the sciatic nerves collected from EAN rats early in the disease (day 10 post-immunozation) before clinical signs started to appear (Hahn et al. 1991). We therefore hypothesized, that neuropathic pain in EAN animals is associated with altered functional properties of primary sensory neurons. To verify this hypothesis, we analyzed isolated nociceptive DRG in the whole-cell mode of the patch clamp technique starting on day 21 post-immunization for 10 days. We chose this time period to ensure that mechanical allodynia reached a stable level and the EAN animals reached a chronic pain state.

4.1.2 Complexity of DRG neuron classification

Isolated DRG neurons represent more than 25 functionally diverse afferent populations that are responsible for a variety of sensory events (Petruska, Napaporn et al. 2000). Among these neurons are the nociceptors, that are also composed of highly specialized sub-populations (Yoshida and Matsuda 1979; Lawson et al. 1985; Harper and Lawson 1985 a; Silverman and Kruger 1988; Petruska, Napaporn et al. 2000). These include Aβ high-threshold mechanoreceptors (HTM), Aδ HTM, Aδ polymodal nociceptors (PMN), Aδ mechanoheat (MH) nociceptors, Aδ cold nociceptors, C HTM, C PMN, C MH nociceptors, C heat nociceptors, C chemonociceptors, and Aδ and C "silent" nociceptors (Petruska, Napaporn et al. 2000). The identification of these specific subgroups has been shown to be quite difficult. Nevertheless, a previous study identified nine sub-groups of acutely dissociated DRG neurons that were classified according to their voltage activated current patterns, as well as their histochemical phenotype (IB_4-binding, immunoreactivity for substance P and calcitonin gene-related peptide (CGRP)), algesic profile (capsaicin, protons, ATP) and AP features (duration, AHP) (Petruska, Napaporn et al. 2000). DRG cells with diameters ranging from 16-45 μm were used in this study, where it was mentioned that taking cell size into account would have simplified sub-group identification. In our study, DRG neurons were classified according to the size, capsaicin sensitivity as well as IB_4-binding capacity. Three different treatment groups were used in our experiments, so that further classification would have made the comparison between the groups quite complicated. Furthermore, EAN induced changes in AP morphology as well as voltage activated currents were analyzed in this study, making it difficult to use these parameters for cell identification. Hence, we were not able to reveal the rich diversity of nociceptors, where each sub-group might have a distinct functional role. EAN might be incorporated in more pronounced changes of nociceptive neurons that we were not able to identify.

4.1.3 Functional findings

In the next step, we analyzed primary nociceptive neurons for alterations in their functional properties that might be associated to the EAN induced neuropathic pain. Our results demonstrate that EAN causes a significant reduction in AP duration of nociceptive DRG neurons due to a reduction of the prominent shoulder in the repolarization phase. Nociceptive neurons of EAN rats also exhibited signs of enhanced excitability such as lower rheobase and higher frequency of evoked AP discharge. These alterations were only found in a subtype of DRG neurons that display sensitivity to capsaicin, which is a selective marker for heat nociception (Snider and McMahon 1998; McCleskey and Gold 1999; Petruska, Napaporn et al. 2000; Caterina and Julius 2001; Vulchanova et al. 2001). Such changes in the intrinsic membrane properties of DRG neurons could explain the persistence of chronic pain observed in EAN rats. The decrease in rheobase and increase in firing frequency did not attain statistical significance with one of the control groups (CFA). A high variability of firing behavior has been observed among the cells of the same treatment group which might have reduced the sensitivity of statistical analysis. This could be due to the fact that despite of classifying the cells according to their capsaicin-sensitivity and IB_4-binding ability, we cannot exclude that our subgroups are still not completely homogenous as previously discussed.

An increased excitability and reduced current threshold has been also demonstrated in other studies which analyzed the response of DRG cells to nerve injury or inflammation (Zhang, Donnelly et al. 1997; Zhang et al. 1999; Abdulla and Smith 2001 a; Weng et al. 2012). Our results regarding altered spike width are also in agreement with other studies, showing shorter AP duration in C and Aδ-fibers following CFA induced peripheral inflammation (Djouhri and Lawson 1999). Consistantly, Oyelese and Kocsis (Oyelese and Kocsis 1996) reported that sciatic nerve damage caused a decrease in the proportion of cutaneous afferent neurons with an inflection in the repolarizing phase of their APs. On the contrary, peripheral nerve axotomy caused broadening of the AP in small nociceptive neurons (Abdulla and Smith 2001 a). Although the different animal models are applied for investigation of pathological pain, they differ in pathogenesis. The EAN model is a combination of peripheral nerve injury and peripheral inflammation (Moalem-Taylor, Allbutt et al. 2007).

Several previous studies have observed no changes in passive membrane properties of DRG neurons of neuropathic pain models (Czeh et al. 1977; Gurtu and Smith 1988; Petersen et al. 1996; Study and Kral 1996). In the present study, resting membrane potential as well as input resistance were unaffected by EAN. A small difference was observed in the capacity of EAN neurons compared to one of the control groups. Since the difference was small and the input resistance was similar between the groups, we conclude that observed changes in AP properties of EAN DRG neurons are not explained by differences in the passive membrane properties. Therefore, we hypothesized that alterations of active currents are responsible for such changes. Consequently, we investigated alterations of TTX_R and TTX_S Na^+ currents, since several lines of evidence have implicated the role of these channels in injury-induced increase in excitability. Indeed, our results show a nerve injury induced switch in Na^+

channels that were seen in the same subpopulation of DRG neurons, where changes of firing properties have been perceived. Although the total transient Na^+ current was unchanged in EAN neurons, the proportion of TTX_R and TTX_S Na^+ currents was dramatically altered. The fast TTX_S Na^+ current was clearly up-regulated in EAN animals, while the fast TTX_R Na^+ current tended to be down-regulated. In control DRG neurons, the TTX_R transient Na^+ current was 3 times as large as the TTX_S current (Fig. 19) which is in agreement with previous studies showing that TTX_R Na^+ current plays the dominant role as it carries most of the total charge during the action potential, from the approach to threshold to the shoulder on the falling phase (Blair and Bean 2002). In EAN DRG, however, TTX_S Na^+ current underlay the majority of the transient inward Na^+ current. This switch in Na^+ currents was also clearly demonstrated in the significantly faster inactivation kinetics of the total transient Na^+ current, reflecting the predominant role of the fast TTX_S Na^+ current in EAN DRG.

Additionally, our results show a reduction in the magnitude of the total persistent Na^+ current of EAN neurons that could be mainly explained by a decrease of the persistent TTX_S current (TTX_S I_{NaP}). Since the persistent Na^+ current does not inactivate during the course of the action potential, the overall decrease in I_{NaP} can explain the reduced hump or shoulder found in EAN neurons. Furthermore, in EAN animals the total transient Na^+ current is composed primarily of a rapidly inactivating TTX_S component in contrast to the control neurons, where the TTX_R current underlies the majority of the I_{NaT} (Fig. 19 C). Consequently, the switch in the composition of total I_{NaT} should result in a rapid inactivation of the transient Na^+ current during electrogenesis, which would produce narrow action potentials. Consistently, the nerve injury induced reduction in the shoulder of the AP observed by Oyelese and Kocsis (Oyelese and Kocsis 1996) in cutaneous afferent neurons was associated with a decrease in the expression of slowly inactivating TTX_R Na^+ current in the subset of neurons (Oyelese, Rizzo et al. 1997). The reduced hump or shoulder results in a faster repolarization of the AP, thus allowing another AP to be fired sooner, consequently leading to repetitive firing at higher than normal frequencies. A decrease in AP duration during peripheral inflammation was also associated with an increase in firing frequency in nociceptive fibers (Djouhri and Lawson 1999).

At depolarized potentials, high frequency firing of intact DRG neurons is mediated by the high threshold, rapidly repriming TTX_R channels as seen from the absence of repetitive firing in small DRGs from $Na_V1.8$ knockout mice (Renganathan, Cummins et al. 2001). In contrast, our results indicate that hyperexcitability, which is believed to underlie pain hypersensitivity in EAN rats, is attributable to an increase in the TTX_S current. Similarly, the ectopic discharges and mechanical allodynia in an animal model of neuropathic pain due to PNL were prevented by low doses of TTX (Lyu et al. 2000; Liu et al. 2001), demonstrating the primary role of TTX_S currents in supporting high frequency firing in neuropathic pain. Furthermore, Kapoor et al. demonstrated that the ectopic firing of primary afferent axons at sites where demyelination took place is triggered by intrinsic TTX-sensitive membrane potential oscillations (Kapoor et al. 1997). In this regards, previous findings have implicated the importance of voltage-sensitive oscillations for sustained spiking both at resting membrane potential and on depolarization in DRGs. Following nerve injury, the proportion of neurons showing

subthreshold oscillations and hence generating ectopic firing were increased. It has been proposed, that the transient TTX_S Na^+ channels play a crucial role in generating the depolarizing limb of subthreshold oscillations. Oscillatory behavior and ectopic spiking were eliminated by $[Na^+]o$ substitution or bath application of lidocaine or tetrodotoxin (TTX), confirming the important role of TTX_S in injury-induced hyperexcitability (Amir et al. 1999). These findings provide a possible explanation of the increased excitability in EAN DRG neurons, where the increase in TTX_S current might lead to an increase of subthreshold oscillations.

The increase in TTX_S current can account for the slightly faster rise time of the AP of the EAN nociceptive neurons. Although it is expected that enhanced TTX_S current should also lead to an alteration of AP threshold, we did not detect any changes in this AP parameter. However, a computer simulation showed that the increase in transient Na^+ conductance can lead to a modest reduction of single AP threshold, but a facilitation of resonance and repetitive spiking (Matzner and Devor 1992). This finding raises the possibility, that the increase in TTX_S Na^+ current might not directly influence the AP threshold. In addition, the results of the electrophysiological measurements might have been influenced by the process of DRG dissociation as will be discussed later.

DRG neurons possess a mixture of Na^+ channel isoforms (Caffrey, Eng et al. 1992; Black, Dib-Hajj et al. 1996), where $Na_V1.7$, $Na_V1.6$, $Na_V1.3$, $Na_V1.2$ and $Na_V1.1$ channel isoforms underlie the TTX_S current, and $Na_V1.8$ and $Na_V1.9$ the TTX_R current (Waxman et al. 1994; Black, Dib-Hajj et al. 1996; Felts, Yokoyama et al. 1997; Cummins et al. 1999; Herzog et al. 2001; Djouhri et al. 2003). The changes of TTX_S and TTX_R currents observed in the DRG neurons of EAN animals are similar to those described in other studies using different chronic pain models. In this regards, chronic constriction injury (CCI) and axotomy of the sciatic nerve are associated with a down-regulation of slowly inactivating TTX_R $Na_V1.8$ and $Na_V1.9$ and an up-regulation of the fast-inactivating/rapidly repriming TTX_S isoform $Na_V1.3$ in nociceptive DRG neurons (Waxman, Kocsis et al. 1994; Dib-Hajj; Cummins and Waxman 1997; Dib-Hajj, Tyrrell et al. 1998; Cummins, Black et al. 2000; Kim, Oh et al. 2002). The $Na_V1.3$ isoform is normally only expressed during early stages of development and is undetectable in the adult rat nervous system (Beckh, Noda et al. 1989; Waxman, Kocsis et al. 1994; Felts, Yokoyama et al. 1997). Similarly, transient demyelination of peripheral afferents is associated with a decrease in expression of TTX_R $Na_V1.8$ channels and an increase in expression of TTX_S $Na_V1.3$ of formerly myelinated DRG neurons. These changes in Na^+ channels were accompanied by spontaneous action potentials in afferent fibers (Wallace, Cottrell et al. 2003). Consistently, both an increase in fast TTX_S currents in parallel with an increased expression of $Na_V1.3$ and $Na_V1.7$ in DRGs has been also observed in models of inflammatory pain due to carrageenan injection (Black, Liu et al. 2004). However, in contrast to mechanical nerve injury, carrageenan injection results also in an increased TTX_R currents (Tanaka et al. 1998; Black, Liu et al. 2004). Similarly, the level of $Na_V1.9$ mRNA in DRG neurons is significantly increased in the CFA model (Tate et al. 1998). In the current study, we found no sings for changes in the TTX_R persistent Na^+ current that is most probably elicited by $Na_V1.9$ in EAN rats. The lack of contribution of $Na_V1.9$ seems to

be in agreement with a previous report, showing that knock-down of this Na^+ channel did not affect thermal or mechanical hypersensitivities following spared nerve injury (SNI) or partial nerve ligation (PNL) (Priest et al. 2005; Amaya et al. 2006).

More than one isoform might contribute to the EAN induced increase in the fast TTX_S component. Of particular interest is the significant increase in the expression of $Na_V1.3$ mRNA and protein level that has been observed in a range of neuropathic pain models and conditions (Waxman, Kocsis et al. 1994; Dib-Hajj, Black et al. 1996; Dib-Hajj et al. 1999; Boucher et al. 2000; Kim et al. 2001; Xiao et al. 2002; Hong, Morrow et al. 2004; Lindia et al. 2005). $Na_V1.3$ protein was also found to accumulate in neuromas of patients with painful neuropathy (Black et al. 2008) and to be up-regulated in second-order dorsal horn neurons after CCI (Hains et al. 2004), raising the possibility that $Na_V1.3$ might underlie the increase in the fast TTX_S current in EAN rats. $Na_V1.3$ can also elicit a TTX_S persistent Na^+ current. Nevertheless, the TTX_S persistent Na^+ current is down-regulated in our study.

Previous studies have also implicated the role of $Na_V1.7$ in neuropathic pain. This Na^+ channel isoform is expressed in nociceptive neurons in a preferential manner and underlies a fast TTX_S current with slow repriming kinetics as well as slow inactivation kinetics that allows $Na_V1.7$ channels to be activated by small depolarizing ramps (Cummins, Howe et al. 1998). Based on these biophysical properties, down-regulation of $Na_V1.7$ in combination with an increase in $Na_V1.3$ could explain the decrease in TTX_S I_{NaP} as well as the enhanced excitability in EAN nociceptive neurons. Towards this end, $Na_V1.7$ protein has been shown to be reduced following sciatic nerve ligation (SNL), spared nerve injury (SNI) and sciatic nerve axotomy (Kim, Oh et al. 2002; Berta, Poirot et al. 2008). Conversely, $Na_V1.7$ mRNA and protein are up-regulated in DRGs after peripheral inflammation induced by carrageenan or complete Freund's adjuvant (CFA) (Black, Liu et al. 2004; Strickland et al. 2008). In addition, knock-down of DRG $Na_V1.7$ significantly prevents the development of hyperalgesia in response to CFA (Yeomans et al. 2005). $Na_V1.6$ also gives rise to a TTX_S transient as well as a persistent Na^+ current, and therefore its down-regulation could also underlie the injury induced decrease in I_{NaP}. Previous studies have shown a down-regulation of $Na_V1.6$ mRNA in DRG neurons after SNL and SNI (Berta, Poirot et al. 2008). Of particular interest is a study showing that in chronic relapsing EAE, an experimental model of multiple sclerosis, demyelination along the optic nerve is accompanied by a down-regulation of $Na_V1.6$ and up-regulation of $Na_V1.2$ within retinal ganglion neurons (Craner et al. 2003).

As described above, the transient TTX_S current isoform $Na_V1.3$, which has rapid inactivation as well as rapid repriming kinetics, might underlie the increased fast TTX_S current as has been shown in other nerve injury models. The rapid recovery from inactivation of $Na_V1.3$ might boost high frequency firing in EAN DRGs. However, a high percentage of TTX_S currents of small nociceptive neurons is inactivated at RMP as they display a quite hyperpolarized midpoint of inactivation. It has been suggested that small DRG neurons have a bistable resting potential, as has been demonstrated for other types of excitable cells (Gola and Niel 1993; O'Donnell and Grace 1995). Under certain conditions, nociceptive neurons may reside at more negative potentials where the TTX_S currents are available for activation. Furthermore, in our measurements the

midpoint of inactivation was at -77mV, leaving nearly half of the TTX_S Na^+ channels available for activation at RMP (~ -63 mV) and at the holding potential used for spike measurements (-70mV). Similarly, a different study showed that a considerable fraction of transient Na^+ current could function at resting membrane potential in $Na_V1.8$ KO neurons, where a compensatory increase in TTX_S current has been observed (Rush, Cummins et al. 2007). For this, TTX_S Na^+ current can play a role in the generation of action potential evoked by a depolarizing current injection from resting membrane potential in EAN DRG neurons.

The different Na^+ channels are not only expressed in the cell body but also along the nerve fibers (Brock, McLachlan et al. 1998; Strassman and Raymond 1999; Black, Renganathan et al. 2002; Black and Waxman 2002; Rush, Craner et al. 2005; Rush, Wittmack et al. 2006). A disruption of Na^+ channel expression has been identified in axons of EAN animal models (Novakovic et al. 1998; Lonigro and Devaux 2009), and also in axonal degeneration in a number of injury models including axotomy (LoPachin et al. 1990), compression injury (Agrawal and Fehlings 1996), nitric oxide exposure (Smith et al. 2001; Garthwaite et al. 2002), and EAE (Lo et al. 2002; Bechtold et al. 2004; Bechtold, Yue et al. 2005). Additionally, it has been demonstrated that voltage-sensitive Na^+ channels accumulate in neuroma endings and in patches of demyelination in both animal neuropathy models and in humans with neuropathic pain (Kretschmer et al. 2002). It has been suggested that observed changes in DRG somatas would also occur in the nerve axons and the terminals, since soma and fiber membrane are shown to have similar properties (Djouhri and Lawson 1999). Consistent with this, the patterns of ectopic discharge generated in nerve end neuromas and in DRG somata are similar and are both selectively blocked by low concentrations of TTX and lidocaine (Devor et al. 1992; Matzner and Devor 1994). It is therefore possible that alterations in Na^+ currents found in EAN nociceptive neurons are mirrored in the axons. As primary afferent axons have a different morphology than DRG somatas, changes in the balance of TTX_S and TTX_R currents might lead to more pronounced alterations. Due to their small diameter they have high input resistance, thus, even a low increase in the densities of Na^+ channels could promote AP electrogenesis in these axons (Waxman et al. 1989; Donnelly 2008).

Although the cell body of nociceptors has been shown to be a very good model for studying the role of different ion channels in electrogenesis, there are still some points to be criticized in this model. This is due to the fact that during the enzymatic and mechanical dissociation process DRG neurons lose their axons, satellite glial cells as well as other non neuronal cells. Consequently, changes in cellular phenotype due to culture conditions or removal from a normal cellular environment might have occurred (Zhang, Donnelly et al. 1997). In this regards, it has been shown that the passive membrane properties of small neurons have been altered after dissociation (higher input resistance and more depolarized RMP). Moreover, excitatory mediators such as substance P and neuropeptide Y (NPY), which are abundant in injured DRG (Wakisaka et al. 1991; Wakisaka et al. 1992; Abdulla and Smith 1999), are washed out during the dissociation process. This altogether may influence the results of the electrophysiological measurements of dissociated cells.

4.1.4 Conclusion

In conclusion, our results show that EAN induced dramatic changes in Na^+ currents of DRG neurons. The TTX_S current in these neurons underlies the majority of transient inward Na^+ current, in contrast to control neurons, where the TTX_R current plays the dominant role. In addition, a significant decrease in persistent TTX_S current has been observed that leads to a reduction of total I_{NaP}. These changes provide a good explanation for the significant decrease in AP duration observed in the same subset of neurons. It can also account for the increased excitability that was found compared to one of the control groups and hence the overall increase in nociceptive sensitivity. However, the mechanism leading to such changes is still unclear. The accompanying autoimmune inflammation in the peripheral nerves of EAN rats can provide a possible explanation for the observed changes. In fact, evidence exists that different immune cells are able to directly increase the excitability of DRG neurons by secreting inflammatory cytokines such as IL-1, IL-6 and TNF (Scholz and Woolf 2007). Neuropathic pain like behavior is attenuated by blocking IL-1- or IL-6-mediated signaling (Arruda et al. 2000; Wolf, Gabay et al. 2006). TNF has been shown to increase TTX_R currents in nociceptive neurons through a signaling pathway that involves TNF receptor 1 (TNFR1) and p38 MAP kinase (Jin and Gereau 2006). Hence, inflammatory mediators might underlie the observed changes of Na^+ currents in nociceptive neurons of EAN animals.

The alteration of Na^+ channel expression observed in our experiments as well as in several recent studies of animal models of nerve lesions suggest that these channels might be good targets for the development of new pharmacological agents. However, further studies are required to identify the specific sodium channel subunits that participate in the development of neuropathic pain, as well as the signal transduction mechanism that lead to such changes.

4.2 Partial sciatic nerve ligation

4.2.1 Increase of the T-type Ca^{2+} current in mice suffering neuropathic pain following PNL of the sciatic nerve

Low voltage-activated T-type Ca^{2+} channels were originally identified in peripheral sensory neurons of the dorsal root ganglion (DRG) and are thought to be signal amplifiers in the peripheral pain pathway. Their up-regulation in sensory neurons may contribute to the hyperexcitability that leads to neuropathic pain. Indeed, our experiments showed that the peak T-type Ca^{2+} current was significantly increased in mice displaying neuropathic pain behavior after partial ligation (PNL) of the sciatic nerve. The increase was observed in a subset of small DRG neurons that displayed sensitivity to capsaicin, a marker of nociceptive neurons capable of responding to noxious heat. Although cap^- cells had higher T-type Ca^{2+} currents under control conditions, the increase of the T-type Ca^{2+} current after ligation was not significant.

Our results are in agreement with previous findings, showing an increase in LVA current in different models of neuropathic pain. In this regards, it has been demonstrated by Jagodic et al. (Jagodic, Pathirathna et al. 2008) that the T-type Ca^{2+} current is up-regulated in small DRG cells in rats after chronic constriction injury

(CCI). In a rat model of streptozotocin-induced painful diabetic neuropathy (PDN), the development of diabetes-induced pain was paralleled with a significant increase in T-type Ca^{2+} current density in medium sized DRG cells from the lumbar ganglia of adult rats (Jagodic, Pathirathna et al. 2007). Additionally, colonic hypersensitivity in a rat model of irritable bowel syndrome was accompanied by an increase in the T-type Ca^{2+} current of small DRG neurons (Marger et al. 2011). Interestingly, other patch clamp recordings of DRG neuron Ca^{2+} channels in chronic constriction injury (CCI) gave contrasting results, where a loss of T-type current in medium sized DRG cells was reported (McCallum, Kwok et al. 2003). In another study, no change in the T-type Ca^{2+} current of AD cells (cells with after depolarizing potential) after axotomy has been detected (Abdulla and Smith 2001 b). Thus it is possible that different experimental conditions or the selection of cells of different diameters can lead to these discrepancies.

Although there is no specific T-type Ca^{2+} channel blocker, several pharmacological blockers and modulators of T-type channels have been shown to alleviate neuropathic pain in vivo. For example, it has been shown that mibefradil accounts for a voltage-dependent inhibition of T-type Ca^{2+} currents in small DRG neurons by stabilizing the channel into inactivated states (Todorovic and Lingle 1998). This drug also reversed symptoms of neuropathic pain in a model of CCI (Dogrul, Gardell et al. 2003). Furthermore, some oxidizing agents that block T-type Ca^{2+} currents of DRG neurons are capable of reversing thermal hyperalgesia due to CCI (Todorovic, Meyenburg et al. 2004). Conversely, reducing agents such as dithiothreitol (DTT) and endogenous L-cysteine are shown to increase T-type Ca^{2+} currents. Injection of them into peripheral fields leads to thermal and mechanical nociception (Todorovic et al. 2001). Moreover, application of Ni^{2+}, a T-type channel blocker, inhibited ectopic discharges from peripheral nerves in a model of segmental spinal mechanical injury (Liu, Zhou et al. 2001). It has also been shown, that T-type Ca^{2+} channels are associated with the development of long-term potentiation (LTP) at synapses between nociceptive afferents and dorsal horn neurons of the spinal cord (Ikeda et al. 2003; Heinke et al. 2004). Collectively, these findings are consistent with a role of T-type Ca^{2+} channels in pathological nociception.

4.2.2 $Ca_V3.2$ does not play a role in the PNL induced neuropathic pain

It is known that $Ca_V3.2$ is the most abundant isoform of T-type channels in small and medium-sized peripheral sensory neurons, while $Ca_V3.1$ and $Ca_V3.3$ isoforms are much less frequently expressed in these neurons (Talley, Cribbs et al. 1999). Consistently, the majority of the T-type current in our experiments was pharmacologically blocked by a low Ni^{2+} concentration (50 µm) in control and PNL mice verifying $Ca_V3.2$ as the underlying subunit. In contrast, $Ca_V3.1$ and $Ca_V3.3$ T-type currents require higher concentrations of Ni^{2+} to be blocked (IC_{50} of 250 µM) (Lee, Gomora et al. 1999). Nevertheless, our data show that the increase in T-type current following peripheral nerve injury is caused by a Ni^{2+} resistant current component. These results were further confirmed with the help of $Ca_V3.2$ knock-out mice. Mice lacking $Ca_V3.2$ still suffered pain hypersensitivity following nerve injury, ruling out a role of $Ca_V3.2$ in supporting neuropathic pain in this animal model. Furthermore, our patch clamp recordings revealed a significant increase of T-type Ca^{2+}

currents in PNL DRG, despite the lack of $Ca_V3.2$. Again, this increase was mediated by a Ni^{2+} insensitive T-type Ca^{2+} current ($Ca_V3.1$ or $Ca_V3.3$). Moreover, our qRT-PCR analysis of DRGs confirmed that the $Ca_V3.2$ T-type channel isoform was not altered following peripheral nerve injury.

Our results are in agreement with a previous in vivo study, where knock-out of $Ca_V3.2$ did not prevent thermal and mechanical hyperalgesia following spinal nerve ligation (Choi, Na et al. 2007), suggesting no significant role for $Ca_V3.2$ channels in this model of neuropathic pain. These experiments together with our present data appear to be in conflict with a pronociceptive role of $Ca_V3.2$ in neuropathic pain suggested in other studies. In this regards, molecular knock-down of $Ca_V3.2$ with intrathecally injected antisense oligodeoxynucleotides in sensory neurons of diabetic rats has been shown to reverse both painful diabetic neuropathy (PDN) as well as the diabetes-induced up-regulation of the T-type Ca^{2+} current density of small and medium sized DRG neurons (Messinger, Naik et al. 2009). Bourinet and colleagues showed that intrathecal administration of $Ca_V3.2$ antisense in intact DRG cells induced a large reduction of T-type currents, and reversed both thermal and mechanical hyperalgesia in rats with CCI (Bourinet, Alloui et al. 2005). However, a reduction of DRG neuron T-type currents of neuropathic pain animals was not reported. The discrepancy between these results and ours could be due to the differences in the type of pain model used. Although all animal models are applied for the investigation of neuropathic pain, they differ in pathology. Alternatively, it may be due to some differences between null knock-out by gene targeting and region-specific knock-down with antisense oligonucleotides. Although it has been shown by Bourinet and colleagues that the antisense treatment directed towards $Ca_V3.2$ did not influence the mRNA levels of the other Ca_V3 genes, it cannot be excluded that there are other unknown off-target effects. In addition, the antisense treatment directed against $Ca_V3.2$ induced a 42% reduction of the mRNA level of this channel subunit within the lumbar DRGs. Thus a 100% knock-down cannot be achieved with the antisense treatment, in contrast to the knock-out approach, where this gene is completely lacking. Also it should be pointed, that some experiments using molecular knock-down of Ca_V3x genes with the antisense application were contradictory. Where an antisense knock-down of $Ca_V3.3$ isoform significantly relieved nociceptive sensitivity in rats with chronic compression of the DRG (CCD) in one study (Wen et al. 2006), knock-down of the same isoform did not reverse neuropathic pain symptoms in rats with CCI in another study (Bourinet, Alloui et al. 2005).

It is also possible that developmental compensatory mechanisms might have eliminated the need for $Ca_V3.2$ in our $Ca_V3.2^{-/-}$ mice. However, this seems to be unlikely, since the $Ca_V3.2$ underlying Ni^{2+} sensitive T-type current was not significantly altered in wild type mice following PNL. In addition, knock-out of $Ca_V3.2$ did not affect the low expression of $Ca_V3.1$ or $Ca_V3.3$ in DRG neurons. The T-type Ca^{2+} current was negligible in control $Ca_V3.2^{-/-}$ mice (-10 pA), indicating no compensation for the loss of $Ca_V3.2$.

Altogether, our results suggest a pronociceptive role of $Ca_V3.1$ or $Ca_V3.3$ in the PNL model of neuropathic pain. Consistently, it has been shown that neuropathic pain due to L_5 spinal nerve ligation (SNL) was reduced in $Ca_V3.1$ knock-out mice compared to

wild type mice, demonstrating the involvement of this T-type Ca^{2+} channel subunit in the development of hypersensitivity after nerve injury (Na, Choi et al. 2008). Furthermore, it has been shown by Ikeda et al. (Ikeda, Heinke et al. 2003) that the T-type Ca^{2+} current induced increase in intracellular Ca^{2+} of dorsal horn neurons potentiates the postsynaptic response during synaptic transmission between the C-fibers and dorsal horn neurons of the spinal cord. $Ca_V3.1$ T-type Ca^{2+} channels are mainly expressed in dorsal horn neurons (Talley, Cribbs et al. 1999), raising the possibility that the $Ca_V3.1$ T-type Ca^{2+} channel is involved in the sensitization necessary for neuropathic pain development at the spinal level as well (Na, Choi et al. 2008). In contrast, another study showed that $Ca_V3.1$ knock-out mice show an increased sensitivity to visceral pain, suggesting that the $Ca_V3.1$ subunit might mediate an antinociceptive mechanism (Kim et al. 2003).

In addition to changes in the T-type current, some previous studies have shown a significant reduction in HVA Ca^{2+} current following axotomy (Abdulla and Smith 2001 b) and CFA induced inflammation (Lu, Zhang et al. 2010). A reduction in HVA currents has been also observed following nerve injury in the present study, however, this change did not attain significance. Also, no differences were shown in the $Ca_V3.2$ knock-out mice with respect to the HVA currents. However, it should be mentioned that a fluoride (F-) based internal solution was used in this study, to facilitate rundown of HVA Ca^{2+} currents and allow the isolation of T-type currents. Additionally, HVA currents require besides Mg^{2+}, cAMP and ATP in the pipette solution for stability, unlike LVA currents that are more resistant to rundown. Hence, it is difficult to detect reliable/positive changes in HVA currents in the PNL model based on our measurements.

4.2.3 T-type Ca^{2+} current enhancement is associated with an increase in excitability of DRG neurons following PNL

Under pathological conditions, primary sensory neurons can be sensitized by various mechanisms, leading to their activation by stimuli that would not have been intense enough to cause activation under normal conditions. This can cause pain symptoms as mechanical allodynia observed in the PNL mice. This altered pain response can be evidenced electrophysiologically by observing a lower threshold for nociceptor activation, an increase in spontaneous activity, and/or an increase in frequency of firing in response to a suprathreshold stimulus (Messinger, Naik et al. 2009). Indeed, the significant up-regulation of the T-type current was paralleled by an increased excitability in the same subset of cap^+ DRG neurons following PNL, as evidenced by a considerable reduction of AP threshold. However, the decreased AP threshold might be rather a result of altered Na^+ currents than of changes in T-type currents. Indeed, multiple alterations of Na^+ currents have been described in animal models of traumatic nerve injury (Waxman, Kocsis et al. 1994; Dib-Hajj, Black et al. 1996; Cummins and Waxman 1997; Dib-Hajj, Tyrrell et al. 1998; Cummins, Black et al. 2000; Kim, Oh et al. 2002). However, in this study, action potential recordings were made at a regular resting potential of -70 mV. Performing action potential measurements from more hyperpolarized potentials and analysis of AP series may reveal the influence of the increased T-type current on excitability. In this regards, previous data suggested a significant role of T-type channels in increasing the excitability of a specific subset of

IB_4^+ and cap^+ DRG neurons by reducing the rheobase for action potential firing (Nelson et al. 2005) and contributing to the entry of Ca^{2+} during action potentials (Blair and Bean 2002; Nelson, Joksovic et al. 2005). Although the expression of T-type Ca^{2+} currents in small nociceptive neurons is of moderate density (Todorovic and Jevtovic-Todorovic 2007), its up-regulation could be enough to induce firing as these cells have high input resistance (Nelson et al. 2007). Also, another study found that the increase in the T-type Ca^{2+} current density in a model of painful diabetic neuropathy (PDN) was associated with greater afterdepolarizing potentials (ADP) as well as increased excitability due to a lower threshold for repetitive spike firing in diabetic than in control cells (Jagodic, Pathirathna et al. 2007).

The unique function of T-type currents in neuronal excitability is based on their biophysical characteristics. T-type Ca^{2+} current activate near resting membrane potential. Hence, a small depolarization of the cell membrane can lead to the activation of T-type Ca^{2+} channel and Ca^{2+} entry. This in turn will further depolarize the plasma membrane, thus initiating an action potential (Cain 2010). Transient membrane hyperpolarization can also cause T-type Ca^{2+} channel induced burst firing, which is a phenomenon called “rebound bursting”. At normal neuronal resting membrane potentials, the majority of T-type Ca^{2+} channels are in an inactivated state (Fox et al. 1987; Perez-Reyes 2003). Transient membrane hyperpolarizations (e.g during AHP) will lead to a fast recovery of these channels from inactivation. For this, a larger number of T-type Ca^{2+} channels are available for opening upon subsequent membrane depolarizations, thus, enhancing their ability to trigger action potential bursts.

In conclusion, our present data suggest a role of LVA-currents in the increased cellular excitability and nociceptive sensitivity following peripheral nerve injury. Our pharmacological examination, however, challenges the pronociceptive role of $Ca_V3.2$ suggested in previous studies and shows that $Ca_V3.1$ and/or $Ca_V3.3$ T-type Ca^{2+} current subunits are rather responsible for such changes. However, further analyses are needed to find out which of the two Ni^{2+} resistant subunits underlie the overall increase in T-type Ca^{2+} currents. Knowing this will help in the development of subtype specific blockers for treatment of neuropathic pain.

References

Abdulla, F. A. and P. A. Smith (1999). "Nerve injury increases an excitatory action of neuropeptide Y and Y_2-agonists on dorsal root ganglion neurons." Neuroscience **89**(1): 43-60.

Abdulla, F. A. and P. A. Smith (2001 a). "Axotomy- and Autotomy-Induced Changes in the Excitability of Rat Dorsal Root Ganglion Neurons." J Neurophysiol **85**(2): 630-43.

Abdulla, F. A. and P. A. Smith (2001 b). "Axotomy- and Autotomy-Induced Changes in Ca^{2+} and K^+ Channel Currents of Rat Dorsal Root Ganglion Neurons." J Neurophysiol **85**(2): 644-58.

Agrawal, S. K. and M. G. Fehlings (1996). "Mechanisms of Secondary Injury to Spinal Cord Axons *In Vitro*: Role of Na^+, Na^+-K^+-ATPase, the Na^+-H^+ Exchanger, and the Na^+-Ca^{2+} Exchanger." J Neurosci **16**(2): 545-52.

Akopian, A. N., L. Sivilotti, et al. (1996). "A tetrodotoxin-resistant voltage-gated sodium channel expressed by sensory neurons." Nature **379**(6562): 257-62.

Amaya, F., I. Decosterd, et al. (2000). "Diversity of Expression of the Sensory Neuron-Specific TTX-Resistant Voltage-Gated Sodium Ion Channels SNS and SNS2." Mol Cell Neurosci **15**(4): 331-42.

Amaya, F., H. Wang, et al. (2006). "The Voltage-Gated Sodium Channel $Na_v1.9$ Is an Effector of Peripheral Inflammatory Pain Hypersensitivity." J Neurosci **26**(50): 12852-60.

Amir, R., M. Michaelis, et al. (1999). "Membrane Potential Oscillations in Dorsal Root Ganglion Neurons: Role in Normal Electrogenesis and Neuropathic Pain." J Neurosci **19**(19): 8589-96.

Arruda, J. L., S. Sweitzer, et al. (2000). "Intrathecal anti-IL-6 antibody and IgG attenuates peripheral nerve injury-induced mechanical allodynia in the rat: possible immune modulation in neuropathic pain." Brain Res **879**(1-2): 216-25.

Asbury, A. K. (1990). "Guillain-Barré syndrome: historical aspects." Ann Neurol **27 Suppl**: S2-6.

Babbedge, R. C., A. J. Soper, et al. (1996). "In vitro characterization of a peripheral afferent pathway of the rat after chronic sciatic nerve section." J Neurophysiol **76**(5): 3169-77.

Baccaglini, P. I. and P. G. Hogan (1983). "Some rat sensory neurons in culture express characteristics of differentiated pain sensory cells." Proc Natl Acad Sci U S A **80**(2): 594-8.

Baker, M. D. and H. Bostock (1997). "Low-Threshold, Persistent Sodium Current in Rat Large Dorsal Root Ganglion Neurons in Culture." J Neurophysiol **77**(3): 1503-13.

Basbaum, A. I., & Jessel, T.M. (2000). Principles of Neural Science. New York, McGraw-Hill.

Basbaum, A. I., D. M. Bautista, et al. (2009). "Cellular and molecular mechanisms of pain." Cell **139**(2): 267-84.

Bean, B. P. (1985). "Two kinds of calcium channels in canine atrial cells. Differences in kinetics, selectivity, and pharmacology." J Gen Physiol **86**(1): 1-30.

Bechtold, D. A., R. Kapoor, et al. (2004). "Axonal protection using flecainide in experimental autoimmune encephalomyelitis." Ann Neurol **55**(5): 607-16.

Bechtold, D. A., X. Yue, et al. (2005). "Axonal protection in experimental autoimmune neuritis by the sodium channel blocking agent flecainide." Brain **128**(Pt 1): 18-28.

Beckh, S., M. Noda, et al. (1989). "Differential regulation of three sodium channel messenger RNAs in the rat central nervous system during development." EMBO J **8**(12): 3611-6.

Berta, T., O. Poirot, et al. (2008). "Transcriptional and functional profiles of voltage-gated Na^+ channels in injured and non-injured DRG neurons in the SNI model of neuropathic pain." Mol Cell Neurosci **37**(2): 196-208.

Bessou, P., P. R. Burgess, et al. (1971). "Dynamic properties of mechanoreceptors with unmyelinated (C) fibers." J Neurophysiol **34**(1): 116-31.

Bessou, P. and E. R. Perl (1969). "Response of cutaneous sensory units with unmyelinated fibers to noxious stimuli." J Neurophysiol **32**(6): 1025-43.

Black, J. A., S. Dib-Hajj, et al. (1996). "Spinal sensory neurons express multiple sodium channel alpha-subunit mRNAs." Brain Res Mol Brain Res **43**(1-2): 117-31.

Black, J. A., S. Liu, et al. (2004). "Changes in the expression of tetrodotoxin-sensitive sodium channels within dorsal root ganglia neurons in inflammatory pain." Pain **108**(3): 237-47.

Black, J. A., L. Nikolajsen, et al. (2008). "Multiple sodium channel isoforms and mitogen-activated protein kinases are present in painful human neuromas." Ann Neurol **64**(6): 644-53.

Black, J. A., M. Renganathan, et al. (2002). "Sodium channel $Na_v1.6$ is expressed along nonmyelinated axons and it contributes to conduction." Brain Res Mol Brain Res **105**(1-2): 19-28.

Black, J. A. and S. G. Waxman (2002). "Molecular Identities of Two Tetrodotoxin-Resistant Sodium Channels in Corneal Axons." Exp Eye Res **75**(2): 193-9.

Blair, N. T. and B. P. Bean (2002). "Roles of Tetrodotoxin (TTX)-Sensitive Na^+ Current, TTX-Resistant Na^+ Current, and Ca^{2+} Current in the Action Potentials of Nociceptive Sensory Neurons." J Neurosci **22**(23): 10277-90.

Boucher, T. J., K. Okuse, et al. (2000). "Potent Analgesic Effects Of GDNF In Neuropathic Pain States." Science **290**(5489): 124-7.

Bourinet, E., A. Alloui, et al. (2005). "Silencing of the $Ca_V3.2$ T-type calcium channel gene in sensory neurons demonstrates its major role in nociception." EMBO J **24**(2): 315-24.

Brackenbury, W. J. and L. L. Isom (2011). "Na^+ Channel β Subunits: Overachievers of the Ion Channel Family." Front Pharmacol **2**: 53.

Bridges, D., S. W. Thompson, et al. (2001). "Mechanisms of neuropathic pain." Br J Anaesth **87**(1): 12-26.

Brock, J. A., E. M. McLachlan, et al. (1998). "Tetrodotoxin-resistant impulses in single nociceptor nerve terminals in guinea-pig cornea." J Physiol **512 (Pt 1)**: 211-7.

Brostoff, S., P. Burnett, et al. (1972). "Isolation and Characterization of a Protein from Sciatic Nerve Myelin responsible for Experimental Allergic Neuritis." Nat New Biol **235**(59): 210-2.

Burgess, P. R. and E. R. Perl (1967). "Myelinated afferent fibres responding specifically to noxious stimulation of the skin." J Physiol **190**(3): 541-62.

Caffrey, J. M., D. L. Eng, et al. (1992). "Three types of sodium channels in adult rat dorsal root ganglion neurons." Brain Res **592**(1-2): 283-97.

Cain, S.M. and T.P. Snutch (2010). "Contribution of T-type calcium channel isoforms to neuronal firing." Channels (Austin) 4(6): 475-82.

Calvo, M., J. M. Dawes, et al. (2012). "The role of the immune system in the generation of neuropathic pain." Lancet Neurol **11**(7): 629-42.

Campbell, J. N. and R. A. Meyer (2006). "Mechanisms of Neuropathic Pain." Neuron **52**(1): 77-92.

Carbone, E. and H. D. Lux (1984). "A low voltage-activated, fully inactivating Ca channel in vertebrate sensory neurones." Nature **310**(5977): 501-2.

Carter, G. T., M. P. Jensen, et al. (1998). "Neuropathic pain in Charcot-Marie-Tooth disease." Arch Phys Med Rehabil **79**(12): 1560-4.

Caterina, M. J. and D. Julius (2001). "The vanilloid receptor: a molecular gateway to the pain pathway." Annu Rev Neurosci **24**: 487-517.

Catterall, W. A. (2000). "From Ionic Currents to Molecular Mechanisms: The Structure and Function of Voltage-Gated Sodium Channels." Neuron **26**(1): 13-25.

Catterall, W. A. (2011). "Voltage-Gated Calcium Channels." Cold Spring Harb Perspect Biol **3**(8): a003947.

Catterall, W. A. (2012). "Voltage-gated sodium channels at 60: structure, function and pathophysiology." J Physiol **590**(Pt 11): 2577-89.

Cervero, F. and J. M. Laird (2003). "Role of ion channels in mechanisms controlling gastrointestinal pain pathways." Curr Opin Pharmacol **3**(6): 608-12.

Cesare, P. and P. McNaughton (1996). "A novel heat-activated current in nociceptive neurons and its sensitization by bradykinin." Proc Natl Acad Sci U S A **93**(26): 15435-9.

Chattopadhyay, M., M. Mata, et al. (2008). "Continuous δ-Opioid Receptor Activation Reduces Neuronal Voltage-Gated Sodium Channel ($Na_V1.7$) Levels through Activation of Protein Kinase C in Painful Diabetic Neuropathy." J Neurosci **28**(26): 6652-8.

Chen, C. C., K. G. Lamping, et al. (2003). "Abnormal Coronary Function In Mice Deficient In α_{1H} T-type Ca^{2+} channels." Science **302**(5649): 1416-8.

Choi, S., H. S. Na, et al. (2007). "Attenuated pain responses in mice lacking $Ca_V3.2$ T-type channels." Genes Brain Behav **6**(5): 425-31.

Coggeshall, R. E., S. Tate, et al. (2004). "Differential expression of tetrodotoxin-resistant sodium channels $Na_V1.8$ and $Na_V1.9$ in normal and inflamed rats." Neurosci Lett **355**(1-2): 45-8.

Coste, B., M. Crest, et al. (2007). "Pharmacological Dissection and Distribution of NaN/$Na_V1.9$, T-type Ca^{2+} Currents, and Mechanically Activated Cation Currents in Different Populations of DRG Neurons." J Gen Physiol **129**(1): 57-77.

Costigan, M., J. Scholz, et al. (2009). "Neuropathic Pain: A Maladaptive Response of the Nervous System to Damage." Annu Rev Neurosci **32**: 1-32.

Coulter, D. A., J. R. Huguenard, et al. (1989). "Characterization of ethosuximide reduction of low-threshold calcium current in thalamic neurons." Ann Neurol **25**(6): 582-93.

Craner, M. J., A. C. Lo, et al. (2003). "Abnormal sodium channel distribution in optic nerve axons in a model of inflammatory demyelination." Brain **126**(Pt 7): 1552-61.

Cribbs, L. L., J. H. Lee, et al. (1998). "Cloning and Characterization of α1H From Human Heart, a Member of the T-type Ca^{2+} Channel Gene Family." Circ Res **83**(1): 103-9.

Cummins, T. R., J. A. Black, et al. (2000). "Glial-Derived Neurotrophic Factor Upregulates Expression of Functional SNS and NaN Sodium Channels and Their Currents in Axotomized Dorsal Root Ganglion Neurons." J Neurosci **20**(23): 8754-61.

Cummins, T. R., S. D. Dib-Hajj, et al. (1999). "A Novel Persistent Tetrodotoxin-Resistant Sodium Current In SNS-Null And Wild-Type Small Primary Sensory Neurons." J Neurosci **19**(24): RC43.

Cummins, T. R., J. R. Howe, et al. (1998). "Slow Closed-State Inactivation: A Novel Mechanism Underlying Ramp Currents in Cells Expressing the hNE/PN1 Sodium Channel." J Neurosci **18**(23): 9607-19.

Cummins, T. R., A. M. Rush, et al. (2009). "Voltage-clamp and current-clamp recordings from mammalian DRG neurons." Nat Protoc **4**(8): 1103-12.

Cummins, T. R. and S. G. Waxman (1997). "Downregulation of Tetrodotoxin-Resistant Sodium Currents and Upregulation of a Rapidly Repriming Tetrodotoxin-Sensitive Sodium Current in Small Spinal Sensory Neurons after Nerve Injury." J Neurosci **17**(10): 3503-14.

Czeh, G., N. Kudo, et al. (1977). "Membrane Properties And Conduction Velocity In Sensory Neurones Following Central Or Peripheral Axotomy." J Physiol **270**(1): 165-80.

Decosterd, I., R. R. Ji, et al. (2002). "The pattern of expression of the voltage-gated sodium channels $Na_V1.8$ and $Na_V1.9$ does not change in uninjured primary sensory neurons in experimental neuropathic pain models." Pain **96**(3): 269-77.

Devor, M., P. D. Wall, et al. (1992). "Systemic lidocaine silences ectopic neuroma and DRG discharge without blocking nerve conduction." Pain **48**(2): 261-8.

Dib-Hajj, S., J. A. Black, et al. (1996). "Down-regulation of transcripts for Na channel α-SNS in spinal sensory neurons following axotomy." Proc Natl Acad Sci U S A **93**(25): 14950-4.

Dib-Hajj, S. D., J. Fjell, et al. (1999). "Plasticity of sodium channel expression in DRG neurons in the chronic constriction injury model of neuropathic pain." Pain **83**(3): 591-600.

Dib-Hajj, S. D., L. Tyrrell, et al. (1998). "NaN, a novel voltage-gated Na channel, is expressed preferentially in peripheral sensory neurons and down-regulated after axotomy." Proc Natl Acad Sci U S A **95**(15): 8963-8.

Djouhri, L., L. Bleazard, et al. (1998). "Association of somatic action potential shape with sensory receptive properties in guinea-pig dorsal root ganglion neurones." J Physiol **513 (Pt 3)**: 857-72.

Djouhri, L., X. Fang, et al. (2003). "The TTX-resistant sodium channel $Na_V1.8$ (SNS/PN3): expression and correlation with membrane properties in rat nociceptive primary afferent neurons." J Physiol **550**(Pt 3): 739-52.

Djouhri, L. and S. N. Lawson (1999). "Changes in somatic action potential shape in guinea-pig nociceptive primary afferent neurones during inflammation *in vivo*." J Physiol **520 Pt 2**: 565-76.

Dogrul, A., L. R. Gardell, et al. (2003). "Reversal of experimental neuropathic pain by T-type calcium channel blockers." Pain **105**(1-2): 159-68.

Donnelly, D. F. (2008). "Spontaneous action potential generation due to persistent sodium channel currents in simulated carotid body afferent fibers." J Appl Physiol (1985) **104**(5): 1394-401.

Dubel, S. J., T. V. Starr, et al. (1992). "Molecular cloning of the alpha-1 subunit of an omega-conotoxin-sensitive calcium channel." Proc Natl Acad Sci U S A **89**(11): 5058-62.

Dubreuil, A. S., H. Boukhaddaoui, et al. (2004). "Role of T-type Calcium Current in Identified D-Hair Mechanoreceptor Neurons Studied *In Vitro*." J Neurosci **24**(39): 8480-4.

Elliott, A. A. and J. R. Elliott (1993). "Characterization of TTX-sensitive and TTX-resistant sodium currents in small cells from adult rat dorsal root ganglia." J Physiol **463**: 39-56.

Ertel, E. A., K. P. Campbell, et al. (2000). "Nomenclature of Voltage-Gated Calcium Channels." Neuron **25**(3): 533-5.

Fang, X., L. Djouhri, et al. (2006). "Intense Isolectin-B4 Binding in Rat Dorsal Root Ganglion Neurons Distinguishes C-fiber Nociceptors with Broad Action Potentials and High $Na_V1.9$ Expression." J Neurosci **26**(27): 7281-92.

Fang, X., S. McMullan, et al. (2005). "Electrophysiological differences between nociceptive and non-nociceptive dorsal root ganglion neurones in the rat *in vivo*." J Physiol **565**(Pt 3): 927-43.

Felts, P. A., S. Yokoyama, et al. (1997). "Sodium channel α-subunit mRNAs I, II, III, NaG, Na6 and hNE (PN1): different expression patterns in developing rat nervous system." Brain Res Mol Brain Res **45**(1): 71-82.

Fink, L., W. Seeger, et al. (1998). "Real-time quantitative RT-PCR after laser-assisted cell picking." Nat Med **4**(11): 1329-33.

Fjell, J., P. Hjelmstrom, et al. (2000). "Localization of the tetrodotoxin-resistant sodium channel NaN in nociceptors." Neuroreport **11**(1): 199-202.

Fox, A. P., M. C. Nowycky, et al. (1987). "Kinetic and pharmacological properties distinguishing three types of calcium currents in chick sensory neurones." J Physiol **394**: 149-72.

Fozzard, H. A. and D. A. Hanck (1996). "Structure and function of voltage-dependent sodium channels: comparison of brain II and cardiac isoforms." Physiol Rev **76**(3): 887-926.

Gabriel, C. M., R. A. Hughes, et al. (1998). "Induction of experimental autoimmune neuritis with peripheral myelin protein-22." Brain **121 (Pt 10)**: 1895-902.

Gallego, R. (1983). "The ionic basis of action potentials in petrosal ganglion cells of the cat." J Physiol **342**: 591-602.

Gallego, R. and C. Eyzaguirre (1978). "Membrane and action potential characteristics of A and C nodose ganglion cells studied in whole ganglia and in tissue slices." J Neurophysiol **41**(5): 1217-32.

Gallego, R., I. Ivorra, et al. (1987). "Effects of central or peripheral axotomy on membrane properties of sensory neurones in the petrosal ganglion of the cat." J Physiol **391**: 39-56.

Garthwaite, G., D. A. Goodwin, et al. (2002). "Nitric oxide toxicity in CNS white matter: an *in vitro* study using rat optic nerve." Neuroscience **109**(1): 145-55.

Gilron, I., C. P. Watson, et al. (2006). "Neuropathic pain: a practical guide for the clinician." CMAJ **175**(3): 265-75.

Gola, M. and J. P. Niel (1993). "Electrical and integrative properties of rabbit sympathetic neurones re-evaluated by patch clamping non-dissociated cells." J Physiol **460**: 327-49.

Gold, M. S., D. Weinreich, et al. (2003). "Redistribution of $Na_V1.8$ in Uninjured Axons Enables Neuropathic Pain." J Neurosci **23**(1): 158-66.

Gorke, K. and F. K. Pierau (1980). "Spike potentials and membrane properties of dorsal root ganglion cells in pigeons." Pflugers Arch **386**(1): 21-8.

Gurnett, C. A., M. De Waard, et al. (1996). "Dual Function of the Voltage-Dependent Ca^{2+} Channel $\alpha_2\delta$ Subunit in Current Stimulation and Subunit Interaction." Neuron **16**(2): 431-40.

Gurtu, S. and P. A. Smith (1988). "Electrophysiological characteristics of hamster dorsal root ganglion cells and their response to axotomy." J Neurophysiol **59**(2): 408-23.

Hahn, A. F. (1996). "Experimental allergic neuritis (EAN) as a model for the immune-mediated demyelinating neuropathies." Rev Neurol (Paris) **152**(5): 328-32.

Hahn, A. F., T. E. Feasby, et al. (1991). "P_2-peptide induced experimental allergic neuritis: a model to study axonal degeneration." Acta Neuropathol **82**(1): 60-5.

Hains, B. C., C. Y. Saab, et al. (2004). "Altered Sodium Channel Expression in Second-Order Spinal Sensory Neurons Contributes to Pain after Peripheral Nerve Injury." J Neurosci **24**(20): 4832-9.

Handwerker, H. O., S. Kilo, et al. (1991). "Unresponsive Afferent Nerve Fibres In The Sural Nerve Of The Rat." J Physiol **435**: 229-42.

Harper, A. A. and S. N. Lawson (1985 a). "Electrical properties of rat dorsal root ganglion neurones with different peripheral nerve conduction velocities." J Physiol **359**: 47-63.

Harper, A. A. and S. N. Lawson (1985 b). "Conduction velocity is related to morphological cell type in rat dorsal root ganglion neurones." J Physiol **359**: 31-46.

Heinemann, S. H., H. Terlau, et al. (1992). "Calcium channel characteristics conferred on the sodium channel by single mutations." Nature **356**(6368): 441-3.

Heinke, B., E. Balzer, et al. (2004). "Pre- and postsynaptic contributions of voltage-dependent Ca^{2+} channels to nociceptive transmission in rat spinal lamina I neurons." Eur J Neurosci **19**(1): 103-11.

Herzog, R. I., T. R. Cummins, et al. (2001). "Persistent TTX-Resistant Na^{+} Current Affects Resting Potential and Response to Depolarization in Simulated Spinal Sensory Neurons." J Neurophysiol **86**(3): 1351-64.

Hille, B. (2001). Ion Channels of Excitable Membranes. Sunderland, Massachusetts U.S.A., Sinauer Associates, Inc.

Ho, T. W., G. M. McKhann, et al. (1998). "Human Autoimmune Neuropathies." Annu Rev Neurosci **21**: 187-226.

Hockerman, G. H., B. Z. Peterson, et al. (1997). "Molecular Determinants Of Drug Binding And Action On L-Type Calcium Channels." Annu Rev Pharmacol Toxicol **37**: 361-96.

Hoffman, P. M., J. M. Powers, et al. (1980). "Experimental allergic neuritis. I. Rat strain differences in the response to bovine myelin antigens." Brain Res **195**(2): 355-62.

Hogan, Q. H., J. B. McCallum, et al. (2000). "Painful neuropathy decreases membrane calcium current in mammalian primary afferent neurons." Pain **86**(1-2): 43-53.

Hong, S., T. J. Morrow, et al. (2004). "Early painful diabetic neuropathy is associated with differential changes in tetrodotoxin-sensitive and -resistant sodium channels in dorsal root ganglion neurons in the rat." J Biol Chem **279**(28): 29341-50.

Hughes, R. A. and D. R. Cornblath (2005). "Guillain-Barré syndrome." Lancet **366**(9497): 1653-66.

Hughes, R. A., R. D. Hadden, et al. (1999). "Pathogenesis of Guillain-Barré syndrome." J Neuroimmunol **100**(1-2): 74-97.

Huguenard, J. R. (1996). "Low-Threshold Calcium Currents in Central Nervous System Neurons." Annu Rev Physiol **58**: 329-48.

Ikeda, H., B. Heinke, et al. (2003). "Synaptic Plasticity In Spinal Lamina I Projection Neurons That Mediate Hyperalgesia." Science **299**(5610): 1237-40.

Isom, L. L., K. S. De Jongh, et al. (1992). "Primary structure and functional expression of the beta 1 subunit of the rat brain sodium channel." Science **256**(5058): 839-42.

Jagodic, M. M., S. Pathirathna, et al. (2008). "Upregulation of the T-type calcium current in small rat sensory neurons after chronic constrictive injury of the sciatic nerve." J Neurophysiol **99**(6): 3151-6.

Jagodic, M. M., S. Pathirathna, et al. (2007). "Cell-Specific Alterations of T-Type Calcium Current in Painful Diabetic Neuropathy Enhance Excitability of Sensory Neurons." J Neurosci **27**(12): 3305-16.

Jeftinija, S. (1994). "The role of tetrodotoxin-resistant sodium channels of small primary afferent fibers." Brain Res **639**(1): 125-34.

Jimenez, C., E. Bourinet, et al. (2000). "Determinants of voltage-dependent inactivation affect Mibefradil block of calcium channels." Neuropharmacology **39**(1): 1-10.

Jin, X. and R. W. t. Gereau (2006). "Acute p38-Mediated Modulation of Tetrodotoxin-Resistant Sodium Channels in Mouse Sensory Neurons by Tumor Necrosis Factor-α." J Neurosci **26**(1): 246-55.

Kadlubowski, M. and R. A. Hughes (1979). "Identification of the neuritogen for experimental allergic neuritis." Nature **277**(5692): 140-1.

Kajander, K. C. and G. J. Bennett (1992). "Onset of a painful peripheral neuropathy in rat: a partial and differential deafferentation and spontaneous discharge in A beta and A delta primary afferent neurons." J Neurophysiol **68**(3): 734-44.

Kapoor, R., Y. G. Li, et al. (1997). "Slow sodium-dependent potential oscillations contribute to ectopic firing in mammalian demyelinated axons." Brain **120 (Pt 4)**: 647-52.

Kellenberger, S., T. Scheuer, et al. (1996). "Movement of the Na^+ Channel Inactivation Gate during Inactivation." J Biol Chem **271**(48): 30971-9.

Kiefer, R., B. C. Kieseier, et al. (2001). "The role of macrophages in immune-mediated damage to the peripheral nervous system." Prog Neurobiol **64**(2): 109-27.

Kim, C. H., Y. Oh, et al. (2001). "The changes in expression of three subtypes of TTX sensitive sodium channels in sensory neurons after spinal nerve ligation." Brain Res Mol Brain Res **95**(1-2): 153-61.

Kim, C. H., Y. Oh, et al. (2002). "Changes in three subtypes of tetrodotoxin sensitive sodium channel expression in the axotomized dorsal root ganglion in the rat." Neurosci Lett **323**(2): 125-8.

Kim, D., D. Park, et al. (2003). "Thalamic Control Of Visceral Nociception Mediated By T-Type Ca^{2+} Channels." Science **302**(5642): 117-9.

Kim, Y. I., H. S. Na, et al. (1998). "Cell type-specific changes of the membrane properties of peripherally-axotomized dorsal root ganglion neurons in a rat model of neuropathic pain." Neuroscience **86**(1): 301-9.

Kiss, T. (2008). "Persistent Na-channels: origin and function. A review." Acta Biol Hung **59 Suppl**: 1-12.

Koerber, H. R., R. E. Druzinsky, et al. (1988). "Properties of somata of spinal dorsal root ganglion cells differ according to peripheral receptor innervated." J Neurophysiol **60**(5): 1584-96.

Kohno, T., R. R. Ji, et al. (2005). "Peripheral axonal injury results in reduced μ opioid receptor pre- and post-synaptic action in the spinal cord." Pain **117**(1-2): 77-87.

Koltzenburg, M., C. L. Stucky, et al. (1997). "Receptive Properties of Mouse Sensory Neurons Innervating Hairy Skin." J Neurophysiol **78**(4): 1841-50.

Kostyuk, P. G., N. S. Veselovsky, et al. (1981). "Ionic currents in the somatic membrane of rat dorsal root ganglion neurons-I. Sodium currents." Neuroscience **6**(12): 2423-30.

Kress, M., M. Koltzenburg, et al. (1992). "Responsiveness and functional attributes of electrically localized terminals of cutaneous C-fibers in vivo and in vitro." J Neurophysiol **68**(2): 581-95.

Kress, M. and P. W. Reeh (1996). "More sensory competence for nociceptive neurons in culture." Proc Natl Acad Sci U S A **93**(26): 14995-7.

Kretschmer, T., L. T. Happel, et al. (2002). "Accumulation of PN1 and PN3 Sodium Channels in Painful Human Neuroma-Evidence from Immunocytochemistry." Acta Neurochir (Wien) **144**(8): 803-10; discussion 810.

Lacerda, A. E., H. S. Kim, et al. (1991). "Normalization of current kinetics by interaction between the α1 and β subunits of the skeletal muscle dihydropyridine-sensitive Ca^{2+} channel." Nature **352**(6335): 527-30.

Lawson, S. N., E. I. Harper, et al. (1985). "Monoclonal antibody 2C5: a marker for a subpopulation of small neurones in rat dorsal root ganglia." Neuroscience **16**(2): 365-74.

Lee, J. H., A. N. Daud, et al. (1999). "Cloning and Expression of a Novel Member of the Low Voltage-Activated T-Type Calcium Channel Family." J Neurosci **19**(6): 1912-21.

Lee, J. H., J. C. Gomora, et al. (1999). "Nickel Block of Three Cloned T-Type Calcium Channels: Low Concentrations Selectively Block α1H." Biophys J **77**(6): 3034-42.

Lee, K. H., K. Chung, et al. (1986). "Correlation of cell body size, axon size, and signal conduction velocity for individually labelled dorsal root ganglion cells in the cat." J Comp Neurol **243**(3): 335-46.

Lewin, G. R. and R. Moshourab (2004). "Mechanosensation and Pain." J Neurobiol **61**(1): 30-44.

Lindia, J. A., M. G. Kohler, et al. (2005). "Relationship between sodium channel Nav1.3 expression and neuropathic pain behavior in rats." Pain **117**(1-2): 145-53.

Liu, X., J. L. Zhou, et al. (2001). "Ion channels associated with the ectopic discharges generated after segmental spinal nerve injury in the rat." Brain Res **900**(1): 119-27.

Llinas, R. R. (1988). "The Intrinsic Electrophysiological Properties Of Mammalian Neurons: Insights Into Central Nervous System Function." Science **242**(4886): 1654-64.

Lo, A. C., J. A. Black, et al. (2002). "Neuroprotection of axons with phenytoin in experimental allergic encephalomyelitis." Neuroreport **13**(15): 1909-12.

Lonigro, A. and J. J. Devaux (2009). "Disruption of neurofascin and gliomedin at nodes of Ranvier precedes demyelination in experimental allergic neuritis." Brain **132**(Pt 1): 260-73.

LoPachin, R. M., Jr., V. R. LoPachin, et al. (1990). "Effects of axotomy on distribution and concentration of elements in rat sciatic nerve." J Neurochem **54**(1): 320-32.

Lopez de Armentia, M., C. Cabanes, et al. (2000). "Electrophysiological properties of identified trigeminal ganglion neurons innervating the cornea of the mouse." Neuroscience **101**(4): 1109-15.

Lu, S. G., X. L. Zhang, et al. (2010). "Persistent Inflammation Alters the Density and Distribution of Voltage-Activated Calcium Channels in Subpopulations of Rat Cutaneous DRG neurons." Pain **151**(3): 633-43.

Luongo, L., M. Sajic, et al. (2008). "Spinal changes associated with mechanical hypersensitivity in a model of Guillain-Barré syndrome." Neurosci Lett **437**(2): 98-102.

Lyu, Y. S., S. K. Park, et al. (2000). "Low dose of tetrodotoxin reduces neuropathic pain behaviors in an animal model." Brain Res **871**(1): 98-103.

Ma, C. and R. H. LaMotte (2005). "Enhanced excitability of dissociated primary sensory neurons after chronic compression of the dorsal root ganglion in the rat." Pain **113**(1-2): 106-12.

Malin, S. A., B. M. Davis, et al. (2007). "Production of dissociated sensory neuron cultures and considerations for their use in studying neuronal function and plasticity." Nat Protoc **2**(1): 152-60.

Malmberg, A. B. and A. I. Basbaum (1998). "Partial sciatic nerve injury in the mouse as a model of neuropathic pain: behavioral and neuroanatomical correlates." Pain **76**(1-2): 215-22.

Mantyh, P. W. (2006). "Cancer pain and its impact on diagnosis, survival and quality of life." Nat Rev Neurosci **7**(10): 797-809.

Marger, F., A. Gelot, et al. (2011). "T-type calcium channels contribute to colonic hypersensitivity in a rat model of irritable bowel syndrome." Proc Natl Acad Sci U S A **108**(27): 11268-73.

Martinez, V., D. Fletcher, et al. (2010). "Small fibre impairment predicts neuropathic pain in Guillain-Barré syndrome." Pain **151**(1): 53-60.

Matzner, O. and M. Devor (1992). "Na^+ conductance and the threshold for repetitive neuronal firing." Brain Res **597**(1): 92-8.

Matzner, O. and M. Devor (1994). "Hyperexcitability at sites of nerve injury depends on voltage-sensitive Na^+ channels." J Neurophysiol **72**(1): 349-59.

McCallum, J. B., W. M. Kwok, et al. (2003). "Loss of T-type calcium current in sensory neurons of rats with neuropathic pain." Anesthesiology **98**(1): 209-16.

McCallum, J. B., W. M. Kwok, et al. (2006). "Painful Peripheral Nerve Injury Decreases Calcium Current in Axotomized Sensory Neurons." Anesthesiology **105**(1): 160-8.

McCarter, G. C., D. B. Reichling, et al. (1999). "Mechanical transduction by rat dorsal root ganglion neurons in vitro." Neurosci Lett **273**(3): 179-82.

McCleskey, E. W. and M. S. Gold (1999). "Ion Channels Of Nociception." Annu Rev Physiol **61**: 835-56.

McNulty, M. M. and D. A. Hanck (2004). "State-Dependent Mibefradil Block of Na^+ Channels." Mol Pharmacol **66**(6): 1652-61.

McQuay, H. J., M. Tramer, et al. (1996). "A systematic review of antidepressants in neuropathic pain." Pain **68**(2-3): 217-27.

Mendell, L. M. (1966). "Physiological properties of unmyelinated fiber projection to the spinal cord." Exp Neurol **16**(3): 316-32.

Messinger, R. B., A. K. Naik, et al. (2009). "In vivo silencing of the $Ca_V3.2$ T-type calcium channels in sensory neurons alleviates hyperalgesia in rats with streptozocin-induced diabetic neuropathy." Pain **145**(1-2): 184-95.

Meyer, R. A., K. D. Davis, et al. (1991). "Mechanically insensitive afferents (MIAs) in cutaneous nerves of monkey." Brain Res **561**(2): 252-61.

Meyer zu Horste, G., H. P. Hartung, et al. (2007). "From bench to bedside--experimental rationale for immune-specific therapies in the inflamed peripheral nerve." Nat Clin Pract Neurol **3**(4): 198-211.

Meyer zu Horste, G., W. Hu, et al. (2008). "The immunocompetence of Schwann cells." Muscle Nerve **37**(1): 3-13.

Millan, M. J. (1999). "The induction of pain: an integrative review." Prog Neurobiol **57**(1): 1-164.

Milner, P., C. A. Lovelidge, et al. (1987). "P0 myelin protein produces experimental allergic neuritis in Lewis rats." J Neurol Sci **79**(3): 275-85.

Moalem-Taylor, G., H. N. Allbutt, et al. (2007). "Pain hypersensitivity in rats with experimental autoimmune neuritis, an animal model of human inflammatory demyelinating neuropathy." Brain Behav Immun **21**(5): 699-710.

Moldovan, M., S. Alvarez, et al. (2013). "Axonal voltage-gated ion channels as pharmacological targets for pain." Eur J Pharmacol **708**(1-3): 105-12.

Morgan, K., E. B. Stevens, et al. (2000). "β3: An additional auxiliary subunit of the voltage-sensitive sodium channel that modulates channel gating with distinct kinetics." Proc Natl Acad Sci U S A **97**(5): 2308-13.

Mori, Y., T. Friedrich, et al. (1991). "Primary structure and functional expression from complementary DNA of a brain calcium channel." Nature **350**(6317): 398-402.

Moulin, D. E., N. Hagen, et al. (1997). "Pain in Guillain-Barré syndrome." Neurology **48**(2): 328-31.

Myers, R. R., H. M. Heckman, et al. (1996). "Reduced Hyperalgesia in Nerve-Injured WLD mice: Relationship to Nerve Fiber Phagocytosis, Axonal Degeneration, and Regeneration in Normal Mice." Exp Neurol **141**(1): 94-101.

Na, H. S., S. Choi, et al. (2008). "Attenuated neuropathic pain in $Ca_V3.1$ null mice." Mol Cells **25**(2): 242-6.

Nelson, M. T., P. M. Joksovic, et al. (2005). "The Endogenous Redox Agent L-Cysteine Induces T-Type Ca^{2+} Channel-Dependent Sensitization of a Novel Subpopulation of Rat Peripheral Nociceptors." J Neurosci **25**(38): 8766-75.

Nelson, M. T., J. Woo, et al. (2007). "Reducing Agents Sensitize C-Type Nociceptors by Relieving High-Affinity Zinc Inhibition of T-Type Calcium Channels." J Neurosci **27**(31): 8250-60.

Nilius, B., P. Hess, et al. (1985). "A novel type of cardiac calcium channel in ventricular cells." Nature **316**(6027): 443-6.

Nordin, M., B. Nystrom, et al. (1984). "Ectopic sensory discharges and paresthesiae in patients with disorders of peripheral nerves, dorsal roots and dorsal columns." Pain **20**(3): 231-45.

Novakovic, S. D., S. R. Levinson, et al. (1998). "Disruption and reorganization of sodium channels in experimental allergic neuritis." Muscle Nerve **21**(8): 1019-32.

Nowycky, M. C., A. P. Fox, et al. (1985). "Three types of neuronal calcium channel with different calcium agonist sensitivity." Nature **316**(6027): 440-3.

Nystroem, B. and K. E. Hagbarth (1981). "Microelectrode recordings from transected nerves in amputees with phantom limb pain." Neurosci Lett **27**(2): 211-6.

O'Donnell, P. and A. A. Grace (1995). "Synaptic Interactions among Excitatory Afferents to Nucleus Accumbens Neurons: Hippocampal Gating of Prefrontal Cortical Input." J Neurosci **15**(5 Pt 1): 3622-39.

Okamoto, M., H. Baba, et al. (2001). "Functional reorganization of sensory pathways in the rat spinal dorsal horn following peripheral nerve injury." J Physiol **532**(Pt 1): 241-50.

Oyelese, A. A. and J. D. Kocsis (1996). "$GABA_A$-Receptor-Mediated Conductance and Action Potential Waveform in Cutaneous and Muscle Afferent Neurons of the Adult Rat: Differential Expression and Response to Nerve Injury." J Neurophysiol **76**(4): 2383-92.

Oyelese, A. A., M. A. Rizzo, et al. (1997). "Differential Effects of NGF and BDNF on Axotomy-Induced Changes in $GABA_A$-Receptor-Mediated Conductance and Sodium Currents in Cutaneous Afferent Neurons." J Neurophysiol **78**(1): 31-42.

Pathirathna, S., S. M. Todorovic, et al. (2005). "5α-reduced-reduced neuroactive steroids alleviate thermal and mechanical hyperalgesia in rats with neuropathic pain." Pain **117**(3): 326-39.

Pentland, B. and S. M. Donald (1994). "Pain in the Guillain-Barré syndrome: a clinical review." Pain **59**(2): 159-64.

Perez-Reyes, E. (2003). "Molecular Physiology of Low-Voltage-Activated T-type Calcium Channels." Physiol Rev **83**(1): 117-61.

Perez-Reyes, E., L. L. Cribbs, et al. (1998). "Molecular characterization of a neuronal low-voltage-activated T-type calcium channel." Nature **391**(6670): 896-900.

Perez-Reyes, E., H. S. Kim, et al. (1989). "Induction of calcium currents by the expression of the α1-subunit of the dihydropyridine receptor from skeletal muscle." Nature **340**(6230): 233-6.

Petersen, M., J. Zhang, et al. (1996). "Abnormal spontaneous activity and responses to norepinephrine in dissociated dorsal root ganglion cells after chronic nerve constriction." Pain **67**(2-3): 391-7.

Petruska, J. C., J. Napaporn, et al. (2000). "Subclassified Acutely Dissociated Cells of Rat DRG: Histochemistry and Patterns of Capsaicin-, Proton-, and ATP-Activated Currents." J Neurophysiol **84**(5): 2365-79.

Pragnell, M., M. De Waard, et al. (1994). "Calcium channel β-subunit binds to a conserved motif in the I-II cytoplasmic linker of the α1-subunit." Nature **368**(6466): 67-70.

Priest, B. T. and G. J. Kaczorowski (2007). "Blocking sodium channels to treat neuropathic pain." Expert Opin Ther Targets **11**(3): 291-306.

Priest, B. T., B. A. Murphy, et al. (2005). "Contribution of the tetrodotoxin-resistant voltage-gated sodium channel $Na_V1.9$ to sensory transmission and nociceptive behavior." Proc Natl Acad Sci U S A **102**(26): 9382-7.

Ramer, M. S., G. D. French, et al. (1997). "Wallerian degeneration is required for both neuropathic pain and sympathetic sprouting into the DRG." Pain **72**(1-2): 71-8.

Randall, A. D. and R. W. Tsien (1997). "Contrasting biophysical and pharmacological properties of T-type and R-type calcium channels." Neuropharmacology **36**(7): 879-93.

Rasminsky, M. (1981). "Hyperexcitability of pathologically myelinated axons and positive symptoms in multiple sclerosis." Adv Neurol **31**: 289-97.

Renganathan, M., T. R. Cummins, et al. (2001). "Contribution of $Na_V1.8$ Sodium Channels to Action Potential Electrogenesis in DRG Neurons." J Neurophysiol **86**(2): 629-40.

Reuter, H. (1979). "Properties of Two Inward Membrane Currents in the Heart." Annu Rev Physiol **41**: 413-24.

Rinaldi, S. and H. J. Willison (2008). "Ganglioside antibodies and neuropathies." Curr Opin Neurol **21**(5): 540-6.

Ritter, A. M. and L. M. Mendell (1992). "Somal membrane properties of physiologically identified sensory neurons in the rat: effects of nerve growth factor." J Neurophysiol **68**(6): 2033-41.

Rose, R. D., H. R. Koerber, et al. (1986). "Somal action potential duration differs in identified primary afferents." Neurosci Lett **63**(3): 259-64.

Roy, M. L. and T. Narahashi (1992). "Differential Properties of Tetrodotoxin-sensitive and Tetrodotoxin-resistant Sodium Channels in Rat Dorsal Root Ganglion Neurons." J Neurosci **12**(6): 2104-11.

Rush, A. M., M. J. Craner, et al. (2005). "Contactin regulates the current density and axonal expression of tetrodotoxin-resistant but not tetrodotoxin-sensitive sodium channels in DRG neurons." Eur J Neurosci **22**(1): 39-49.

Rush, A. M., T. R. Cummins, et al. (2007). "Multiple sodium channels and their roles in electrogenesis within dorsal root ganglion neurons." J Physiol **579**(Pt 1): 1-14.

Rush, A. M., E. K. Wittmack, et al. (2006). "Differential modulation of sodium channel $Na_V1.6$ by two members of the fibroblast growth factor homologous factor 2 subfamily." Eur J Neurosci **23**(10): 2551-62.

Ruth, P., A. Rohrkasten, et al. (1989). "Primary Structure Of The Beta Subunit Of The DHP-Sensitive Calcium Channel From Skeletal Muscle." Science **245**(4922): 1115-8.

Ruts, L., J. Drenthen, et al. (2010). "Pain in Guillain-Barré syndrome: a long-term follow-up study." Neurology **75**(16): 1439-47.

Sangameswaran, L., S. G. Delgado, et al. (1996). "Structure and Function of a Novel Voltage-gated, Tetrodotoxin-resistant Sodium Channel Specific to Sensory Neurons." J Biol Chem **271**(11): 5953-6.

Sangameswaran, L., L. M. Fish, et al. (1997). "A Novel Tetrodotoxin-sensitive, Voltage-gated Sodium Channel Expressed in Rat and Human Dorsal Root Ganglia." J Biol Chem **272**(23): 14805-9.

Sather, W. A. and E. W. McCleskey (2003). "Permeation And Selectivity In Calcium Channels." Annu Rev Physiol **65**: 133-59.

Sawant-Mane, S., S. J. Piddlesden, et al. (1996). "CD59 homologue regulates complement-dependent cytolysis of rat Schwann cells." J Neuroimmunol **69**(1-2): 63-71.

Schmidt, R., M. Schmelz, et al. (1995). "Novel Classes of Responsive and Unresponsive C Nociceptors in Human Skin." J Neurosci **15**(1 Pt 1): 333-41.

Scholz, J. and C. J. Woolf (2007). "The neuropathic pain triad: neurons, immune cells and glia." Nat Neurosci **10**(11): 1361-8.

Scroggs, R. S. and A. P. Fox (1992). "Calcium Current Variation Between Acutely Isolated Adult Rat Dorsal Root Ganglion Neurons Of Different Size." J Physiol **445**: 639-58.

Seltzer, Z., R. Dubner, et al. (1990). "A novel behavioral model of neuropathic pain disorders produced in rats by partial sciatic nerve injury." Pain **43**(2): 205-18.

Shin, H. C., E. F. McFarlane, et al. (1989). "Induction of experimental allergic neuritis with synthetic peptides from myelin P2 protein." Neurosci Lett **102**(2-3): 309-12.

Shin, J. B., C. Martinez-Salgado, et al. (2003). "A T-type calcium channel required for normal function of a mammalian mechanoreceptor." Nat Neurosci **6**(7): 724-30.

Silverman, J. D. and L. Kruger (1988). "Lectin and neuropeptide labeling of separate populations of dorsal root ganglion neurons and associated "nociceptor" thin axons in rat testis and cornea whole-mount preparations." Somatosens Res **5**(3): 259-67.

Sindrup, S. H. and T. S. Jensen (1999). "Efficacy of pharmacological treatments of neuropathic pain: an update and effect related to mechanism of drug action." Pain **83**(3): 389-400.

Singer, D., M. Biel, et al. (1991). "The Roles Of The Subunits In The Function Of The Calcium Channel." Science **253**(5027): 1553-7.

Smith, E. S. and G. R. Lewin (2009). "Nociceptors: a phylogenetic view." J Comp Physiol A Neuroethol Sens Neural Behav Physiol **195**(12): 1089-106.

Smith, K. J., R. Kapoor, et al. (2001). "Electrically active axons degenerate when exposed to nitric oxide." Ann Neurol **49**(4): 470-6.

Snider, W. D. and S. B. McMahon (1998). "Tackling Pain at the Source: New Ideas about Nociceptors." Neuron **20**(4): 629-32.

Snutch, T. P. and P. B. Reiner (1992). "Ca^{2+} channels: diversity of form and function." Curr Opin Neurobiol **2**(3): 247-53.

Sommer, C., A. Lalonde, et al. (1995). "Quantitative neuropathology of a focal nerve injury causing hyperalgesia." J Neuropathol Exp Neurol **54**(5): 635-43.

Soong, T. W., A. Stea, et al. (1993). "Structure And Functional Expression Of A Member Of The Low Voltage-Activated Calcium Channel Family." Science **260**(5111): 1133-6.

Stahl, S. M. (1998). "Basic psychopharmacology of antidepressants, part 1: Antidepressants have seven distinct mechanisms of action." J Clin Psychiatry **59 Suppl 4**: 5-14.

Starr, T. V., W. Prystay, et al. (1991). "Primary structure of a calcium channel that is highly expressed in the rat cerebellum." Proc Natl Acad Sci U S A **88**(13): 5621-5.

Stebbing, M. J., S. Eschenfelder, et al. (1999). "Changes in the action potential in sensory neurones after peripheral axotomy in vivo." Neuroreport **10**(2): 201-6.

Stoll, G., B. Schmidt, et al. (1991). "Presence of the terminal complement complex (C5b-9) precedes myelin degradation in immune-mediated demyelination of the rat peripheral nervous system." Ann Neurol **30**(2): 147-55.

Strassman, A. M. and S. A. Raymond (1999). "Electrophysiological Evidence for Tetrodotoxin-Resistant Sodium Channels in Slowly Conducting Dural Sensory Fibers." J Neurophysiol **81**(2): 413-24.

Strickland, I. T., J. C. Martindale, et al. (2008). "Changes in the expression of $Na_V1.7$, $Na_V1.8$ and $Na_V1.9$ in a distinct population of dorsal root ganglia innervating

the rat knee joint in a model of chronic inflammatory joint pain." Eur J Pain **12**(5): 564-72.

Study, R. E. and M. G. Kral (1996). "Spontaneous action potential activity in isolated dorsal root ganglion neurons from rats with a painful neuropathy." Pain **65**(2-3): 235-42.

Stys, P. K., H. Sontheimer, et al. (1993). "Noninactivating, tetrodotoxin-sensitive Na^+ conductance in rat optic nerve axons." Proc Natl Acad Sci U S A **90**(15): 6976-80.

Takahashi, M., M. J. Seagar, et al. (1987). "Subunit structure of dihydropyridine-sensitive calcium channels from skeletal muscle." Proc Natl Acad Sci U S A **84**(15): 5478-82.

Takigawa, T., H. Yasuda, et al. (2000). "The Sera from GM1 Ganglioside Antibody Positive Patients with Guillain-Barré Syndrome or Chronic Inflammatory Demyelinating Polyneuropathy Blocks Na^+ Currents in Rat Single Myelinated Nerve Fibers." Intern Med **39**(2): 123-7.

Talley, E. M., L. L. Cribbs, et al. (1999). "Differential Distribution of Three Members of a Gene Family Encoding Low Voltage-Activated (T-type) Calcium Channels." J Neurosci **19**(6): 1895-911.

Tanabe, T., H. Takeshima, et al. (1987). "Primary structure of the receptor for calcium channel blockers from skeletal muscle." Nature **328**(6128): 313-8.

Tanaka, M., T. R. Cummins, et al. (1998). "SNS Na^+ channel expression increases in dorsal root ganglion neurons in the carrageenan inflammatory pain model." Neuroreport **9**(6): 967-72.

Tandrup, T., C. J. Woolf, et al. (2000). "Delayed loss of small dorsal root ganglion cells after transection of the rat sciatic nerve." J Comp Neurol **422**(2): 172-80.

Tate, S., S. Benn, et al. (1998). "Two sodium channels contribute to the TTX-R sodium current in primary sensory neurons." Nat Neurosci **1**(8): 653-5.

Todorovic, S. M. and V. Jevtovic-Todorovic (2007). "Regulation of T-Type Calcium Channels in the Peripheral Pain Pathway." Channels (Austin) **1**(4): 238-45.

Todorovic, S. M., V. Jevtovic-Todorovic, et al. (2001). "Redox Modulation of T-Type Calcium Channels in rat Peripheral Nociceptors." Neuron **31**(1): 75-85.

Todorovic, S. M. and C. J. Lingle (1998). "Pharmacological Properties of T-Type Ca^{2+} Current in Adult Rat Sensory Neurons: Effects of Anticonvulsant and Anesthetic Agents." J Neurophysiol **79**(1): 240-52.

Todorovic, S. M., A. Meyenburg, et al. (2004). "Redox modulation of peripheral T-type Ca^{2+} channels in vivo: alteration of nerve injury-induced thermal hyperalgesia." Pain **109**(3): 328-39.

Tsien, R. W., D. Lipscombe, et al. (1988). "Multiple types of neuronal calcium channels and their selective modulation." Trends Neurosci **11**(10): 431-8.

Vassilev, P. M., T. Scheuer, et al. (1988). "Identification Of An Intracellular Peptide Segment Involved In Sodium Channel Inactivation." Science **241**(4873): 1658-61.

Vulchanova, L., T. H. Olson, et al. (2001). "Cytotoxic targeting of isolectin IB4-binding sensory neurons." Neuroscience **108**(1): 143-55.

Wakisaka, S., K. C. Kajander, et al. (1991). "Increased neuropeptide Y (NPY)-like immunoreactivity in rat sensory neurons following peripheral axotomy." Neurosci Lett **124**(2): 200-3.

Wakisaka, S., K. C. Kajander, et al. (1992). "Effects of peripheral nerve injuries and tissue inflammation on the levels of neuropeptide Y-like immunoreactivity in rat primary afferent neurons." Brain Res **598**(1-2): 349-52.

Waksman, B. H. and R. D. Adams (1955). "Allergic Neuritis: An Experimental Disease Of Rabbits Induced By The Injection Of Peripheral Nervous Tissue And Adjuvants." J Exp Med **102**(2): 213-36.

Wall, P. D. and M. Devor (1983). "Sensory afferent impulses originate from dorsal root ganglia as well as from the periphery in normal and nerve injured rats." Pain **17**(4): 321-39.

Wall, P. D. and M. Gutnick (1974). "Ongoing activity in peripheral nerves: The physiology and pharmacology of impulses originating from a neuroma." Exp Neurol **43**(3): 580-93.

Wallace, V. C., D. F. Cottrell, et al. (2003). "Focal Lysolecithin-Induced Demyelination of Peripheral Afferents Results in Neuropathic Pain Behavior That Is Attenuated by Cannabinoids." J Neurosci **23**(8): 3221-33.

Watanabe, E., A. Fujikawa, et al. (2000). "Nav2/NaG Channel Is Involved in Control of Salt-Intake Behavior in the CNS." J Neurosci **20**(20): 7743-51.

Waxman, S. G., J. A. Black, et al. (1989). "Low density of sodium channels supports action potential conduction in axons of neonatal rat optic nerve." Proc Natl Acad Sci U S A **86**(4): 1406-10.

Waxman, S. G., J. D. Kocsis, et al. (1994). "Type III Sodium Channel mRNA Is Expressed in Embryonic But Not Adult Spinal Sensory Neurons, and Is Reexpressed Following Axotomy." J Neurophysiol **72**(1): 466-70.

Waxman, S. G., D. A. Utzschneider, et al. (1994). "Enhancement of action potential conduction following demyelination: experimental approaches to restoration of function in multiple sclerosis and spinal cord injury." Prog Brain Res **100**: 233-43.

Weber, F., R. Rudel, et al. (2000). "Anti-GM1 antibodies can block neuronal voltage-gated sodium channels." Muscle Nerve **23**(9): 1414-20.

Weidner, C., M. Schmelz, et al. (1999). "Functional Attributes Discriminating Mechano-Insensitive and Mechano-Responsive C Nociceptors in Human Skin." J Neurosci **19**(22): 10184-90.

Wen, X. J., Z. J. Li, et al. (2006). "Intrathecal administration of Cav3.2 and Cav3.3 antisense oligonucleotide reverses tactile allodynia and thermal hyperalgesia in rats following chronic compression of dorsal root of ganglion." Acta Pharmacol Sin **27**(12): 1547-52.

Weng, X., T. Smith, et al. (2012). "Chronic inflammatory pain is associated with increased excitability and hyperpolarization-activated current (I_h) in C- but not Aδ-nociceptors." Pain **153**(4): 900-14.

White, G., D. M. Lovinger, et al. (1989). "Transient low-threshold Ca^{2+} current triggers burst firing through an afterdepolarizing potential in an adult mammalian neuron." Proc Natl Acad Sci U S A **86**(17): 6802-6.

Williams, M. E., P. F. Brust, et al. (1992). "Structure And Functional Expression Of An Omega-Conotoxin-Sensitive Human N-Type Calcium Channel." Science **257**(5068): 389-95.

Winer, J. B. (2001). "Guillain Barré syndrome." Mol Pathol **54**(6): 381-5.

Wolf, G., E. Gabay, et al. (2006). "Genetic impairment of interleukin-1 signaling attenuates neuropathic pain, autotomy, and spontaneous ectopic neuronal activity, following nerve injury in mice." Pain **120**(3): 315-24.

Wood, J. N. (2000). "Pathobiology of visceral pain: molecular mechanisms and therapeutic implications. II. Genetic approaches to pain therapy." Am J Physiol Gastrointest Liver Physiol **278**(4): G507-12.

Woolf, C. J. and Q. Ma (2007). "Nociceptors-Noxious Stimulus Detectors." Neuron **55**(3): 353-64.

Woolf, C. J., P. Shortland, et al. (1995). "Reorganization of central terminals of myelinated primary afferents in the rat dorsal horn following peripheral axotomy." J Comp Neurol **360**(1): 121-34.

Wu, G., M. Ringkamp, et al. (2002). "Degeneration of Myelinated Efferent Fibers Induces Spontaneous Activity in Uninjured C-Fiber Afferents." J Neurosci **22**(17): 7746-53.

Xiao, H. S., Q. H. Huang, et al. (2002). "Identification of gene expression profile of dorsal root ganglion in the rat peripheral axotomy model of neuropathic pain." Proc Natl Acad Sci U S A **99**(12): 8360-5.

Yeomans, D. C., S. R. Levinson, et al. (2005). "Decrease in Inflammatory Hyperalgesia by Herpes Vector-Mediated Knockdown of $Na_V1.7$ Sodium Channels in Primary Afferents." Hum Gene Ther **16**(2): 271-7.

Yoshida, S. and Y. Matsuda (1979). "Studies on sensory neurons of the mouse with intracellular-recording and horseradish peroxidase-injection techniques." J Neurophysiol **42**(4): 1134-45.

Yu, F. H., R. E. Westenbroek, et al. (2003). "Sodium Channel β4, a New Disulfide-Linked Auxiliary Subunit with Similarity to β2." J Neurosci **23**(20): 7577-85.

Yuki, N., K. Susuki, et al. (2004). "Carbohydrate mimicry between human ganglioside GM1 and *Campylobacter jejuni* lipooligosaccharide causes Guillain-Barré syndrome." Proc Natl Acad Sci U S A **101**(31): 11404-9.

Zamponi, G. W., E. Bourinet, et al. (1996). "Nickel block of a family of neuronal calcium channels: subtype- and subunit-dependent action at multiple sites." J Membr Biol **151**(1): 77-90.

Zhang, J. M., D. F. Donnelly, et al. (1997). "Axotomy Increases the Excitability of Dorsal Root Ganglion Cells With Unmyelinated Axons." J Neurophysiol **78**(5): 2790-4.

Zhang, J. M., X. J. Song, et al. (1999). "Enhanced Excitability of Sensory Neurons in Rats With Cutaneous Hyperalgesia Produced by Chronic Compression of the Dorsal Root Ganglion." J Neurophysiol **82**(6): 3359-66.

Zhang, Z., Z. Y. Zhang, et al. (2008). "Mechanical allodynia and spinal up-regulation of $P2X_4$ receptor in experimental autoimmune neuritis rats." Neuroscience **152**(2): 495-501.

Declaration

I, hereby confirm that this work is my own. This thesis has been written independently and with no other sources and aids than stated. The presented thesis has not been submitted to another university and I have not applied for a doctorate procedure so far.

Hiermit versichere ich, dass die vorgelegte Arbeit (abgesehen von den ausdrücklich bezeichneten Hilfsmitteln) persönlich, selbständig und ohne Benutzung anderer als der angegebenen Hilfsmittel angefertigt wurde. Aus anderen Quellen direkt oder indirekt übernommenen Daten und Konzepte sind unter Angabe der Quelle kenntlich gemacht worden.

Die vorliegende Arbeit wurde an keiner anderen Hochschule als Dissertation eingereicht. Ich habe früher noch keinen Promotionsversuch unternommen.

Ort, Datum Unterschrift